EGG-TMI-8058
June 1988

C1

INFORMAL REPORT

TMI-2 CORE BORE GAMMA RAY SPECTROSCOPY MEASUREMENTS

Charles V. McIsaac
Douglas W. Akers

Idaho National Engineering Laboratory

Managed by the U.S. Department of Energy

EG&G Idaho

Work performed under DOE Contract No. DE-AC07-76ID01570

DISCLAIMER

EGG-TMI-8058

TMI-2 CORE BORE GAMMA RAY SPECTROSCOPY MEASUREMENTS

Charles V. McIsaac
Douglas W. Akers

Published June 1988

EG&G Idaho, Inc.
Idaho Falls, Idaho 83415

Prepared for the
U.S. Department of Energy
Idaho Operations Office
Under DOE Contract No. DE AC07-76ID01570

ABSTRACT

Gamma spectroscopy measurements were performed on TMI-2 core samples to evaluate the distribution of gamma-ray-emitting radionuclides, structural materials (^{60}Co), and uranium fuel (^{144}Ce) in the lower portion of the reactor core. A core boring machine, similar in design to the boring machines employed to extract geological core samples, was used during July and August, 1986, to drill through the entire height of the damaged TMI-2 reactor core at ten different locations. At nine of these locations, core samples measuring 0.064 m in diameter by about 1.8 m long were extracted from the reactor core. The core bore samples contained sections of intact fuel rods, crust layers surrounding the central core region, and previously molten ceramic material.

This report presents the results of the high-resolution gamma ray spectroscopy measurements that were performed on the nine core bore samples. The results indicate that undamaged regions of the fuel rod sections retained their original fission product inventories. Of the amount of ^{137}Cs originally retained in the fuel that was assimilated into the previously molten ceramic material, less than 2% was retained in the ceramic material. The results also show that the concentrations of ^{106}Ru, ^{125}Sb, and ^{60}Co in the ceramic material are as much as a factor of ten higher than their corresponding concentrations in the intact fuel rods.

SUMMARY

Gamma spectroscopy measurements were performed on TMI-2 core samples to evaluate the distribution of gamma-ray-emitting radionuclides, structural materials (^{60}Co), and uranium fuel (^{144}Ce) in the lower portion of the reactor core. At nine core locations, core bore samples measuring 0.0635 m in diameter by about 1.8 m long were extracted from the reactor core.

The core grid drilling locations were chosen to provide two core bore samples from near the center of the core, one sample from near mid-radius, and six samples from the periphery of the core. Three of the locations sampled corresponded to the locations of burnable poison fuel assemblies, and the other six locations corresponded to control rod fuel assemblies. The closed-circuit television (CCTV) inspections of the core bore holes indicated that the solid ceramic structure located near the mid-plane of the core had the shape of an inverted cone; it was about 1.2-m thick near the center of the core and was between 0.30- and 0.60-m thick near the core periphery. Based on these observations, it was anticipated that the core bore samples would consist of varying lengths of stratified cores of the previously molten material and bundles of intact fuel rod stubs from the bottom of the reactor core. Because of the shape of the central core region, it was expected that the bores extracted from peripheral locations would contain little or no ceramic material, but would contain the longest fuel rod sections.

Following their arrival at the Idaho National Engineering Laboratory (INEL), the nine core bore samples were unloaded from their shipping containers, and the cutting heads were removed from the cores. The samples were placed in transport canisters and assayed, using a high-resolution gamma ray spectrometer/scanner system. Each core bore sample was initially scanned over the entire length of the canister to determine the relative distribution of gross gamma ray intensity as a function of position along the axial centerline of the sample. After evaluation of the initial gross intensity measurements, isotopic gamma spectroscopy measurements were

performed at 2.5-cm intervals along the entire length of each core bore, with longer count times used at positions which corresponded to interesting features as determined from the initial gross intensity profile.

The gamma spectroscopy results indicate that the average activities of ^{134}Cs, ^{137}Cs, ^{144}Ce, and ^{154}Eu in regions of the fuel rod bundles removed from the bottoms of the rods are reasonably constant from one core bore sample to the next. The relative abundances of ^{134}Cs, ^{137}Cs, ^{106}Ru, and ^{144}Ce in cross sections of the core bore fuel bundles agree quite well with their ORIGEN2-calculated core average relative abundances. However, the average activities of ^{60}Co, ^{106}Ru, and ^{125}Sb in the intact fuel rods exhibit significantly more variation, which suggests that these radionuclides are distributed less evenly than the fuel-related radionuclides. However, at the time these measurements were made, only small amounts of these radionuclides remained, which probably contributed to the wide variation observed.

In contrast to the results for the intact fuel rod portions of the core bores, the gamma spectroscopic results indicate that ^{106}Ru, ^{125}Sb, and ^{60}Co are the dominant activities in most of the ceramic and agglomerate materials in the core bores (i.e., the upper crust, central core region, and lower crust) and that the bulk of the activity for these radionuclides appears to be associated with the metallic phases. The data also indicate that the structural materials containing phases (from the ^{60}Co distribution) do not contain ^{125}Sb and ^{106}Ru at the same locations, which suggests that the two radionuclides may be retained by different mechanisms in the debris.

If the intact fuel rods retained their original inventories of ^{137}Cs throughout the regions for which average activities were determined, as has been indicated by other examinations, the gamma spectroscopy data suggest that about 98% of the ^{137}Cs originally present in the intact fuel was transported out of the ceramic and agglomerate portions of the previously molten fuel.

To provide a basis for comparing the results of the gamma ray spectroscopy measurement results with radiochemical analyses that are now being performed, radionuclide concentrations in the various materials in the core bore samples were calculated. The average concentrations of ^{134}Cs, ^{137}Cs, ^{106}Ru, and ^{144}Ce in the intact fuel rods were, respectively, 135, 6190, 165, and 276 μCi/g. These concentrations agree to within about 20% of the expected fuel concentrations as determined from ORIGEN2. The measured concentrations of ^{125}Sb and ^{154}Eu are 92 and 24.5 μCi/g, respectively, which are both approximately one-half their expected concentrations.

The results indicate that the concentrations of ^{137}Cs in the ceramic and agglomerate segments are, respectively, only about 1% and 4% of the average ^{137}Cs concentration in the intact fuel rods. The concentrations of ^{60}Co, ^{125}Sb, and ^{106}Ru are, on the other hand, between factors of 5 and 10 higher in the previously molten material than in the bulk material of the fuel bundles.

In summary, the gamma spectroscopy data suggest that much of the original inventory of fission products has been retained in the intact fuel rods; that the more volatile radionuclides (e.g., ^{137}Cs) have been significantly depleted from the previously molten materials; and that the majority of the less volatile radionuclides and materials that probably remained as metallics (^{125}Sb and ^{106}Ru) have been retained in the previously molten materials in the metallic phases.

ACKNOWLEDGMENTS

The work documented in this report required the effort of a large number of individuals in a number of organizations at EG&G. Much of the initial systems development work was done by David Struttman and Alan Procter, with assistance from other members of the Applied Physics Group. Measurements were mostly performed through the efforts of Alan Marley and Gilbert Roybal, with assistance from Pete Randolph and Don Staples. Also, the assistance of Malcolm Russell and Richard Garner in reviewing this report is appreciated.

CONTENTS

FIGURES

TABLES

TMI-2 CORE BORE GAMMA RAY SPECTROSCOPY MEASUREMENTS

1. INTRODUCTION

The Unit 2 pressurized water reactor at Three Mile Island (TMI-2) experienced a loss-of-coolant accident on March 28, 1979, that resulted in severe damage to the core. Since the accident, considerable effort has been expended to improve our understanding of the physical mechanisms that controlled the core damage progression. An integral part of that effort has been focused on characterizing the end-state configuration of the reactor core and assessing the distribution of fission products within core materials. This report presents the results of gamma ray spectroscopy measurements that were performed on nine core bore samples extracted from the TMI-2 reactor core during July and August, 1986. The primary objective of these measurements was to determine the distribution of gamma-ray-emitting radionuclides, structural materials (^{60}Co), and uranium fuel (^{144}Ce) in the lower portion of the reactor core for comparison with radiochemical analysis data.

Prior to 1986, examinations of the active core region were limited to visual and acoustical examinations and mechanical probings of the upper region of the core. The first visual inspections of the core were performed during 1982 using a closed-circuit television (CCTV) system.[1] The inspections revealed the presence of a large void in the upper region of the core. The void extended axially about 1.6 m into the active fuel region and radially, in some locations, to the core former wall, occupying a volume of about 9.3 m^3, or approximately 26% of the original core region.[2] Relatively intact fuel rods were observed in the peripheral regions of the core, and a bed of granular rubble was seen to extend over most of the diameter of the core. After the CCTV inspection on August 12, 1982, the debris bed was probed by lowering a stainless steel rod through two control rod guide tube openings. The probes indicated that the debris bed was as deep as 0.94 m and that it rested on a hard layer of solidified core material.[1]

Following the success of the exploratory probings, the first samples of debris bed material were collected during September and October, 1983. At this time, a total of six samples were retrieved from the debris bed at grid locations H8 and E9 which were, respectively, near the center and mid-radius of the core. At each location, samples were collected from the surface of the bed and at depths of 0.08 and 0.56 m below the surface of the debris bed. Five additional samples were extracted from the debris bed at these same two grid locations during March 1984. These samples were collected at depths down to 0.94 m at location E9 and at depths down to 0.77 m at location H8.[1]

In order to complete the end-state characterization of the reactor core, a core boring machine, similar in design to the boring machines employed to extract geological core samples, was built and subsequently used during July and August, 1986, to drill axially down through the core at ten different locations.[3] At nine of these locations, core samples measuring 0.0635 m in diameter by about 1.8 m long were extracted from the reactor core. At the other location, the core bore sample contained only a short section (<0.15-m long) of one fuel rod. Immediately following the removal of each of the nine core samples, the core bore hole was visually inspected using a CCTV system. The inspections revealed that damage to the core was much more extensive than originally estimated. A region of previously molten material having a volume estimated to be about 10% of the original core volume was confirmed to be present in the lower, central region of the core. This solid ceramic structure was about 1.2-m thick at the center of the core and tapered to a thickness of between about 0.30 and 0.60 m near the core periphery. Sections of standing intact fuel rods were present between the bottom surface of the solid ceramic structure and the fuel rod lower endfittings.

The examinations of the reactor core described above provided a basis for estimating a credible end-state core configuration, which is shown in Figure 1.[4] Video examinations of the walls of the core bore holes revealed two distinct regions between the hard crust (located at about the mid-plane of the original core) and the lower fuel assembly endfittings:

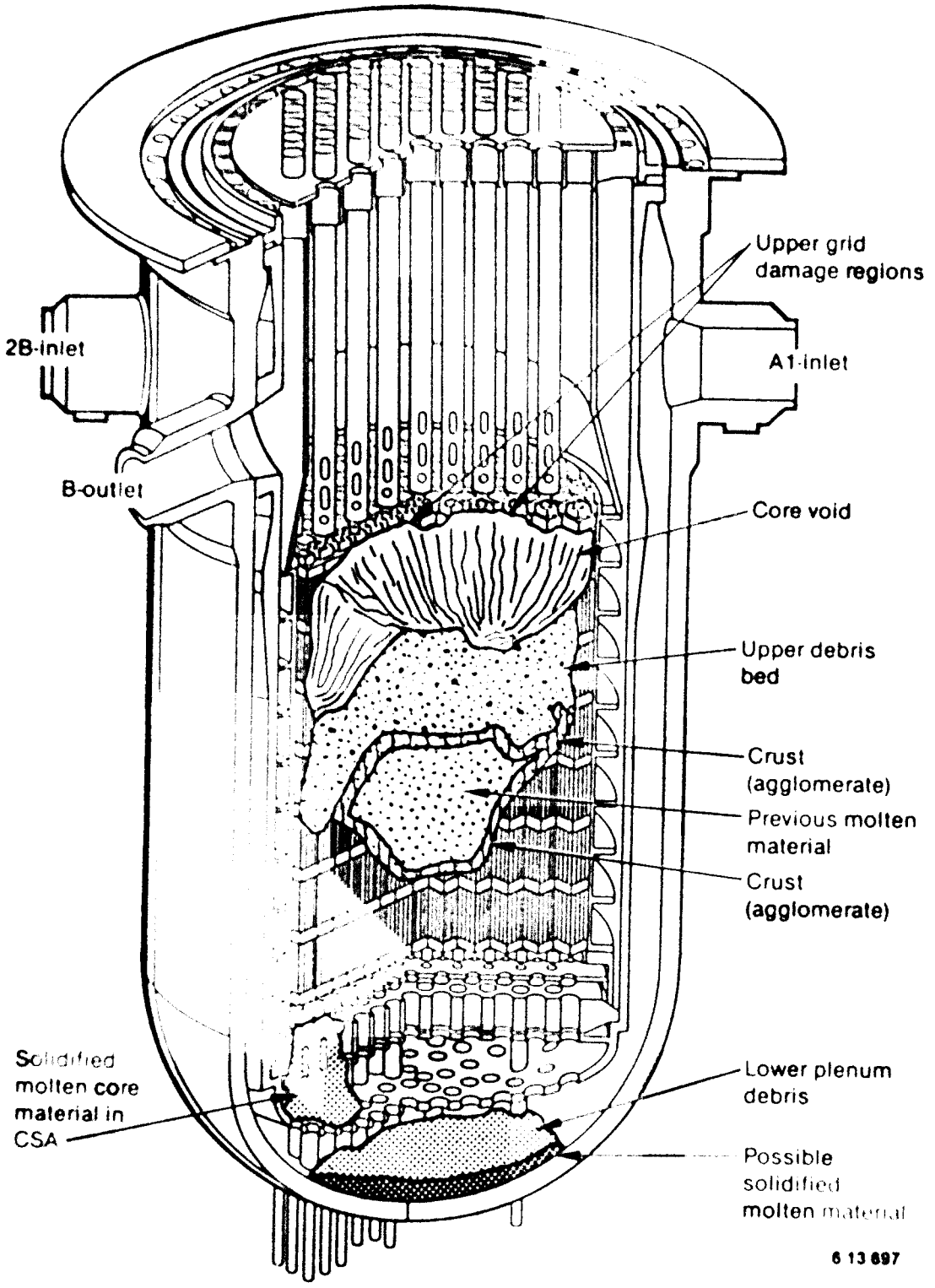

Figure 1. End-state reactor core configuration.

(1) a region of previously molten material that included the hard crust and (2) a region of intact standing fuel rods that extended from the bottom of the previously molten region to the lower fuel assembly endfittings. The previously molten region was observed to be composed of two types of material, namely, (a) material appearing to have a uniform, homogeneous structure that was void of any intact fuel rod components and (b) material that contained generally degraded but intact fuel pellets and/or fuel rod segments. Type (a) material is hereafter referred to as ceramic material and type (b) as agglomerate material.

In Section 2, the core grid locations at which samples were taken are identified, and the condition of the core at each location is briefly described. The methods employed to perform the gamma ray spectroscopy analyses of the core bore samples are described in Section 3. The results of these examinations and analyses are presented and discussed in Section 4, and general observations and conclusions are then summarized in Section 5.

2. END-STATE CORE CONFIGURATION AND CORE BORE SAMPLING LOCATIONS

The TMI-2 active core consisted of 177 individual fuel assemblies, of which 61 were full-length control rod assemblies, 8 were partial-length control rod assemblies, 68 were burnable poison assemblies, and 40 were peripheral (orifice) assemblies.[5] Each of the fuel assemblies is a 15 x 15 array of 208 fuel rods, 16 guide tubes, and 1 instrument tube. Each assembly is about 0.217 m square. The guide tubes provide an envelope which either directs the movement of control rods or positions the fixed burnable poison and orifice rods when they are first inserted. The neutron absorber used in the full-length control rods is a solid metal alloy containing 80 wt% silver, 15 wt% indium, and 5 wt% cadmium. The control rod cladding is cold-worked 304 stainless steel. The neutron absorber used in the majority of the burnable poison assemblies is Al_2O_3-B_4C. The burnable poison rods are clad in zircaloy-4.

The types of assemblies from which the ten core bores were drilled and their grid locations are shown in Figure 2. Grid locations are identified by numbers (north-south) and letters (west-east). The pattern of sampling shown provides east-west and southwest-northeast diametral cross-sectional samples, as well as two radial sample cross sections from the core center to the north and another to the southeast. These nine core bores provided two samples from near the center of the core, one sample from near mid-radius, and six samples from around the core periphery. A summary of the grid locations of the assemblies that were sampled is listed in Table 1. As indicated in Table 1, fuel assemblies G-8, G-12, K-6, and N-5 are burnable poison assemblies having ^{235}U enrichments of 2.64 wt%, while the remaining six assemblies are full-length control rod assemblies having ^{235}U enrichments of 1.98 wt%.

As was previously mentioned, following removal of each of the nine core bore samples, the core bore hole was visually examined using a CCTV system. The results of these observations were combined with the core probe data and the acoustic topography data to construct contour maps that

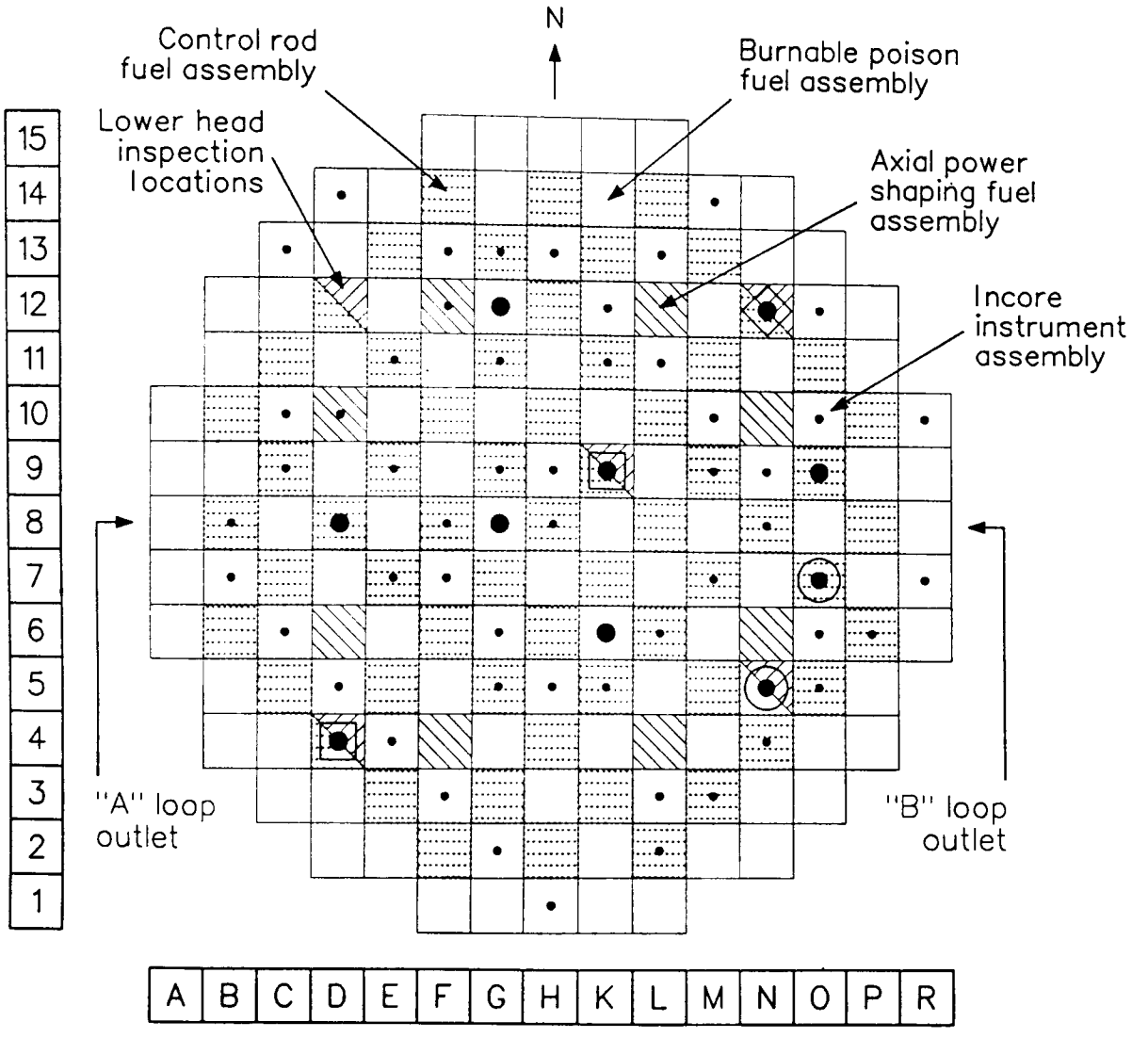

Drilling Locations

G	12
N	12
K	9
O	9
D	8
G	8
O	7
N	5
D	4

LN88025-1

Figure 2. Core bore drilling locations.

TABLE 1. SUMMARY OF DESCRIPTIVE INFORMATION FOR CORE BORE FUEL ASSEMBLIES

Core Bore Number	Element Number	^{235}U Enrichment	Type of Assembly
K-9	105	1.98	Control rod
G-8	74	2.64	Burnable poison
D-8	32	1.98	Control rod
G-12	78	2.64	Burnable poison
N-12	150	1.98	Control rod
O-9	159	1.98	Control rod
O-7	157	1.98	Control rod
N-5	143	2.64	Burnable poison
D-4	28	1.98	Control rod
K-6	102	2.64	Burnable poison

defined the spatial distributions of the upper debris bed, the agglomerate region, the previously molten homogeneous ceramic region, and the region of standing intact fuel rods. Figure 3 shows these regions as they extend across the K row of fuel assemblies and the position of the K-9 core bore hole. The core locations are referenced to the 298-ft elevation, which is the elevation of the core support plate. As shown in Figure 3, the standing fuel rod stubs support the agglomerate and molten ceramic regions. The agglomerate region forms a shell around the periphery of the previously molten ceramic material. At the location of the K-9 fuel assembly, this shell is only 0.10- to 0.15-m thick at the interface of the agglomerate layer and the standing fuel rod stubs.[3] Compared with other locations that were sampled, the previously molten homogeneous material extends to its greatest depth at the location of the K-9 fuel assembly, which (as shown on Figure 3) extends from the top of the core bore hole down to near the top of the second spacer grid, a distance of almost 1.3 m. Previously molten material was observed between fuel rods at positions as low as 0.10 m above the bottoms of the rods.

Figures 4(a), 4(b), 4(c), and 4(d) respectively show these same four regions as they extend across the D, G, N, and O rows of the fuel assemblies. Figure 4 also shows the positions of the D-4, D-8, G-8, G-12, N-5, N-12, O-7, and O-9 core bore holes. As shown, the agglomerate shell is relatively thin under the previously molten homogeneous ceramic in the

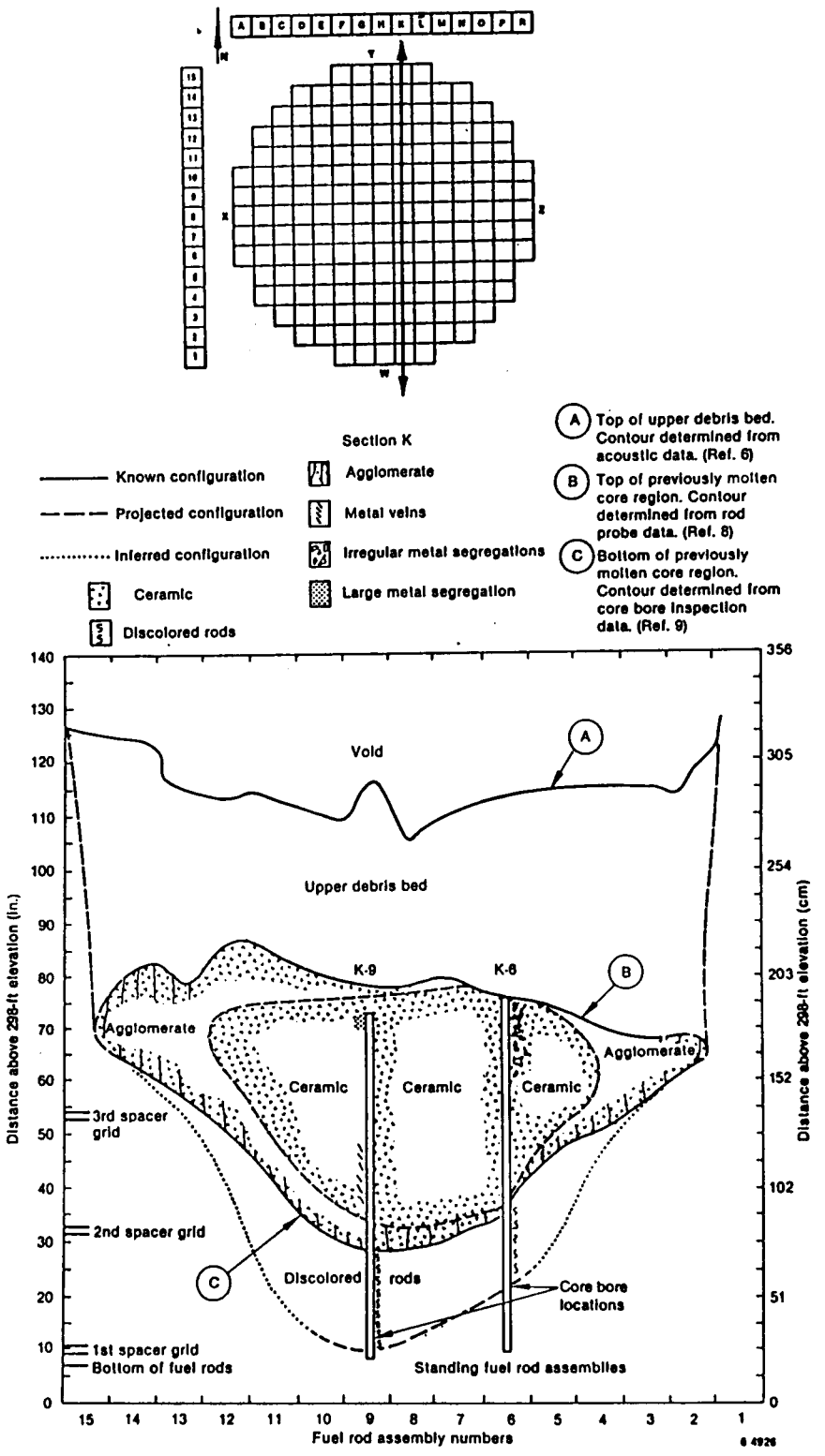

Figure 3. Core cross section showing end-state configuration through Row K of fuel assemblies.

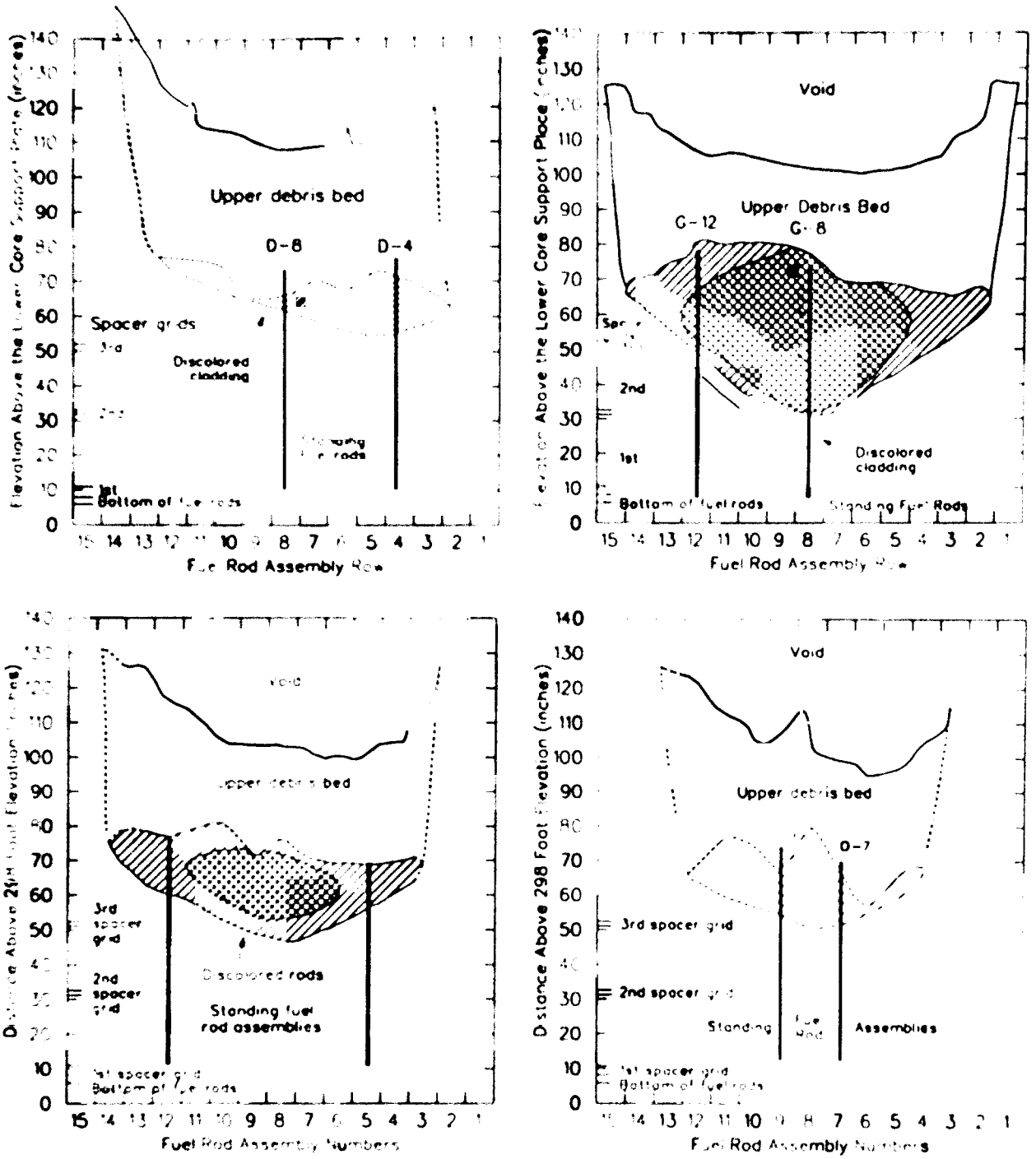

Figure 4. Core cross sections showing end-state configurations through Rows D, G, M, and O of fuel assemblies.

central region of the core, but increases in thickness towards the outer regions and forms all of the degraded core material above the standing fuel rod stubs at the locations of the outer fuel assemblies. This postulated distribution of agglomerate material in the core is supported by the fact that previously molten homogeneous ceramic material was not observed in any of the peripheral core bore holes (i.e., D-4, D-8, N-5, N-12, O-7, and O-9). Figures 3 and 4 illustrate that the heights of the standing fuel rod stubs above the bottom of the core vary from about 0.80 m at the center of the core to between 1.3 and 1.5 m at the periphery of the core.

Detailed descriptions of the types of materials and lengths of fuel rods contained in each of the core bore samples are provided in Section 4.1.

3. ANALYTICAL METHODS

This section describes the methods used to perform the gamma ray spectroscopy examinations on the nine core bore samples.

3.1 Photographic Examinations

After the core bores had been examined by gamma spectroscopy, they were transported to the Auxiliary Reactor Reactor (ARA) for disassembly and visual examination. Methods of photographic examination are discussed in Reference 4. A final core bore examination report will be published in the latter part of 1988.

3.2 Gamma Ray Spectroscopy Measurements

A description of the collimated gamma ray spectrometer/scanner system used to analyze the core bore samples is provided in Section 3.2.1. Engineering drawings of the scanner bed and the detector housing and collimator are provided in Appendix A, figures A-1 through A-3. The gamma spectral analysis program written for the IBM personal computer that was used to analyze the core bore spectra is described in Section 3.2.2. The analytical methods and the assumptions used to derive sample self-attenuation correction factors for the signature gamma rays of the radionuclides that were detected are discussed in Section 3.2.3.

3.2.1 Gamma Ray Spectrometer/Scanner System

A special-purpose gamma ray spectrometer/scanner system was developed to examine the highly radioactive core bore samples obtained from the TMI-2 reactor core.[6] Components of spectrometer instrumentation are identified in figure 5. Input gamma rays are processed in order by the detector, amplifier, analog-to-digital converter (ADC), and micro multi-channel analyzer (MCA). Details of system design and operation are included in References 7 and 8.

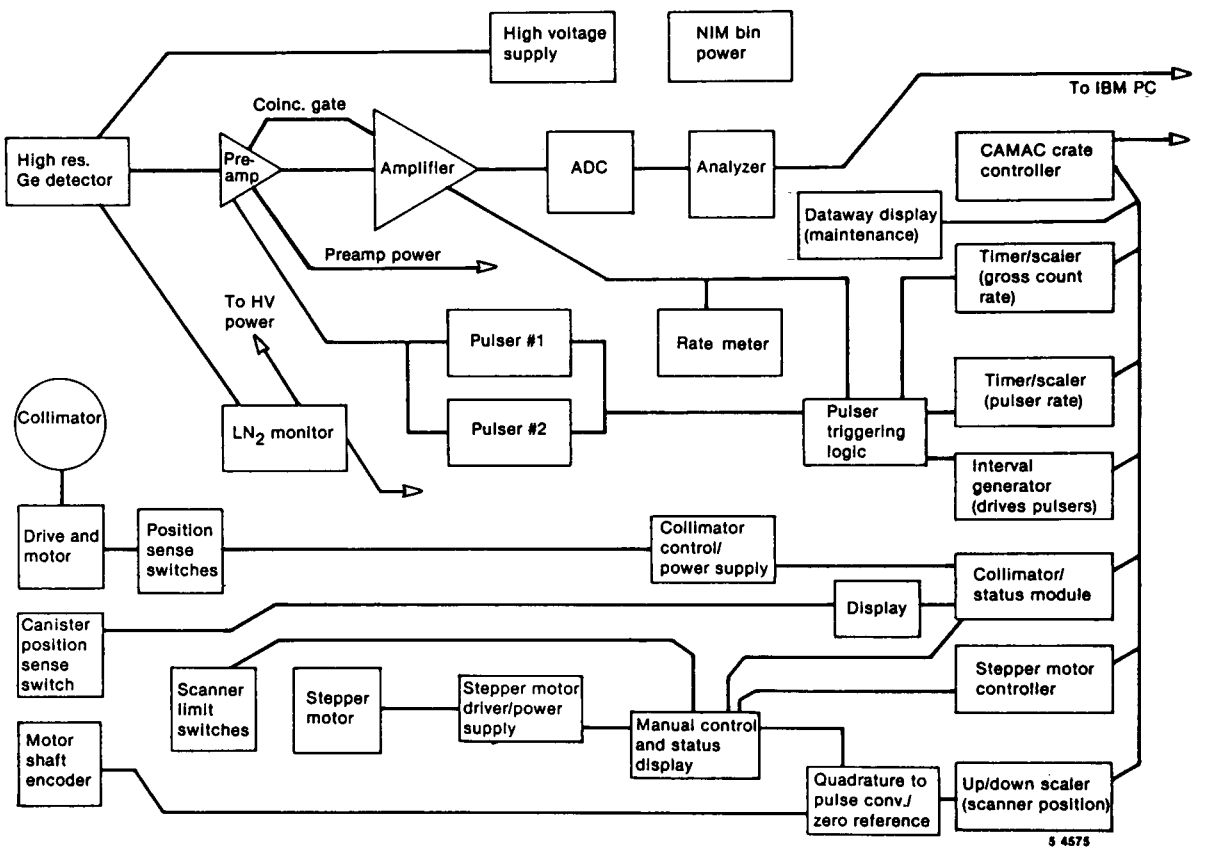

Figure 5. Spectrometer instrumentation diagram.

Samples to be analyzed are laid on a moving trolley that rides on the scanner bed. The detector/shield/collimator assembly, which is located at the center of the scanner bed, views the sample from above. The trolley motor control module includes a position encoder that allows a scan position to be determined to 0.254 cm.

In order to assure that the energy flux to the detector is kept below its saturation limit, the detector is surrounded by a shield made of tungsten alloy and lead, as shown in Figure 6. Figure A-3 in Appendix A shows the arrangement of the slits and the calibration source holder. The fixed calibration source provides a means of conveniently monitoring spectrometer gain over long periods of time; the blank position is used when a determination of gamma ray leakage through the shield is desired.

The length and size of the collimator slit and the distance between the collimator and the core bore sample determine the volume of the core bore sample that is within the field of view of the detector (see Appendix A). During the analyses of the core bore samples, the distance between the collimator and the axial centerlines of the core bore samples was maintained at 0.38 m. Using geometrical optics, the volume of the canister that is within the field of view of the detector can be calculated in a straightforward manner. Because the width of the collimator slit that was used is close to the diameter of the core bore canister (i.e., 6.35 cm) in the direction perpendicular to the axial centerline of the core bore canister, about 80% of the diameter of the canister is within the umbra of the detector's field of view (i.e., that region of the field of view where the detector's counting efficiency is constant).

Each core bore sample was initially gamma-scanned over the entire length of the core bore canister to determine the relative gamma ray intensity as a function of position along the axial centerline. During each of these scans, the spectrometer's ADC input count rate was recorded on an analog chart recorder while the core bore sample was moved at a constant rate through the field of view of the detector. The resulting count rate profiles were used to locate the top and bottom ends of the core

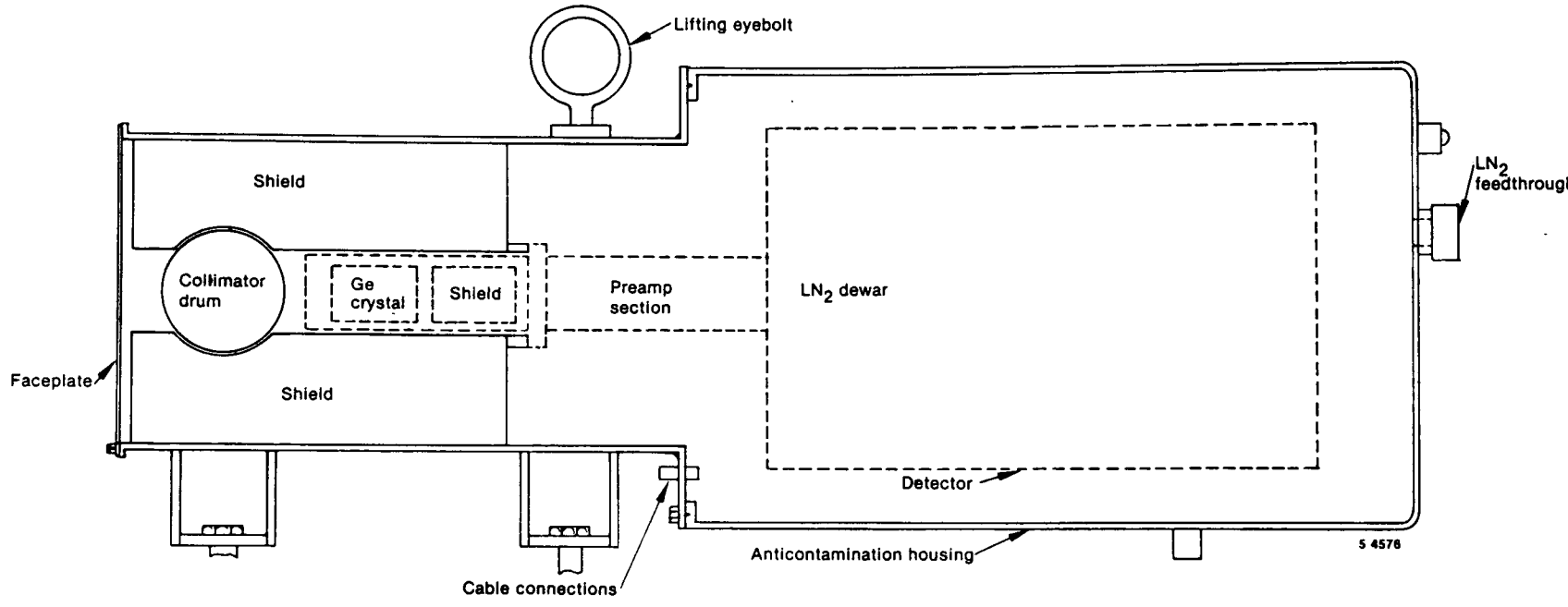

Figure 6. Cross-sectional view of detector and collimator.

bore samples. They were also used to define regions of interest that would be examined during the subsequent incremental isotopic gamma spectral measurements.

Isotopic gamma spectral measurements were normally performed at intervals of 2.5 cm over the entire length of each sample. Measurements were also made at locations beyond the ends of each core bore sample to determine background levels of the radionuclides of interest. For some core bore samples, intervals smaller than 2.5 cm were used in order to more closely examine regions of the gamma ray intensity profiles that exhibited anomalous features. The count live time that was normally used at each scan position was 100 s; however, the count live time was increased to 600 s at a few locations on each of the core bore samples in order to enhance detection sensitivity.

3.2.2 Gamma Spectral Analysis Program

The gamma spectral analysis program converts the gamma radiation measured by the detector into usable information on the identity and quantity of radionuclides present in the sample material. Originally, it was anticipated that the analysis of the core bore spectra would be performed using a commercially available gamma spectral analysis program. However, no software programs were available at the time the measurements were made that met the requirements for the core bore scanner system. Consequently, a program was developed using available software that was suitable for the gamma scanner measurements. The code developed, called RICKI, is a compact, user-interactive gamma spectral analysis program written for the IBM personal computer (IBM/PC) using the IBM Disk Operating System (DOS), Version 3.1.[9]

RICKI is written in BASIC language and compiled using the IBM/PC BASIC compiler version 2.01. System requirements for the present version of RICKI are an IBM/PC with the enhanced graphics adapter, disk files for spectral data, a radionuclide gamma ray library, two temporary files for sorting, and a printer. RICKI locates peaks, computes centroids and areas,

and identifies spectral peaks by energy via a user-specified library file. Peak analysis is a multi-operation process, including peak and background location, peak integration, and comparison of peak centroid energies with library data. The peak search algorithm utilizes an optimized second derivative filter for efficient and reliable peak identification. A Gaussian is fit to each peak found, using a modified version of Mukoyama's linear least-squares fitting method.[10]

Corrections for detector efficiency as a function of energy are applied to all peaks. Two forms of efficiency estimation are available: (1) a functional efficiency = A exp $[B/E_1^N]E_1^C$ where A, B, C, and N are parameters calculated from a least-squares analysis and E_1 is the peak centroid energy and (2) a tabular interpolation based on a cubic spline fit. The dead-time pile-up correction is derived from the ratio of pulses injected into the spectrum to the area of the spectral peak resulting from this injection. Applying this correction requires that a pulse generator inject pulses of known height into the detector's "TEST" input during acquisition of spectra. Averaged activities for all identified radionuclides are computed by sorting peaks by identification and calculating weighted averages. For a more detailed description of the RICKI gamma spectral analysis algorithms, the reader is referred to Reference 9.

3.2.3 Corrections for Sample Self-Attenuation

The absolute counting efficiency of the spectrometer that was used to analyze the core bore samples was determined by making multiple measurements of a rectangular plane source calibration standard. The standard was positioned at a distance that duplicated the counting geometry that was employed to analyze the core bore samples. However, the physical characteristics of the plane source calibration standard were different from the physical characteristics of the actual core bore samples in two important respects, namely: (a) the plane source standard was less than 2-mm thick, whereas the core bore canisters contained materials that were usually 5-cm thick, and (b) the density of the plane source standard, which

was basically blotting paper sandwiched between two sheets of plexiglass, was about a factor of five to ten less than the densities of the materials present in the core bore samples. Because of these differences, the effect of gamma ray self-attenuation within the calibration standard was negligible compared to the effect of self-attenuation within the higher density materials of the core bore samples. The absolute counting efficiency data that were used to convert photopeak count rates to radionuclides activities did not take into account the gamma ray self-attenuation within the materials of the core bore samples.

If, for a given energy, the material within the relatively narrow field of view of the germanium detector can be characterized by a single linear attenuation coefficient u^1, the fraction of gamma rays escaping the sample without any energy loss can be computed in a straightforward manner. For a cylindrically shaped sample viewed by a detector along a diameter of the sample at a distance that is large compared to the diameters of the sample and detector, it has been shown that[11,12]

$$CF(E_1) = \frac{1}{2} \frac{-\ln(T)}{[I\,[-\ln(T)] - L\,[-\ln(T)]]} \qquad (1)$$

where

$CF(E_1)$ = the self-attenuation correction factor for a gamma ray of energy E_1,
L_1 = the modified Struve function of order 1,
I_1 = the modified Bessel function of order 1, and
T = the transmission across the diameter of the sample for a gamma ray of energy E_1.

The transmission across the diameter of the sample is

$$T = \exp(-u^1 D), \qquad (2)$$

where

D = the diameter of the sample, and

u^1 = the linear attenuation coefficient at energy E_1.

Because transmission measurements were not made, the transmission across the diameter of the core bore sample must be computed using a u^1 that is calculated based on an assumed sample composition and density. The linear attenuation coefficient of a compound or mixture of elements is calculated as the product of the mass attenuation coefficient and the mean density of the compound. The mass attenuation coefficient of a compound is calculated as

$$u^m = w^1(u^m)_1 + w^2(U^m)_2 + \ldots + w^n(u^m)_n \qquad (3)$$

where

w^i = the weight fraction of element (i) in the compound, and

$(u^m)_i$ = the mass attenuation coefficient of element (i).

Values of the mass attenuation coefficients for gamma ray energies from 200 keV to 2 MeV are tabulated in Table 2 for oxygen, iron, uranium, UO_2 fuel, and (U-Zr-O) ceramic. The weight percents of uranium and oxygen in the fuel pellets in the fuel rods in the core bore samples were assumed to be the same as they were prior to the accident; namely, 88.15 and 11.85 wt.%, respectively. The ceramic material in the core bores was assumed to be composed of 62.87 wt.% uranium, 12.40 wt.% oxygen, 17.42 wt.% zirconium, and 7.31 wt.% iron, silver, and other trace-level metals, which is the elemental composition of the active core region following oxidation of the cladding.[1,4] It has been estimated that about 4,800 kg of oxygen combined with the cladding during its oxidation.[4] The mass attenuation coefficients for (U-Zr-O) ceramic that are presented in Table 2 were calculated using the mass attenuation coefficients for iron in place of those for zirconium and the trace-level metals; over the energy range of interest, the mass attenuation coefficients of these metals have about the

TABLE 2. MASS ATTENUATION COEFFICIENTS OF ELEMENTS AND COMPOUNDS

Energy (keV)	Mass Attenuation Coefficient (cm^2/g)				
	O[a]	Fe[a]	U[a]	UO_2	(U-Zr-O)
200	0.122	0.150	1.200	1.072	0.807
400	0.096	0.092	0.300	0.276	0.223
600	0.081	0.075	0.153	0.144	0.125
800	0.071	0.066	0.105	0.101	0.091
1000	0.064	0.058	0.082	0.080	0.0737
1200	0.058	0.053	0.068	0.067	0.0631
1400	0.053	0.049	0.059	0.059	0.0560
1600	0.050	0.045	0.054	0.053	0.0510
1800	0.047	0.042	0.050	0.050	0.0476
2000	0.044	0.040	0.047	0.047	0.0449

a. T. Rockwell III, Reactor Shielding Design Manual, Princeton: D. Van Nostrand Company, Inc., 1956, pp. 447 448.

same values. Linear attenuation coefficients were calculated using densities of 10.13 g/cm^3 for fuel pellets[5] and 7.5 g/cm^3 for ceramic material, where the latter density is the average density of the ceramic samples that were removed from the core bore canisters for radiochemical analysis.

For the purpose of comparing gamma ray self-attenuation within the materials of the core bore samples, only the following four simplified source geometries were considered: (a) a single UO_2 fuel pellet clad in zircaloy-4; (b) a single (U-Zr-O) ceramic pellet having the same dimensions as a fuel pellet; (c) a solid (U-Zr-O) right-circular cylinder having a diameter of 6.35 cm; and (d) a fuel rod bundle consisting of closely packed, completely clad fuel fuel rods. The fuel pellet diameter was assumed to be 0.94 cm, and the cladding wall thickness was assumed to be 0.135 cm.[5] The diameter of a closely packed fuel rod bundle is 5.46 cm. The diameter of the (U-Zr-O) ceramic core segment was set equal to the diameter of the core bore canister, 6.35 cm.

The self-attenuation correction factors that were calculated for the UO_2 and (U-Zr-O) pellets are presented in Table 3; similar results for the fuel rod bundle and the 6.35-cm-dia (U-Zr-O) ceramic core segment are presented in Table 4. The data in these tables show that for each of the four categories of samples, the self-attenuation correction factor does not change substantially in the energy range of 1 to 2 MeV. The average values of the correction factors in this energy range are: UO_2 pellet, 1.32 ± 5%; (U-Zr-O) pellet, 1.18 ± 3%; fuel rod bundle, 2.84 ± 15%, and (U-Zr-O) core segment, 2.48 ± 14%. The fact that the self-attenuation correction factor changes very little between 1 and 2 MeV means that, for a given scan position, the relative activities that were measured for radionuclides having primary gamma rays in this energy range should correspond reasonably well with their relative concentrations in the core bore samples. Of the radionuclides that were detected, ^{60}Co, ^{106}Ru, ^{110m}Ag, ^{144}CeD, and ^{154}Eu fall into this category (see Table 5 for gamma ray energies).[13] On the other hand, the primary gamma rays of ^{134}Cs, ^{137}Cs, and ^{125}Sb are lower, being 796, 662, and 428 keV, respectively. Because of increased gamma ray self-attenuation, their measured activities required application of a correction factor to account for the additional self-absorption.

The data in Table 4 also show that the self-attenuation correction factors for a fuel rod bundle are generally about 20% higher than the self-attenuation correction factors for corresponding gamma ray energies for a 6.35-cm-dia (U-Zr-O) core segment. These results indicate that it is valid to compare the radionuclide activities of a fuel bundle with the corresponding radionuclide activities of ceramic pieces that have diameters that are close to the diameter of the fuel bundle. In this case, a difference in measured activity between the two types of samples can be attributed to the samples having different radionuclide inventories. For small-diameter ceramic pieces, self-attenuation is, of course, not as severe as it is for a fuel bundle or large-diameter ceramic core segment. In this latter case, the validity of comparing radionuclide activities, especially those of ^{134}Cs, ^{137}Cs, and ^{125}Sb, in small ceramic fragments with corresponding activities in core bore fuel bundles is questionable because of the large differences in the self-attenuation correction factors for the two types of samples (see Tables 3 and 4).

TABLE 3. SELF-ATTENUATION CORRECTION FACTORS FOR UO_2 AND (U-Zr-O) PELLETS

Energy (keV)	UO_2 Pellet		(U-Zr-O) Pellet	
	Transmission	Correction Factor	Transmission	Correction Factor
200	3.69 E-05	9.34 E+00	3.38 E-03	5.09 E+00
400	7.20 E-02	2.69 E+00	2.08 E-01	1.80 E+00
600	2.54 E-01	1.83 E+00	4.14 E-01	1.42 E+00
800	3.82 E-01	1.56 E+00	5.26 E-01	1.31 E+00
1000	4.67 E-01	1.44 E+00	5.95 E-01	1.24 E+00
1200	5.28 E-01	1.36 E+00	6.41 E-01	1.20 E+00
1400	5.70 E-01	1.31 E+00	6.74 E-01	1.18 E+00
1600	6.04 E-01	1.28 E+00	6.98 E-01	1.16 E+00
1800	6.21 E-01	1.27 E+00	7.15 E-01	1.15 E+00
2000	6.39 E-01	1.26 E+00	7.29 E-01	1.14 E+00

TABLE 4. SELF-ATTENUATION CORRECTION FACTORS FOR FUEL ROD BUNDLE AND COMPARABLY SIZED (U-Zr-O) CERAMIC CORE SEGMENT

Energy (keV)	Fuel Rod Bundle		(U-Zr-O) Segment	
	Transmission	Correction Factor	Transmission	Correction Factor
200	2.11 E-23	4.04 E+01	2.04 E-17	2.98 E+01
400	9.73 E-07	1.09 E+01	2.44 E-05	8.41 E+00
600	5.65 E-04	5.99 E+00	2.60 E-03	4.83 E+00
800	4.81 E-03	4.37 E+00	1.31 E-02	3.63 E+00
1000	1.44 E-02	3.56 E+00	2.99 E-02	3.05 E+00
1200	2.65 E-02	3.13 E+00	4.95 E-02	2.70 E+00
1400	4.23 E-02	2.81 E+00	6.95 E-02	2.48 E+00
1600	5.67 E-02	2.61 E+00	8.81 E-02	2.32 E+00
1800	6.48 E-02	2.52 E+00	1.04 E-01	2.22 E+00
2000	7.44 E-02	2.43 E+00	1.18 E-01	2.14 E+00

TABLE 5. ENERGIES OF THE PREDOMINANT GAMMA RAYS OF THE DETECTED RADIONUCLIDES

Radionuclide	Energy (keV)	Branching Ratio (%)	Intensity Code
^{134}Cs	604.66	97.60	2
	795.76	85.40	1
	1038.50	1.00	2
	1167.90	1.80	2
	1365.13	3.04	3
^{137}Cs	661.65	85.00	1
^{60}Co	1173.21	99.86	2
	1332.46	99.98	1
^{110m}Ag	657.75	94.74	2
	706.67	16.74	2
	763.93	22.36	2
	884.67	72.86	2
	937.48	34.31	1
	1384.27	24.35	2
	1505.00	13.11	2
^{125}Sb	427.89	29.53	1
	463.38	10.48	3
	600.56	17.83	2
	635.90	11.35	3
^{106}Ru	621.80	9.81	3
	1050.10	1.44	2
	1128.00	0.38	1
	2193.28	0.01	2
^{144}Ce	696.50	1.34	2
	1489.20	0.28	2
	2185.70	0.69	1
^{154}Eu	123.14	40.50	2
	723.30	19.70	2
	873.19	11.50	2
	996.32	10.30	2
	1004.76	17.40	2
	1274.45	35.50	1
	1596.48	1.67	3

4. ANALYSIS RESULTS AND DISCUSSION

A discussion of the results of the core bore high-resolution gamma ray spectroscopy measurements that were described in Section 3 is presented in this section. Also included is a summary of the photographic results for comparison with the gamma spectroscopy data. Significant results include the following:

4.1 Photographic Examinations

This section summarizes the results of the examinations of photographs that were taken of the nine core bore samples following their arrival at the INEL (see Appendix B). The physical features that were observed during the examinations of the photographs of the core bores are compared with the previously reported results of CCTV inspections of the core bore holes.[3] These CCTV inspections were performed immediately following the removal of each core bore sample.

A summary of the information obtained from the photographic examinations of the fuel rods contained in the nine core bore samples is listed in Table 6. The maximum lengths of the fuel rods in the nine core bore canisters are itemized, along with the lengths of the standing intact fuel rod stubs that were observed during the video inspections of the core bore holes that, in each case, were done immediately following extraction of the core sample. The lengths of the fuel rods as determined by these two methods are plotted in Figure 7 for comparison. For five of the core bore samples, the lengths of the fuel rods in the core bore canisters were shorter than the observed lengths of the corresponding intact standing fuel rods in the bottom of the reactor vessel. The differences in their lengths range from 5 cm for core bore D-4 to 42 cm for core bore O-7. Two of the core bore samples, G-8 and G-12, contained fuel rods whose maximum lengths were essentially equal to the lengths of the standing fuel rods that were observed using the CCTV.

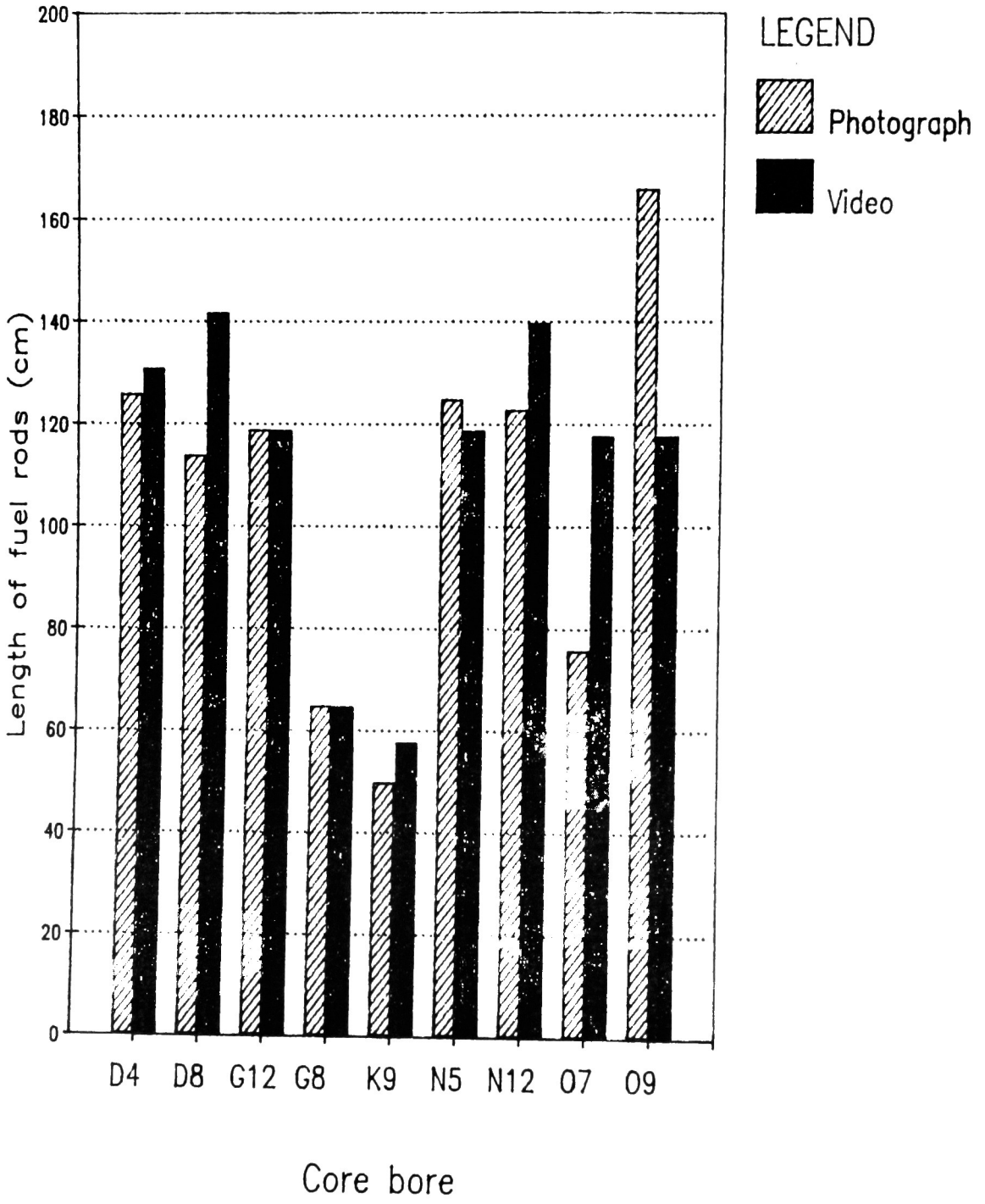

Figure 7. Lengths of fuel rods as determined by photographic and video examinations.

TABLE 6. SUMMARY OF PHOTOGRAPHIC AND VIDEO DATA FOR FUEL RODS

Core Bore Number	Fuel Rod Length (cm) Photograph	Video	Difference (cm)	Damaged Regions[a] of Fuel Rods
K-9	50	58	-8	11 to 38[b]
G-8	65	65	0	0 to 14[b]
D-8	114	142	-28	10 to 20[c], 36 & 61[b]
G-12	119	119	0	23 to 33[b], 61 to 71[b]
N-12	123	140	-17	74 to 86[c], above 74[d]
O-9	166	118	48	71 to 112[d]
O-7	76	118	-42	28 to 46[c], above 61[d]
N-5	125	119	6	None
D-4	126	131	-5	81 to 91[c]

a. Distance from the bottom of the fuel rods in centimeters.

b. Fuel rod cladding is breached.

c. Fuel rods are sheared off.

d. Fuel rods are twisted and otherwise damaged.

On the other hand, core bore samples N-5 and O-9 contained fuel rods that appeared to be longer than the standing fuel rods that were observed at the corresponding locations in the core, the differences in their lengths being 6 cm for core bore N-5 and 48 cm for core bore O-9. The fact that the fuel rod samples that were obtained are often shorter than their observed lengths in the reactor vessel suggests that the upper sections of many of the standing fuel rods were brittle and these sections, or portions thereof, were fragmented and lost during the core drilling. That the lengths of the fuel rods in core bore O-9 are longer than expected is perplexing. Because not all of the bottom ends of the fuel rods are visible in the photograph of the opened O-9 core bore canister, it may be that the bottom ends of some of the fuel rods are actually positioned above the ends that are visible in the photograph.

The locations where the fuel rods in the core bore canisters exhibited obvious damage are also summarized in Table 6. The types of damage include breaches in cladding, rods that are sheared off below the average height of

the rods in the sample, and rods that are twisted or otherwise deformed. Only the fuel rods of core bore sample N-5 showed no indications of damage. Fuel rod cladding in core bore samples K-9, G-8, D-8, and G-12 was breached, the lengths of the breaches ranging from about 1 cm (D-8) to about 27 cm (K-9). As was previously mentioned, it is probable that the breaches were caused by the drill bit during core boring. The upper sections of the fuel rods of core bore samples N-12, O-9, and O-7 were twisted or otherwise deformed.

4.2 Gamma Ray Spectroscopy Measurements

This section presents the results of the high-resolution gamma ray spectroscopy measurements that were performed on the nine core bore samples after their arrival at the INEL. As was previously mentioned in Section 3, each core bore sample was initially gamma-scanned over its entire length to determine gross gamma ray intensity as a function of position along the axial centerline. The resulting gross rate profiles were used to locate the top and bottom ends of the core bore samples and to define regions of interest that should be examined during the subsequent incremental isotopic analyses.

Isotopic gamma ray spectroscopy measurements were performed to determine the quantity and identity of fission products that made up the gross rate profiles. Spectra were obtained at 2.5-cm intervals over the entire length of each core bore sample; however, for some core bores, intervals less than 2.5-cm were used in order to more closely examine regions that exhibited anomalous features, either in the photographic inspections or the gross rate profiles.

However, with the exception of core bore K-9, not all of the spectra that were obtained for each core bore were analyzed. For core bore samples other than K-9, the spectra that were analyzed were those obtained at positions corresponding to significant peaks and valleys in the gamma ray intensity profile and at selected positions throughout the region of the profile that corresponded to the region of the intact fuel rod segments.

4.2.1 Gross Gamma Ray Intensity Profiles

The gross gamma ray intensities produced by the core bore samples plotted as a function of position along the axial centerlines of the nine core bore canisters are shown in Figure 8. In these plots, gamma ray intensity is expressed in units of counts per second (cps) and location is listed in centimeters from the bottom of the fuel stack. The locations of distinct components, such as fuel rod lower plenum springs, fuel stacks, and individual ceramic and agglomerate plug segments, are identified. The location of the large peak (^{60}Co) produced by the Inconel spring in the bottom end of each fuel rod was used to index the beginning of the fuel stack. The lengths of the fuel stacks shown in Figure 8 are based on the lengths of the fuel rods as determined from examinations of the core bore photographs. However, the gross gamma profiles may not agree entirely with the photographic data; because some of the fuel rods did not contain fuel material and, consequently, the gamma scan data did not indicate lengths as long as those observed in the photographs.

Based on the photographic examinations, the lengths of the fuel stacks shown in Figure 8 range from a low of 40.6 cm (core bore K-9) to a high of 157 cm (O-9). Among the the nine core bore samples, K-9, G-8, and O-7 have the shortest fuel stack lengths, with the lengths of the latter two being 55.9 and 67.3 cm, respectively. Core grid locations K-9 and G-8 are near the center of the core, while location O-7 is near the periphery of the core in the southeast quadrant (see Figure 2). The lengths of the fuel stacks of the remaining six core bore samples range from about 105 to 157 cm. The fact that the fuel stack length of core bore sample O-7 is significantly shorter than the fuel stack lengths of core bore samples D-4, N-5, N-12, and O-9, which were also collected from peripheral core grid locations, might be explained in terms of the proximity of grid location O-7 to location R-6. This grid location is thought to be near the pathway by which molten core material relocated into the lower plenum about 224 min after the TMI-2 turbine tripped.[4] Because of its nearness to the relocation pathway, the O-7 fuel assembly could have been subjected to

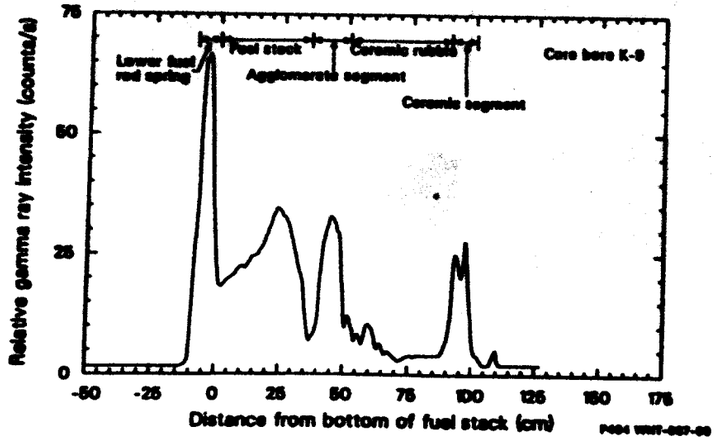

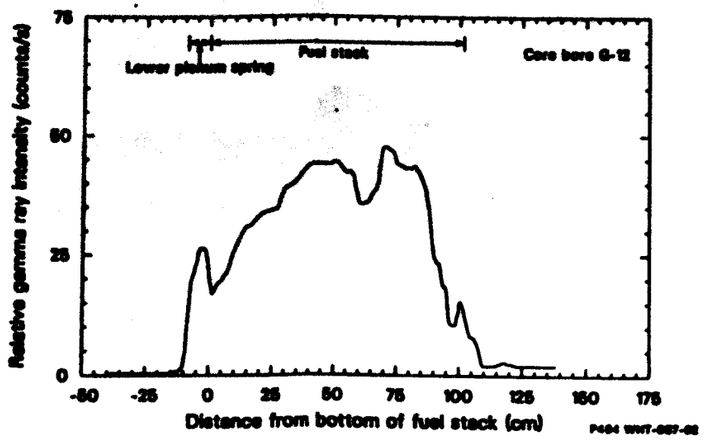

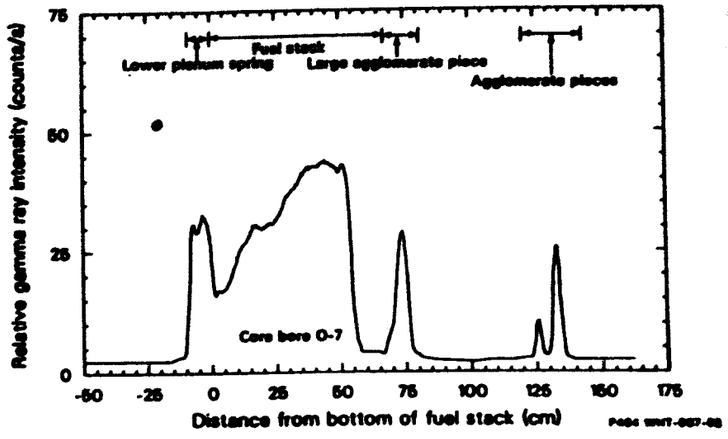

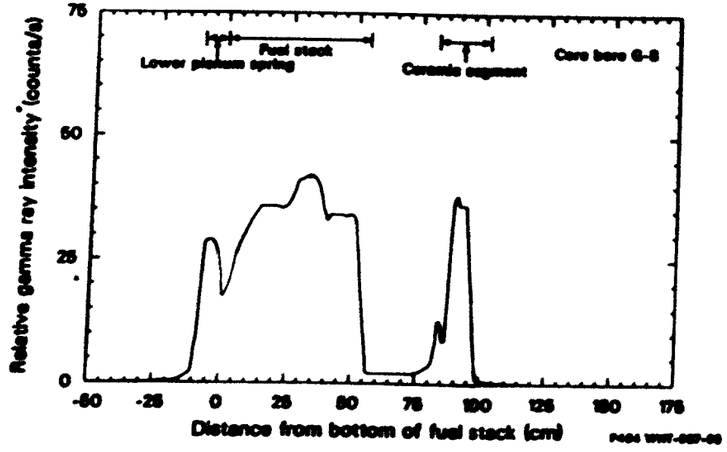

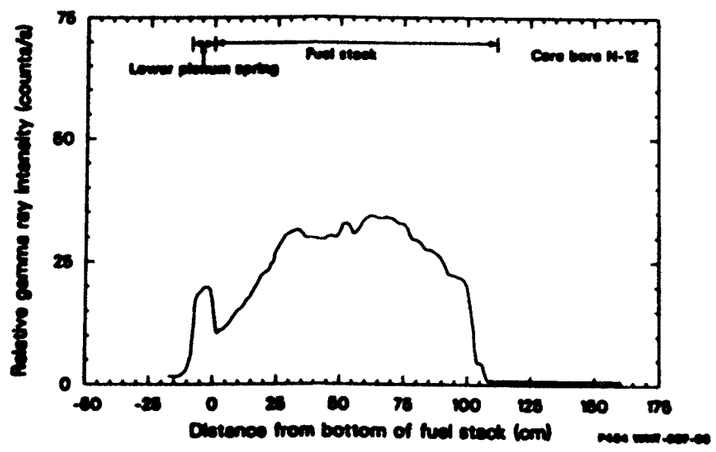

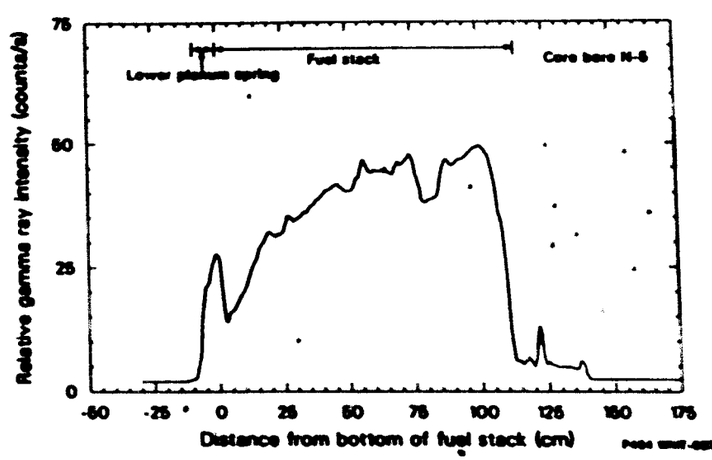

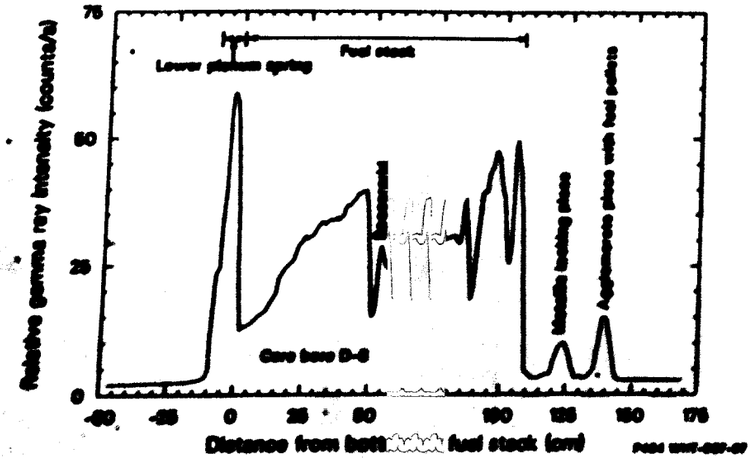

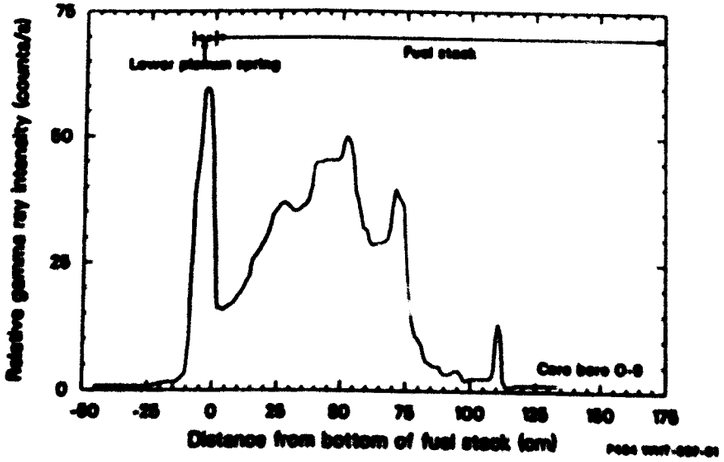

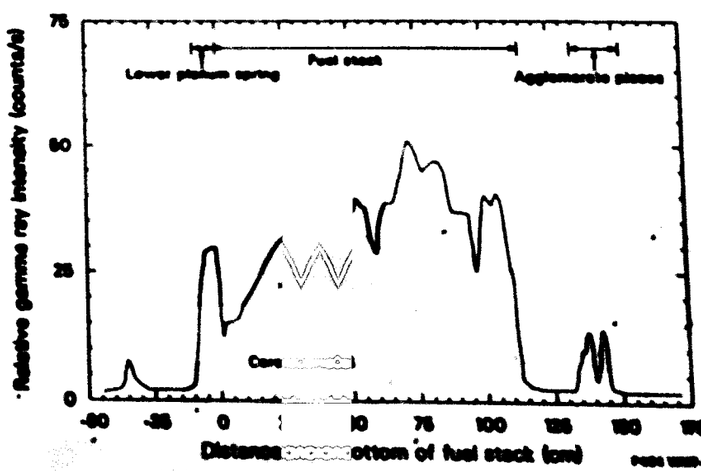

Figure 8. Gamma ray intensity profiles for nine TMI-2 core bore samples.

significant thermal shock and mechanical stress. These forces may have been strong enough to fracture and dislocate the upper sections of the D-7 fuel rod remnants.

The maximum count rates measured at the locations of the fuel rod lower plenum springs ranged from a low of about 20 cps for core bore sample N-12 to a high of about 67 cps for core bore sample K-9. Corresponding count rates for core bore samples D-8 and D-9 are 59 and 60 cps, respectively; while those of the remaining five core bore samples occupy a relatively narrow range between 26 and 33 cps. These variations in activity may be attributed to differences in the production of ^{60}Co by neutron activation and, consequently, differences in the neutron flux and enrichment at these core locations. [A higher enrichment (2.64%) would produce a greater neutron flux than the lower enrichment assemblies.] Also, the presence of control and poison materials would affect the measurable count rates.

The portions of the count rate profiles that correspond to the regions of the fuel rod stacks generally exhibit count rates that increase monotonically with distance from the bottom of the fuel stacks, which shows the increase in burnup closer to the center of the core. The count rate profiles for the fuel stacks are at their maximum near the tops of the fuel stacks. Maximum count rates over the regions of the fuel stacks range from a low of 35 cps for core bore sample K-9 to a high of 51 cps for core bore sample D-4.

The count rate profiles for the fuel stacks of core bore samples D-8 and D-4 exhibit abrupt decreases in count rate that probably correspond to the locations of gaps between fuel pellets. For both of these core bore samples, the first significant decrease in count rate occurs at about the height of the second spacer grid. The heights of the midpoints of the first, second, and third spacer grids, relative to the bottom of the fuel stack, are about -0.013, 0.55, and 1.10 m, respectively.[5] The drill bit penetration rate decreased abruptly when passing through the locations of the spacer grids of the D-8 and D-4 fuel assemblies, and the torque on the

drill bit was temporarily increased to maintain a nominal penetration rate.[3] The above-average mechanical stress at these locations was probably responsible for the apparent voids in the fuel stacks.

The maximum count rates associated with agglomerate core segments are, in general, comparable to those of the corresponding fuel stacks. However, the count rates associated with previously molten core segments and with relatively small individual fragments are significantly lower than the maximum rates recorded for agglomerate core segments. These data suggest that the previously molten regions are significantly depleted in fission product activity as might be expected from previously molten fuel.

4.2.2 Isotopic Activity Profiles

This section presents the results of the isotopic gamma ray spectroscopy examinations. The relative activities, expressed in units of μCi, of ^{134}Cs, ^{137}Cs, ^{110m}Ag, ^{125}Sb, ^{106}Ru, ^{144}Ce, and ^{154}Eu that were measured at positions along the axial centerlines of the nine core bore samples are tabulated in Appendix C, Tables C-1 through C-9. For each position that was scanned, the sum of the activities of these eight radionuclides is also given. Because these data are not corrected for sample self-attenuation, they are not actual measures of the curie content of the core bores. They are, however, indicative of relative changes in activity that can be intercompared. Actual radionuclides concentrations are estimated in Section 4.2.3.

The relative radionuclide activity data tabulated in Tables C-1 through C-9 are presented graphically as discussed in the following subsections. (The ^{134}Cs and ^{110m}Ag data were not plotted, as there are few ^{110m}Ag data points and the ^{134}Cs data follows the ^{137}Cs curves, although at lower concentrations) In these figures, radionuclide activity, expressed in units of μCi, is plotted versus position relative to the bottom of the fuel stack. The distributions of ^{137}Cs along the centerlines of all nine of the core bore samples are shown in Figure 9.

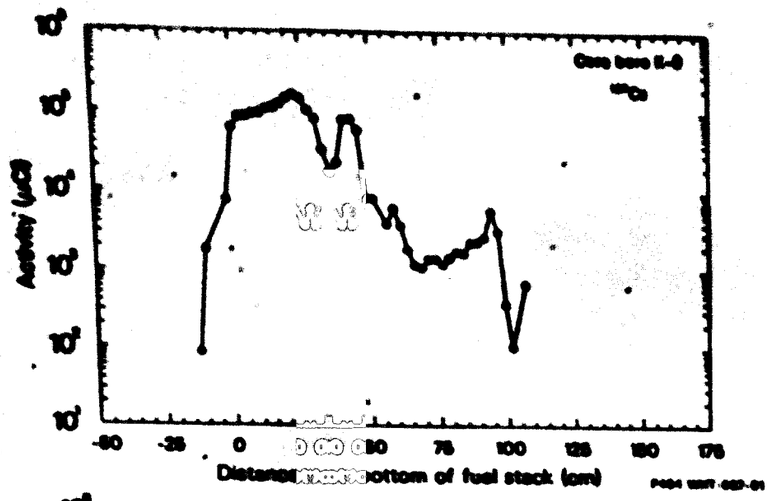

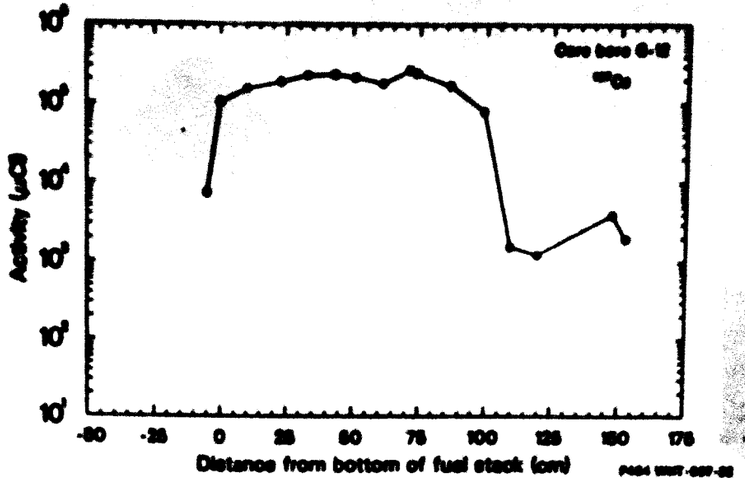

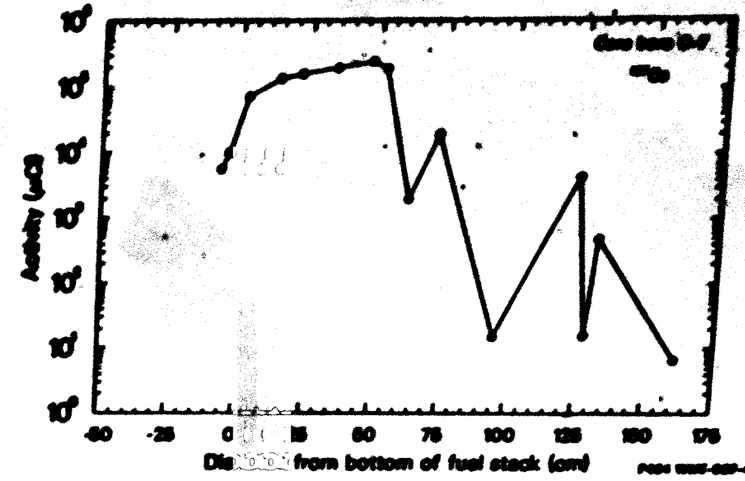

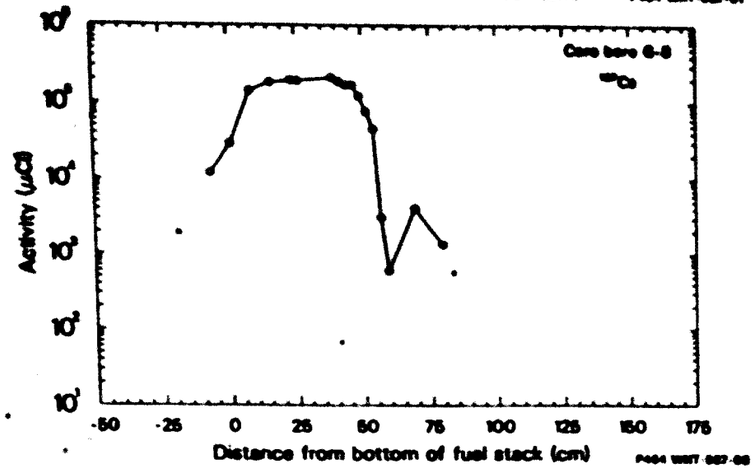

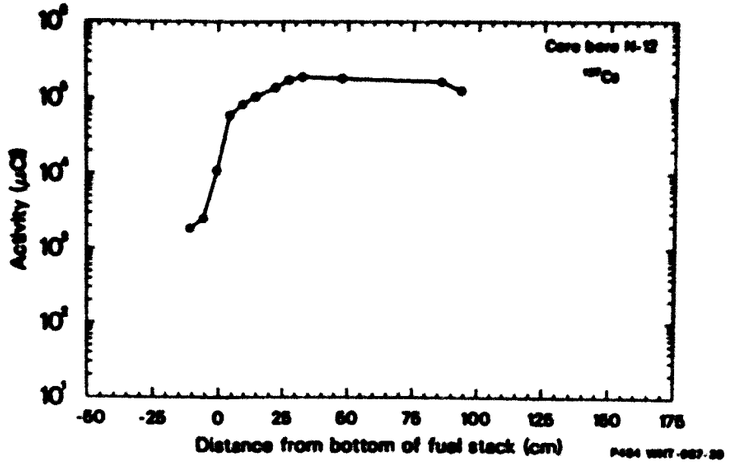

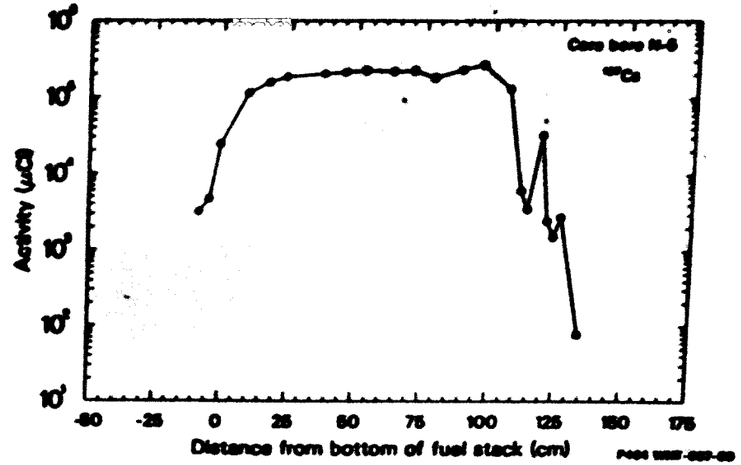

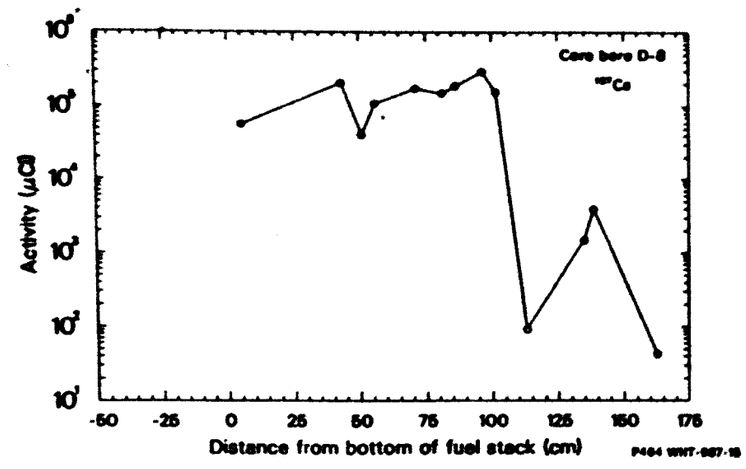

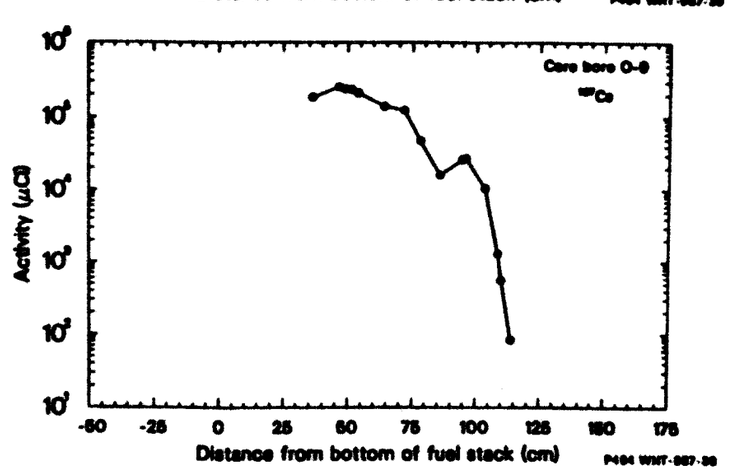

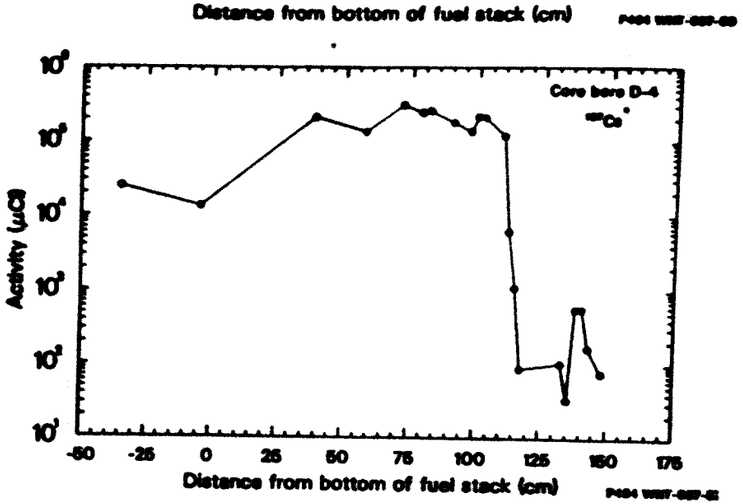

Figure 9. Activity distribution for ^{137}Cs for nine TMI-2 core bore samples.

To interpret the plotted radionuclide data, each core bore was divided into regions where individual isotope concentrations remained relatively constant. These areas have been identified as regions of average activity. A region was considered to be representative if both the ^{137}Cs, and ^{154}Eu (high- and low-volatile fission products, respectively) remained reasonably uniform throughout the region. For example, for core bore N-12, average activities were computed for the region from 0.324 to 0.933 m above the bottom of the fuel stack (i.e., the region of intact fuel rods). Figure 9 indicates that the ^{137}Cs activity of the N-12 fuel stack increases by about a factor of 20 from the bottom of the stack to a height of about 0.30 m; above 0.30 m, the ^{137}Cs activity remains fairly constant.

The activity distribution of ^{154}Eu, shown in Figure 10, is similar to that of ^{137}Cs in that the ^{154}Eu activity profile follows the same pattern as the ^{137}Cs, indicating a similar distribution for both radionuclides as would be expected from intact fuel material. This type of activity profile is common to all core bores in the intact fuel regions.

The determination of average radionuclide activities in incremental cross sections of the core bore fuel rod bundles is complicated by the fact that detection limits for the various radionuclides may cause them to not be detectable at the shorter count times. To increase sensitivity, count times of 600 s were used at some locations to assure that most radionuclides would be measurable. The effect of increasing the count live time is evident in the results for core bore G-12, that are listed in Table C-4. A count live time of 600 s was used at the 0.229-, 0.432-, 0.610-, 0.737-, 0.991-, and 1.194-m scan positions, while a count time of only 100 s was used at the intermediate positions. When a 600-s count time was used, ^{125}Sb, ^{144}Ce, and ^{154}Eu were consistently detected and quantified; but when a 100-s count time was used, they were frequently not detected. Consequently, the approach adopted to compute the average activities entailed using only the real measured values. This approach was used to compute the average activities of ^{134}Cs, ^{137}Cs, ^{60}Co, ^{125}Sb, ^{106}Ru, ^{144}Ce, and ^{154}Eu for the constant activity regions as listed in Table 7.

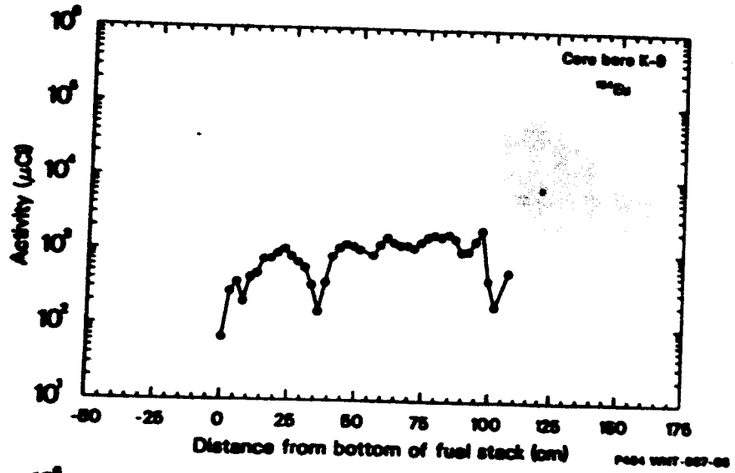

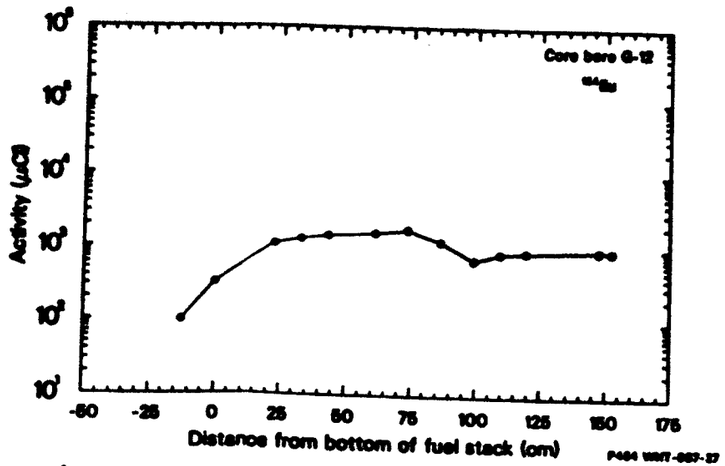

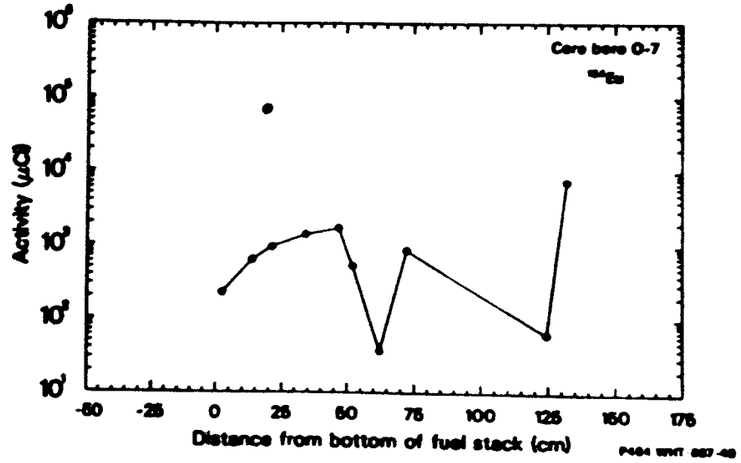

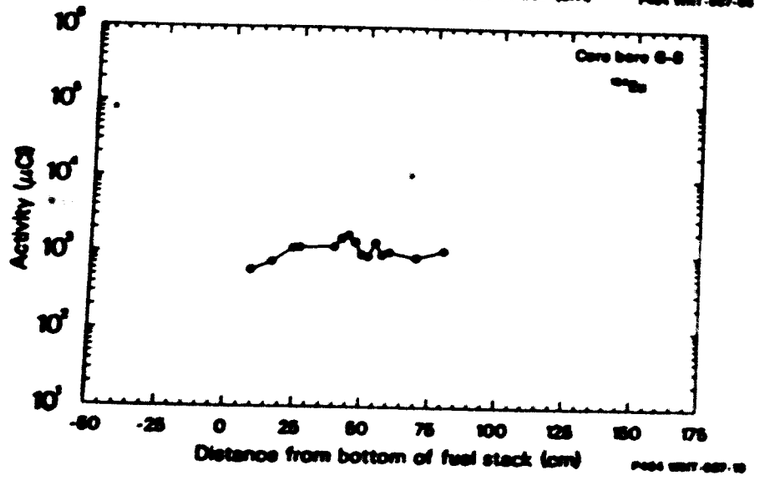

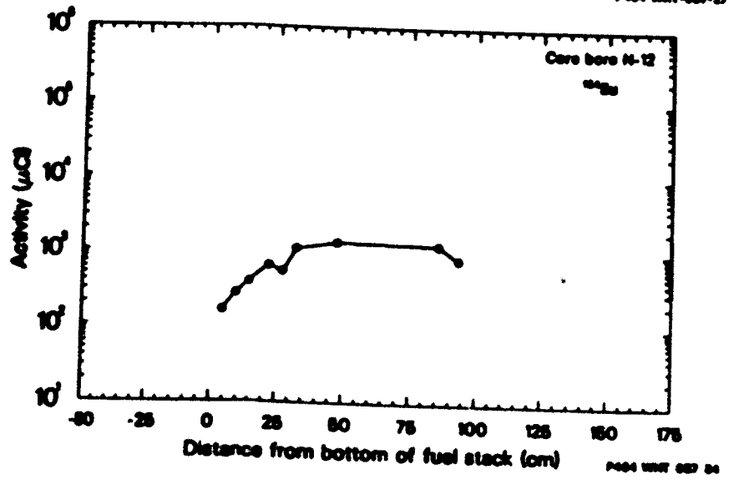

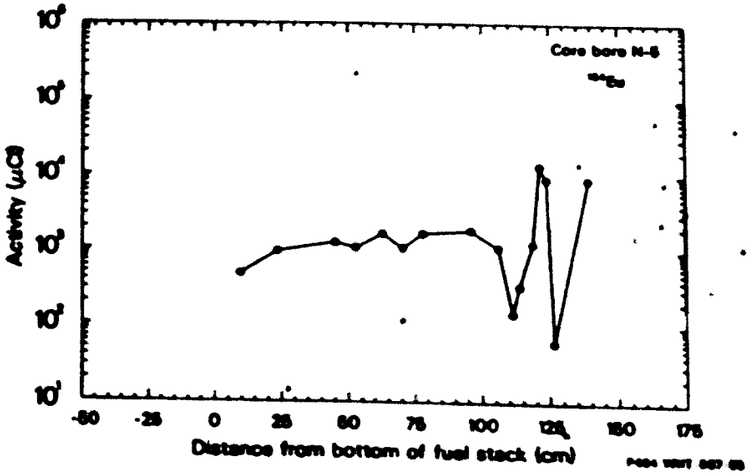

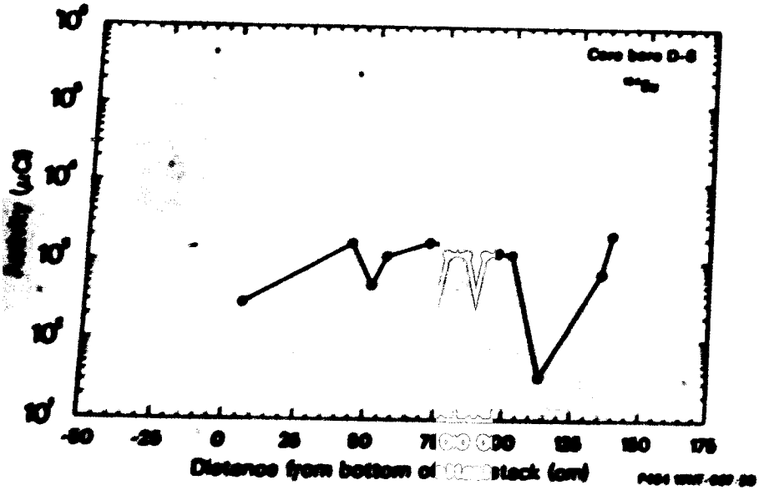

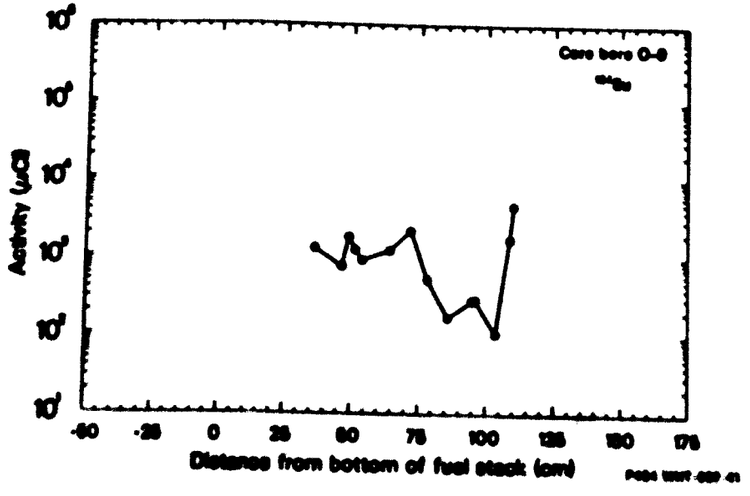

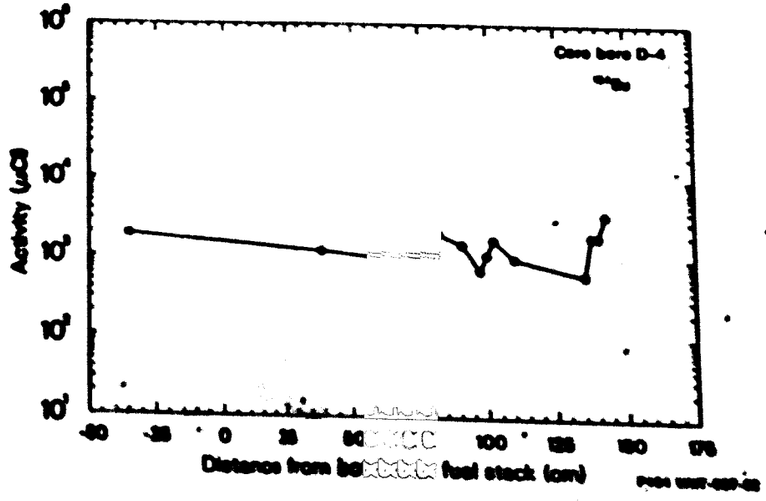

Figure 10. Activity distribution for ^{154}Eu for nine TMI-2 core bore samples.

TABLE 7. AVERAGE UNCORRECTED RADIONUCLIDE ACTIVITIES IN INCREMENTAL CROSS SECTIONS OF FUEL STACKS[a]

Core Bore	Region of Fuel Stack[b]	Average Activity (μCi)							
		^{134}Cs	^{137}Cs	^{60}Co	^{125}Sb	^{106}Ru	^{144}Ce	^{154}Eu	Total
K-9	2.5 to 30.5	2.33 E03	1.12 E05	1.24 E03	1.73 E03	3.61 E03	1.08 E04	6.12 E02	1.32 E05
G-8	8.3 to 48.9	4.38 E03	1.75 E05	1.81 E03	1.60 E03	2.55 E03	1.94 E04	1.18 E03	2.06 E05
D-8	5.1 to 101.6	4.71 E03	1.52 E05	9.07 E02	9.76 E02	7.28 E03	1.72 E04	1.23 E03	1.84 E05
	43.2 to 101.6[c]	5.22 E03	1.64 E05	9.94 E02	9.37 E02	7.28 E03	1.83 E04	1.35 E03	1.98 E05
G-12	10.2 to 86.4	5.30 E03	2.08 E05	2.33 E02	2.21 E03	6.87 E03	1.77 E04	1.37 E03	2.42 E05
N-12	4.4 to 93.3	2.74 E03	1.35 E05	1.42 E02	5.78 E02	5.67 E03	1.88 E04	7.21 E02	1.64 E05
	32.4 to 93.3[c]	4.05 E03	1.64 E05	ND	ND	7.51 E03	2.19 E04	1.13 E03	1.99 E05
O-9	36.2 to 71.8[c]	5.84 E03	1.97 E05	8.74 E03	---[d]	9.29 E03[d]	1.80 E04	1.32 E03	2.40 E05
	36.2 to 113.7	3.49 E03	1.01 E05	5.16 E03	8.48 E03	4.30 E04	8.95 E03	1.21 E03	1.71 E05
O-7	2.5 to 52.1	4.07 E03	1.67 E05	3.37 E03	1.28 E03	7.78 E03	1.89 E04	9.07 E02	2.04 E05
N-5	9.5 to 106.0	4.59 E03	1.96 E05	5.43 E03	1.64 E03	1.43 E04	1.77 E04	1.22 E03	2.41 E05
D-4	38.7 to 109.9	5.65 E03	2.02 E05	4.31 E02	1.14 E03	1.00 E04	2.08 E04	1.46 E03	2.41 E05
	Average[e]:	4.89 E03	1.84 E05	3.00 E03	1.47 E03	8.20 E03	1.91 E04	1.24 E03	2.21 E05
	Std. Dev.:	0.25 E03	0.06 E05	1.18 E03	0.18 E03	1.17 E03	0.05 E04	0.06 E03	0.07 E05

a. Activities are not corrected for sample self-attenuation. Activities are decay-corrected to April 1, 1986.

b. Distance in centimeters from the bottom of the fuel stack.

c. Activities in this region of the fuel stack were used to compute overall average activities.

d. Activity measured at 71.8 cm was ignored.

e. The results for core bore sample K-9 were omitted when the overall average activities were computed. The standard deviation is the one-sigma standard deviation of the average value.

Table 7 also contains the average activities of these seven radionuclides and the associated one-sigma standard deviations. The results for core bore K-9 were omitted when the overall average activities were computed because the K-9 fuel stack was much shorter than the fuel stacks of the majority of the core bore samples and therefore experienced less burnup.

Silver-110m was not included in Table 7 as it was only rarely detected in any of the core bores. For example, over the region of the fuel stack of the K-9 core bore sample, it was detected at only two locations: 0.0 and 0.025 m (see Table C-1). It was probably detected at these locations due to the presence of control rod material (silver), which had been activated to produce ^{110m}Ag in this portion of the core bore. This radionuclide was not detected at any scan positions on core bore samples G-8, G-12, N-12, O-9, or N-5, probably due to the small amount remaining at the time the measurements were performed and the shielding effects of the fuel material in other portions of the core bores.

Among the radionuclides detected in the core bore samples, ^{144}Ce and ^{154}Eu are the most refractory and are expected to have been retained in the fuel with only minor losses due to mechanisms other than radioactive decay. Because they are retained in the fuel, these two radionuclides are used as indicators of the quantity of fuel present and provide a qualitative indication of the retention of other radionuclides as a function of fuel content.

Consequently, to determine the relative retention of some of the more volatile fission products, ratios were calculated to evaluate the retention of several radionuclides in the fuel. The ^{154}Eu data was chosen as the reference, as it was detected more often than the ^{144}Ce. The ratios of ^{137}Cs, ^{106}Ru, and ^{144}Ce to ^{154}Eu activity are listed in Appendix D, Tables D-1 through D-9. Plots of the ^{137}Cs, ^{106}Ru, and ^{144}Ce normalized activity distributions for the nine core bore samples are presented in the following subsections, which discuss the isotopic activity

data and the normalized retention data for the isotopes measured in the intact fuel portions of the core bores. The data are discussed in order from the most to least volatile.

4.2.2.1 Cesium-137. The ^{137}Cs activity profiles shown in Figure 9 indicate that the ^{137}Cs activities remain reasonably constant in the regions of the intact fuel stacks and that the activities are similar in all core bores. The data presented in Table 7 illustrate the similarity of the average ^{137}Cs activity for all core bores. That core bore K-9 exhibits the lowest average ^{137}Cs activity over the region of the fuel stack is probably due to the fact that the fuel rods present in the K-9 core bore are substantially shorter than the fuel rods of the other eight core bore samples and consequently experienced a lower average burnup than the longer rod sections. For core bore O-9, the gamma scan data indicate a large decrease in activity between about 62 and 103 cm. This dramatic decrease in ^{137}Cs activity suggests that fuel pellets were lost from the upper regions of the fuel rod remnants, which is likely because the photographs indicate that the fuel rods in core bore sample O-9 were twisted and severely damaged. Ignoring activities for positions higher than 72 cm, the average ^{137}Cs activity over the region of the O-9 fuel stack falls within the range measured for the remaining core bores.

Also shown in Figure 9 are the ^{137}Cs activity distributions in the previously molten regions of the core bores. The activity distributions indicate that the inventories of ^{137}Cs in the large-diameter (U-Zr-O) ceramic core segments are substantially less than the inventories of ^{137}Cs in the corresponding fuel stacks. The visual examinations indicated the presence of large-diameter ceramic core segments in core bore samples K-9 and G-12 at distances of about 91 and 147 cm from the bottoms of the fuel stacks. The maximum ^{137}Cs activities that were measured for these ceramic core segments are 0.006 and 0.004 Ci, respectively; while the average activities measured for the corresponding fuel stacks are 0.11 and 0.21 Ci. The maximum ^{137}Cs activities of the ceramic segments correspond to only 5.4% and 1.9% of the average ^{137}Cs activities measured for the respective fuel stacks. As the gamma ray self-attenuation correction

factors for large ceramic segments and fuel rod bundles are similar (within 20%), the data indicate significant depletion of ^{137}Cs in the ceramic core segments.

Three core bore samples (K-9, O-7, and D-8) contained large agglomerate core segments at distances of about 43, 72, and 138 cm from the bottoms of their fuel stacks. The maximum ^{137}Cs activities measured for these three core segments were 0.08, 0.02, and 0.004 Ci, respectively. For the K-9 agglomerate segment, the activity is comparable to the K-9 fuel rod bundle, which indicates that the agglomerate sections are depleted in ^{137}Cs content. Also, several of the core bore samples contained ceramic nd/or agglomerate fragments (i.e., pieces much smaller than the diameter of the core bores) with low ^{137}Cs activity, suggesting that these sample fractions are depleted in ^{137}Cs content. The maximum ^{137}Cs activity of these fragments ranges from a low of 0.002 Ci for ceramic fragments in core bore K-9 to a high of 0.03 Ci for the agglomerate fragments in core bore N-5.

Based on ORIGEN2 calculations[1], as of April 1, 1986, the ratio of the core inventory of ^{137}Cs to that of ^{154}Eu was about 134. For each position that was scanned, the ratio of the activity of ^{137}Cs to that of ^{154}Eu was computed. The results for the nine core bore samples are plotted in Figure 11. The graphs in Figure 11 show that the $^{137}Cs/^{154}Eu$ ratio is reasonably constant for the majority of the core bore samples over most of the length of the fuel stack. For several of the core bores (K-9, N-12, and O-7 in particular), the value of the ratio decreases by about a factor of two between the bottom of the fuel stack and a height of about 30 cm. If only those regions of the fuel stacks where the $^{137}Cs/^{154}Eu$ activity ratio remains reasonably constant are considered (i.e., typically regions above 30 cm from the bottoms of the fuel stacks), the average values of the ratio for the individual fuel stacks are approximately equal. They range from a low of 121 for core bore D-8 to a high of 163 for core bore N-5. Similar average values for the remaining seven core bore samples are: K-9, 156; O-7, 150; G-12, 147; N-12, 147; D-4, 145; O-9, 142; and G-8, 139. The mean value and standard

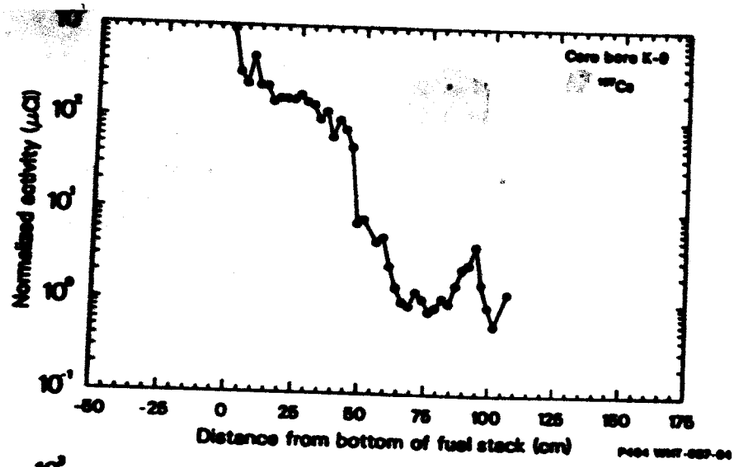

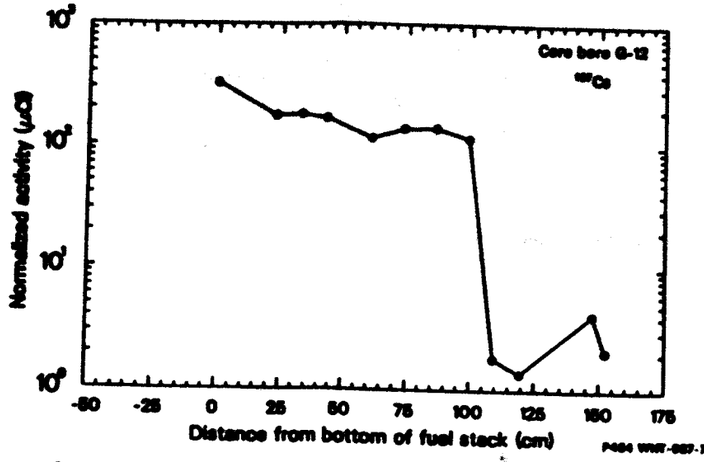

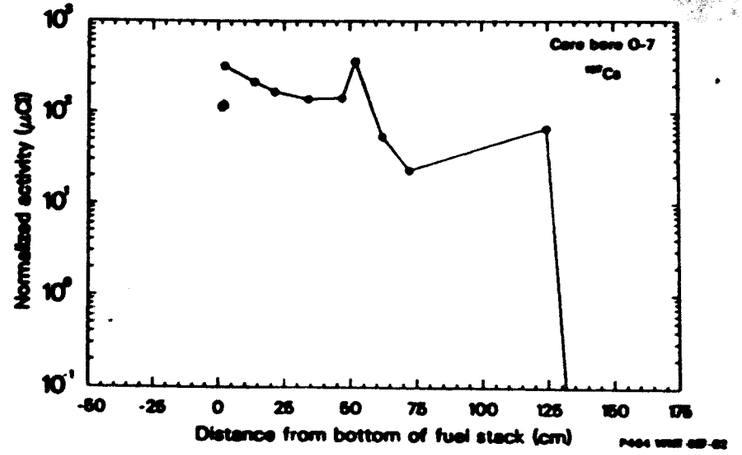

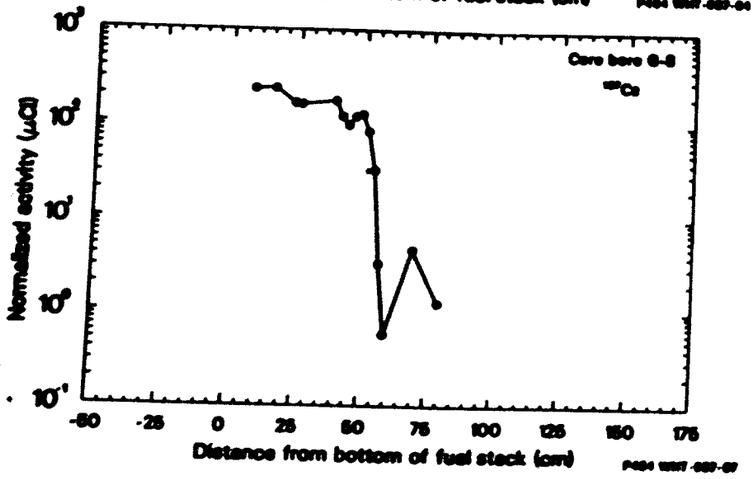

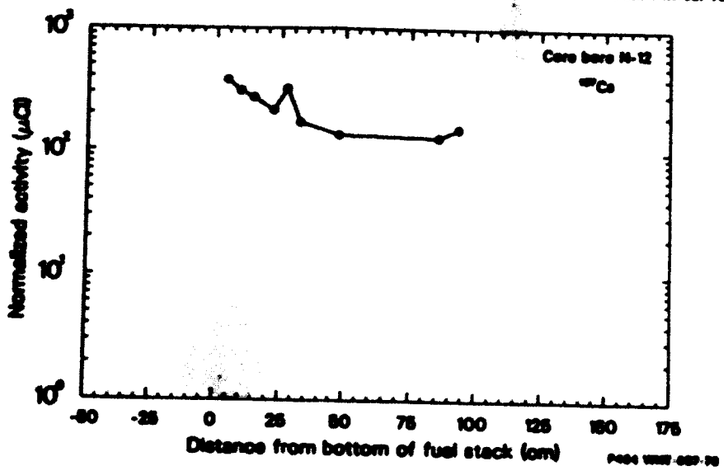

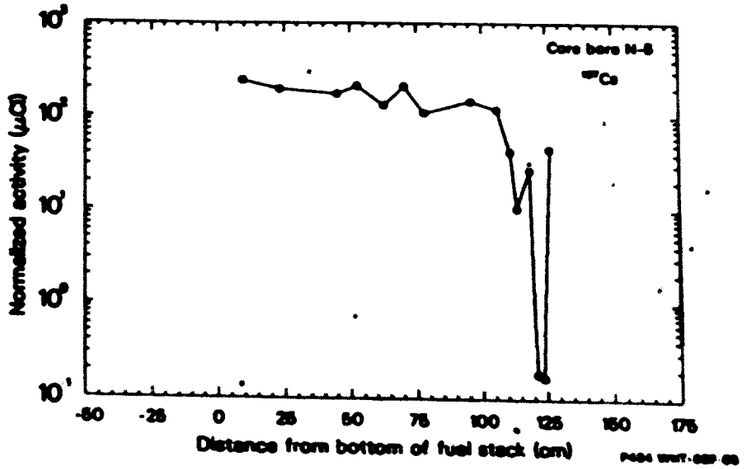

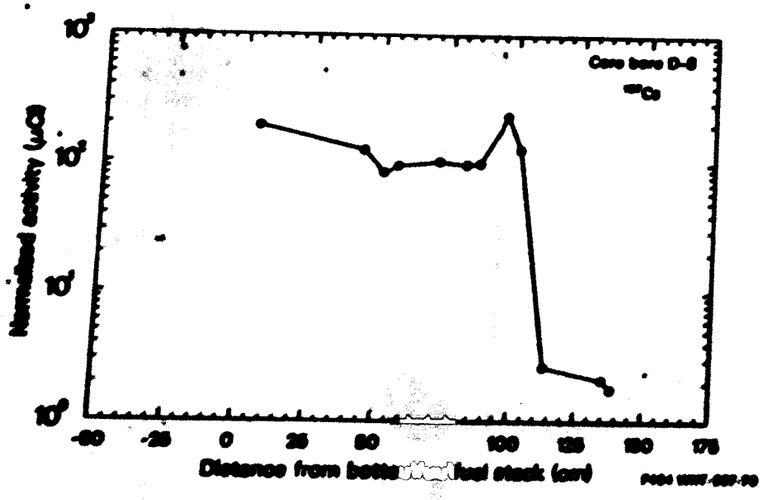

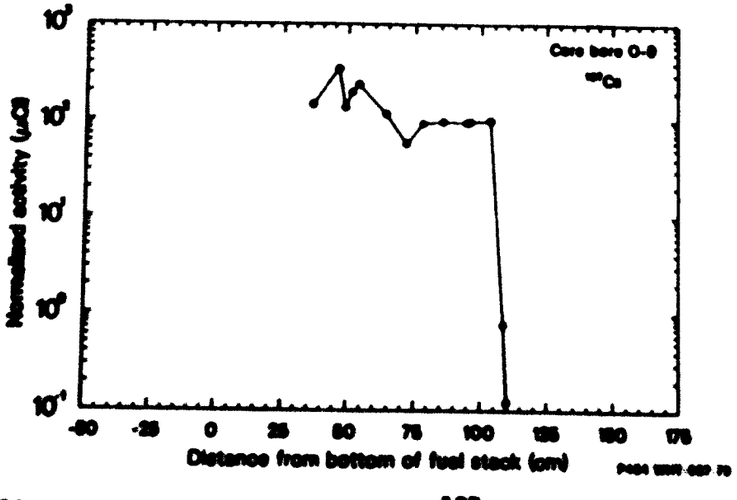

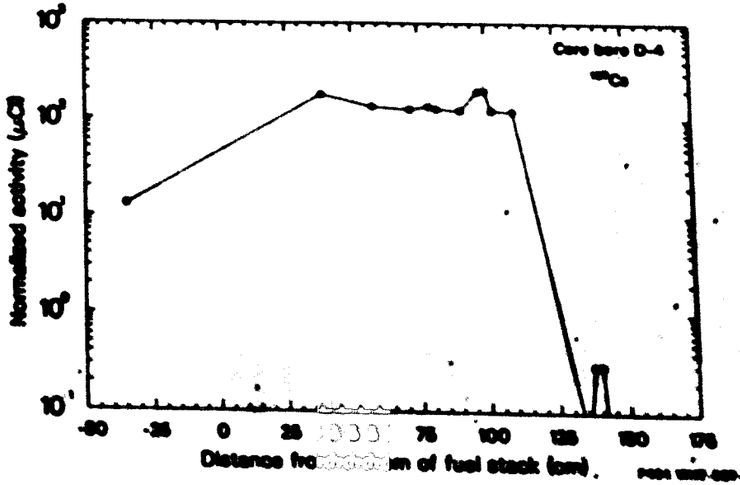

Figure 11. Normalized activity distribution for ^{137}Cs for nine TMI-2 core bore samples.

deviation of the average ratio for all nine fuel stacks is 146 ± 3%. The ratio suggests that the inventory data for ^{154}Eu is higher than would be expected based on the measurement data.

The values of the $^{137}Cs/^{154}Eu$ ratio for the large-diameter (U-Zr-O) ceramic core segments in core bores K-9 and G-12 are 4.1 and 4.2, respectively, while the average values of the ratio for the upper regions of the corresponding fuel stacks are 156 and 147, respectively. Based on the assumption that the ^{154}Eu activity measured at a given location is proportional to the quantity of fuel at that location, these data indicate that the quantity of ^{137}Cs that is associated with fuel in the ceramic core segments is less than 3% of that associated with the fuel in the upper regions of the fuel stacks. In other words, even if all of the ^{137}Cs in the ceramic segments are considered to be associated with fuel, these results indicate that at least 97% of the original inventory of ^{137}Cs in the fuel that combined with zirconium to form a ceramic was lost from the ceramic.

4.2.2.2 Cobalt-60. ^{60}Co is a relatively non-volatile radionuclide that is produced by neutron activation of natural ^{59}Co present in the structural steel. The ^{60}Co activity profiles of the nine core bore samples are shown in Figure 12. The locations of the fuel rod lower plenum springs, which are made of 304 stainless steel are indicated by the large peaks on the left side of the plots. Other peaks in the intact fuel region indicate the location of fuel rod spacer grids. As originally installed in the fuel assemblies, each spacer grid consisted of thirty-two 0.22-m long by 0.033-m high by 0.0005-m thick strips of Inconel-718.

Excluding core bore N-12, average ^{60}Co activities over the regions of the core bore fuel stacks range from a low of about 0.0002 Ci for core bore G-12 to a high of 0.009 Ci for core bore O-9. In the case of core bore N-12, ^{60}Co was detected at only three scan locations on the fuel stack, all of which were within about 22 cm of the bottom of the fuel stack. The average ^{60}Co activity for the N-12 fuel stack is about 0.0001 Ci. Core bore samples G-8, G-12, and N-5 were extracted from

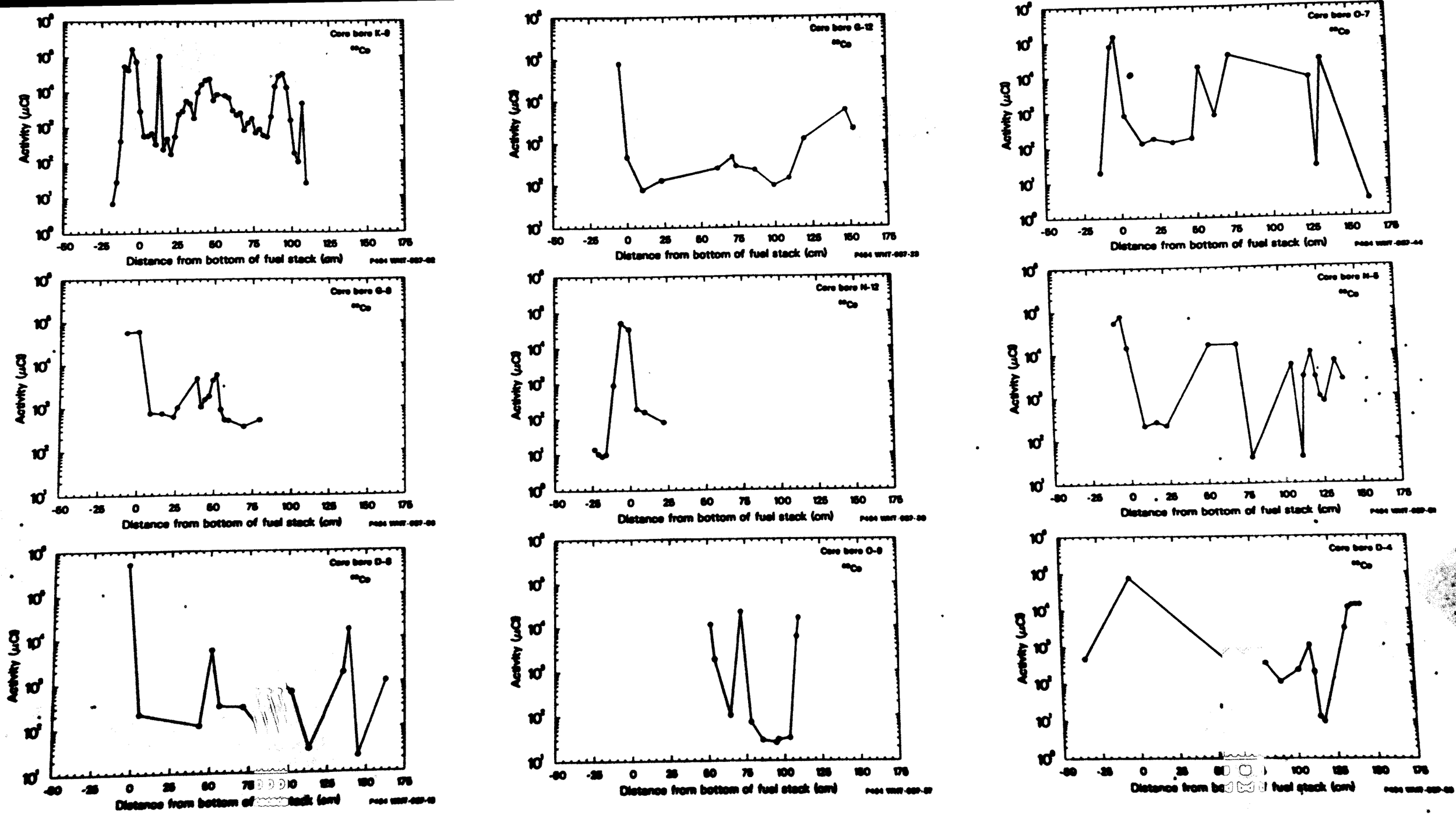

Figure 12. Activity distribution for ^{60}Co for nine TMI-2 core bore samples.

burnable poison fuel assemblies, while the remaining six core bore samples were removed from control rod fuel assemblies. Burnable poison rods are clad in zircaloy-4, while control rods are clad in 304 stainless steel. The fact that the ^{60}Co activity levels over the regions of the fuel stacks are not significantly different for the two types of fuel assemblies suggests that the neutron flux is similar at the spacer grid locations on both types of assemblies as might be expected.

The ^{60}Co activities measured for ceramic and agglomerate materials are generally significantly higher than the activity levels of the core bore fuel rod bundles, which suggests the presence of significant amounts of structural material in the plug regions. In the case of core bore K-9, the good symmetry of the ^{60}Co peak at 91 cm suggests that ^{60}Co is homogeneously distributed in this 7-cm-long ceramic segment.

4.2.2.3 Antimony-125. Antimony-125 is both a fission product and an activation product with several relatively volatile oxide forms. However, the energy required for oxidation is significant, which suggests that this fission product probably remained in a metallic form during the accident. The ^{125}Sb activity distributions presented in Figure 13 and the data listed in Table 7 indicate that ^{125}Sb was frequently not detected during the core bore scans. This is somewhat expected, as the principal gamma ray emission lines for this radionuclide are relatively low in energy and are significantly attenuated by the fuel material present in the core bores.

Excluding core bore N-12, the ^{125}Sb average activities in the fuel stacks range from a low of about 0.0009 Ci for core bore D-8 to a high of about 0.002 Ci for core bore G-12. The ^{125}Sb activity profile of core bore N-5 exhibits a sharp peak at 0.053-m above the bottom of the fuel stack, which corresponds to the location of a broad ^{60}Co peak that is evident in Figure 12. These data suggest that there are accumulations of ^{125}Sb associated with structural materials, as indicated by the ^{60}Co concentrations.

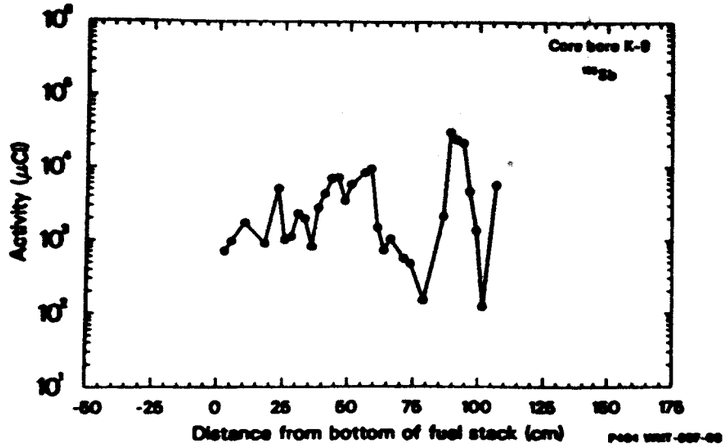

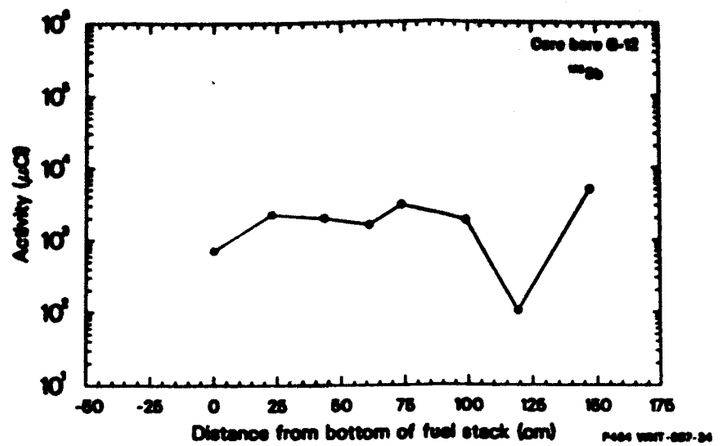

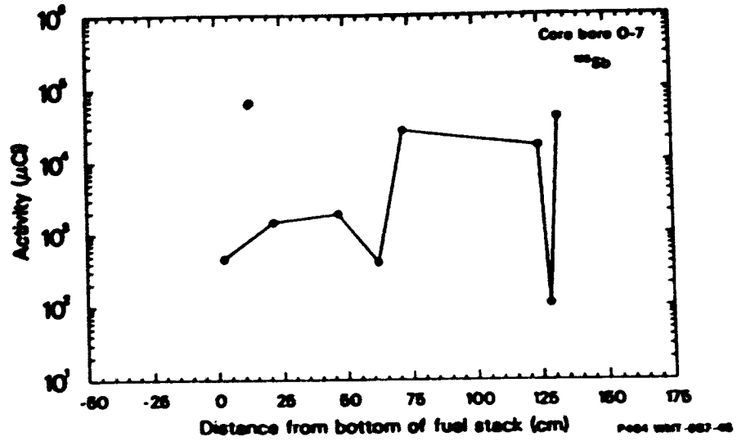

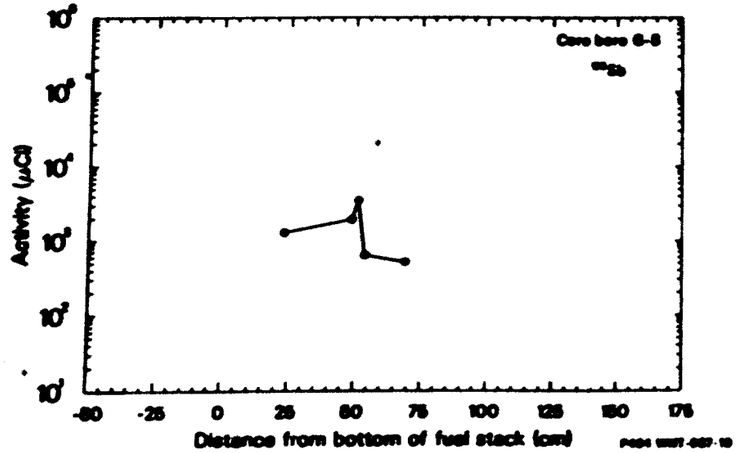

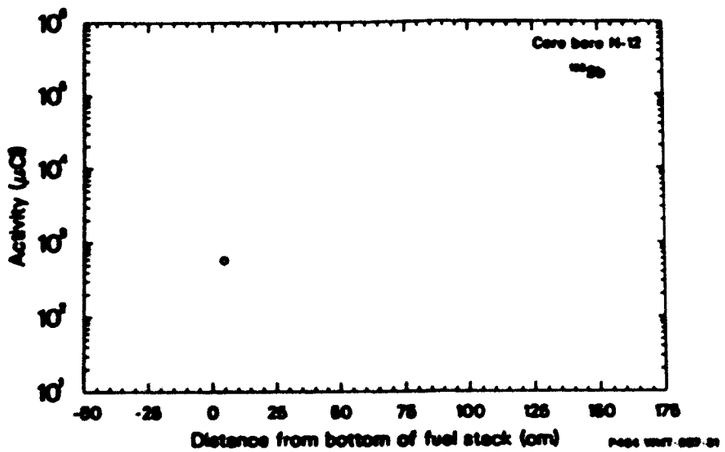

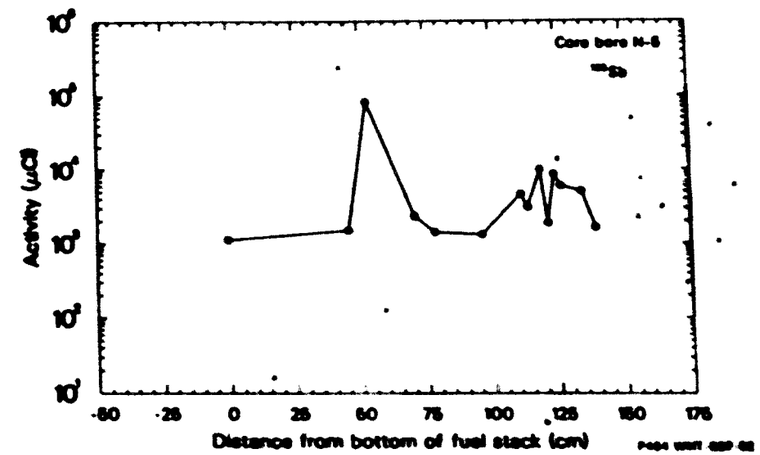

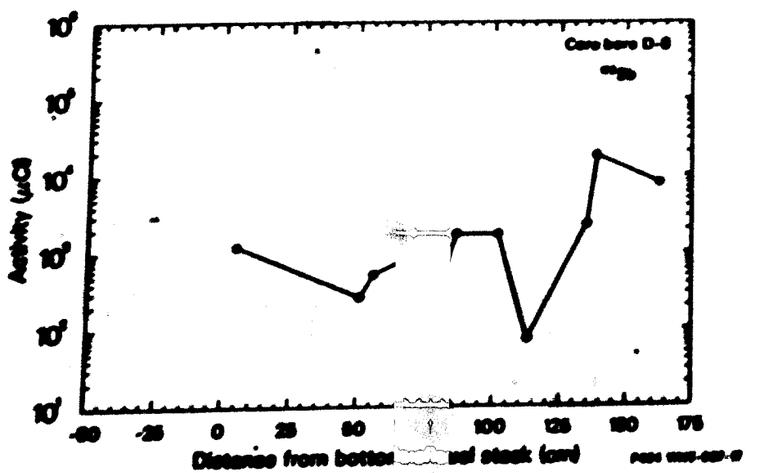

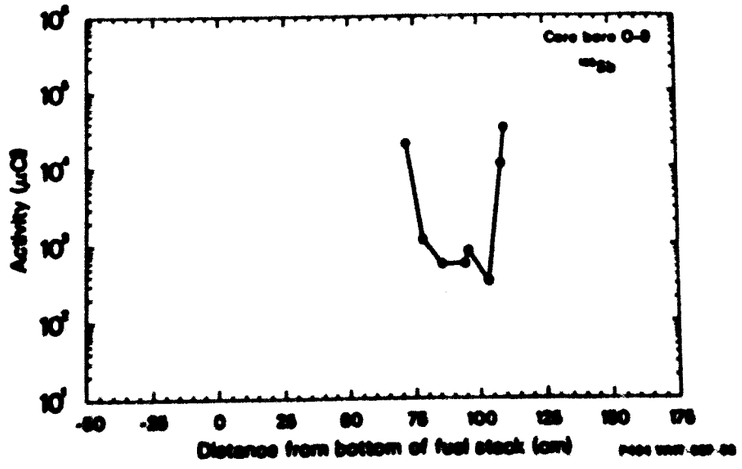

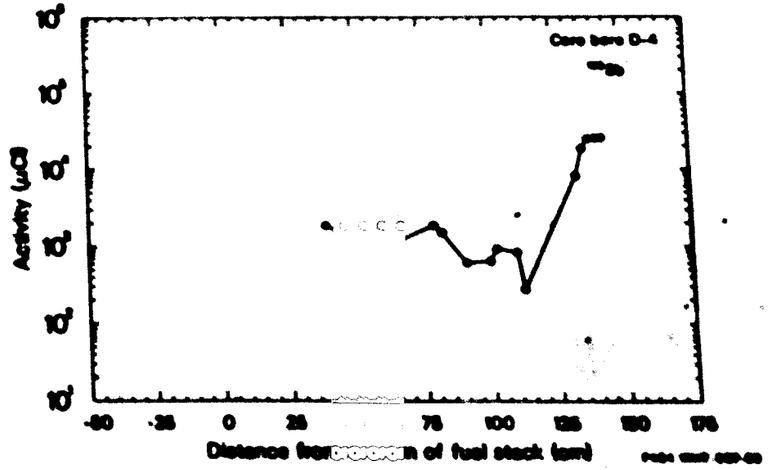

Figure 13. Activity distribution for ^{125}Sb for nine TMI-2 core bore samples.

As was the case with ^{60}Co activities, the ^{125}Sb activities measured for ceramic and agglomerate materials are generally an order of magnitude or more higher than the ^{125}Sb activities of the fuel rod bundles, suggesting accumulations of this isotope in the plug regions. The ^{125}Sb activity profile for core bore K-9 exhibits a broad, fairly symmetrical peak centered at the location of the large ceramic segment. The maximum activity of this peak is 0.03 Ci, which is about a factor of four higher than the maximum ^{125}Sb activity of the agglomerate core segment peak at 0.43 m and about a factor of 17 higher than the average ^{125}Sb activity of the K-9 fuel stack. These data suggest accumulations of ^{125}Sb, with higher concentrations in the upper ceramic region and lower concentrations in the lower agglomerated region.

The maximum ^{125}Sb activity in core bore G-12 was for the ceramic segment (0.005 Ci), while the average activity measured for the fuel stack was about 0.002 Ci. The pronounced ^{125}Sb activity peak that is located about 1.43 m above the bottom of the D-4 fuel stack reaches a maximum activity of 0.03 Ci. The location of this latter peak corresponds to the position of agglomerate fragments in the D-4 canister, which indicates accumulations of activity at these locations.

The maximum ^{125}Sb activities of the agglomerate materials in core bores O-7 and N-5 are 0.04 and 0.009 Ci, respectively which indicate activity accumulations in O-7 but not N-5.

4.2.2.4 Ruthenium-106. Ruthenium, which is a noble metal, is expected to be relatively nonvolatile in its elemental form and requires significant amounts of energy to form the relatively volatile oxide forms. The ^{106}Ru activity profiles presented in Figure 14 are similar to those of the ^{125}Sb. In the intact fuel sections, with the exception of O-9, the average ^{106}Ru activities over the regions of the fuel stacks range from a low of about 0.003 Ci for core bore G-8 to a high of about 0.01 Ci for core bore N-5. In core bore O-9, however, the highest ^{106}Ru activity for the fuel stacks was measured at 1.10 m above the bottom of the stack(0.15 Ci). These data suggest a significant accumulation of structural materials and ^{106}Ru activity at this core location.

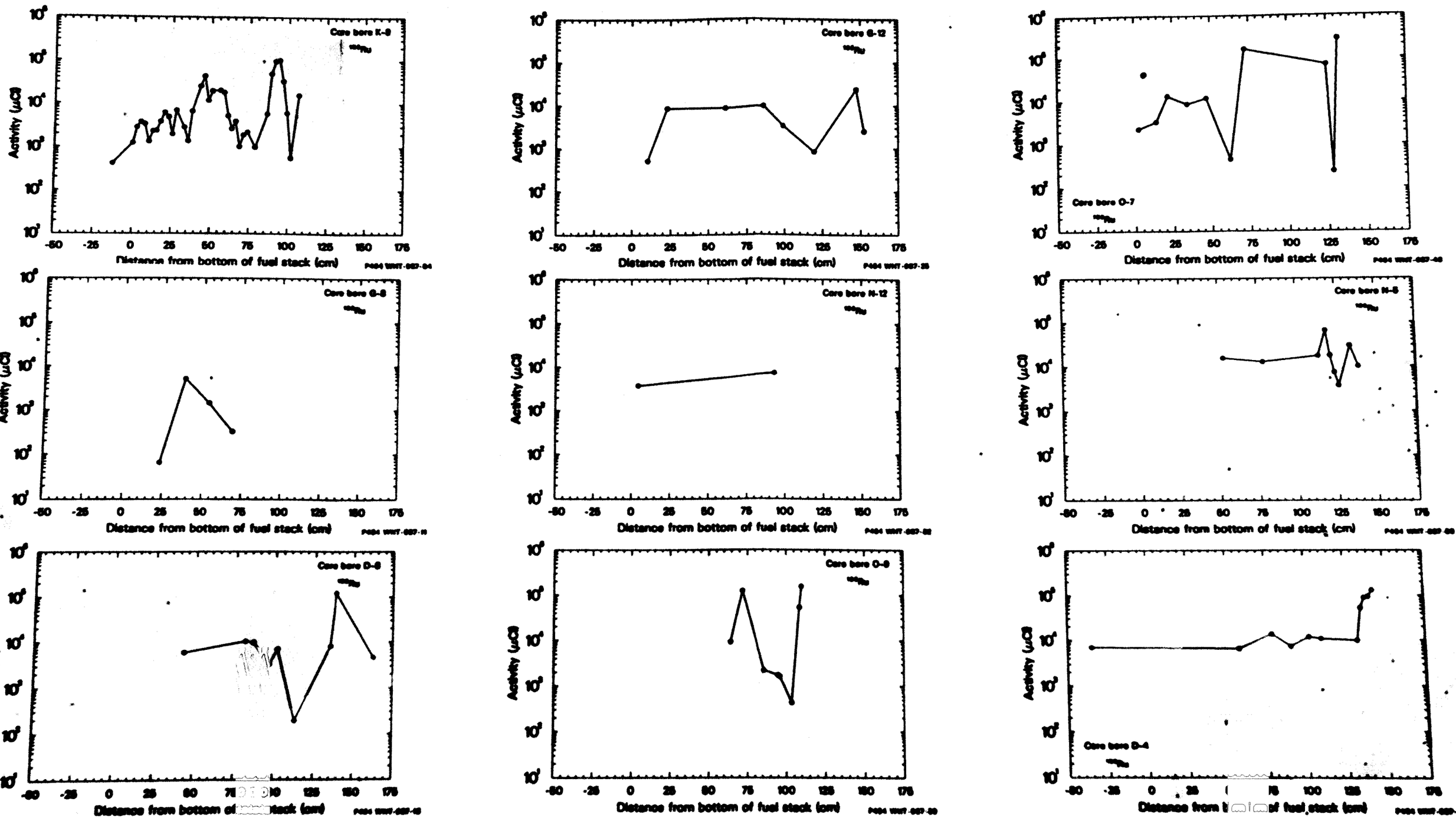

Figure 14. Activity distribution for ^{106}Ru for nine TMI-2 core bore samples.

As was the case with ^{60}Co and ^{125}Sb, the ^{106}Ru activities of the ceramic and agglomerate materials are generally significantly higher than the ^{106}Ru activities measured for the fuel stacks. As was previously mentioned, large ceramic core segments were present in core bore samples K-9 and G-12 at respective distances of 0.91 and 1.47 m from the bottoms of their fuel stacks. The maximum ^{106}Ru activities that were measured at these locations are 0.10 and 0.02 Ci, respectively, while the average ^{106}Ru activities measured for the corresponding fuel stacks are about 0.004 and 0.007 Ci, respectively. These data suggest a high ^{106}Ru concentration in the upper crust layer.

The maximum ^{106}Ru activities of the K-9 and G-12 fuel stacks correspond, respectively, to only about 7% and 40% of the maximum ^{106}Ru activities measured for their respective ceramic core segments. These data suggest that the concentrations of ^{106}Ru in the ceramic materials are as much as an order of magnitude higher than the concentration of ^{106}Ru in the fuel bundles. In the case of core bore sample K-9, the good symmetry of the ^{106}Ru peak at 0.94 m indicates that the ^{106}Ru is uniformly distributed within the 7-cm-long ceramic core segment. As was previously mentioned, three core bore samples, K-9, D-8, and D-7, contained large agglomerate pieces. The maximum ^{106}Ru activities that were measured for these three agglomerate core segments are 0.04, 0.12, and 0.16 Ci, respectively. The maximum ^{106}Ru activities that were measured for the agglomerate fragments in core bores N-5 and D-4 have similar values, the activities being 0.06 and 0.13 Ci, respectively. The agglomerate core segments and fragments, like the ceramic core segments, have ^{106}Ru activities that are significantly higher than the ^{106}Ru activities of the fuel bundles.

Based on ORIGEN2 calculations[1], as of April 1, 1986, the ratio of the core inventory of ^{106}Ru to that of ^{154}Eu was about 5.1. For each position scanned, the ratio of the activity of ^{106}Ru to that of ^{154}Eu was computed. The results for the nine core bore samples are presented in Tables D-1 through D-9 and are plotted in Figure 15. The graphs in Figure 15 show that, for the majority of the core bores, the

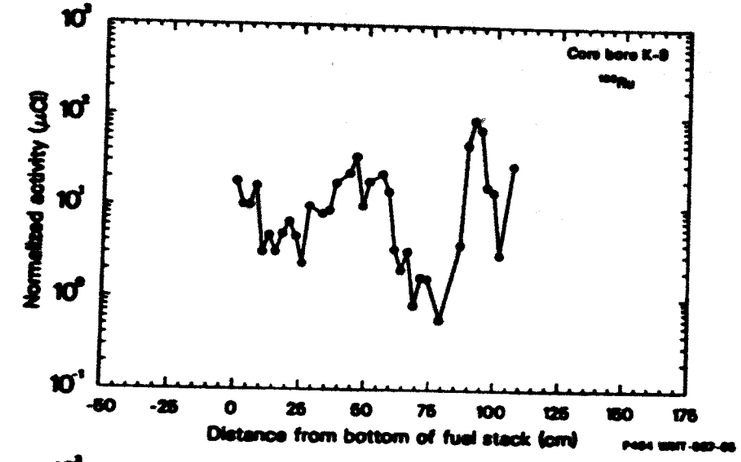

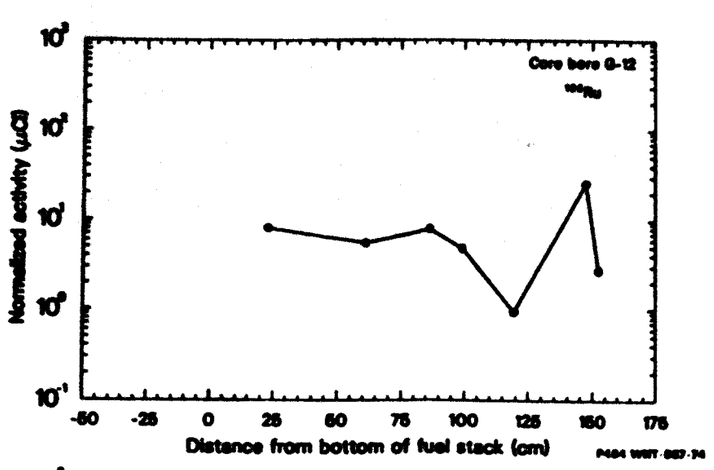

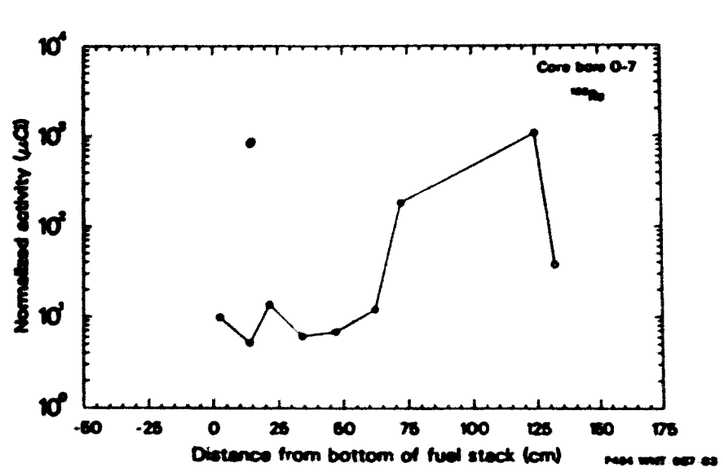

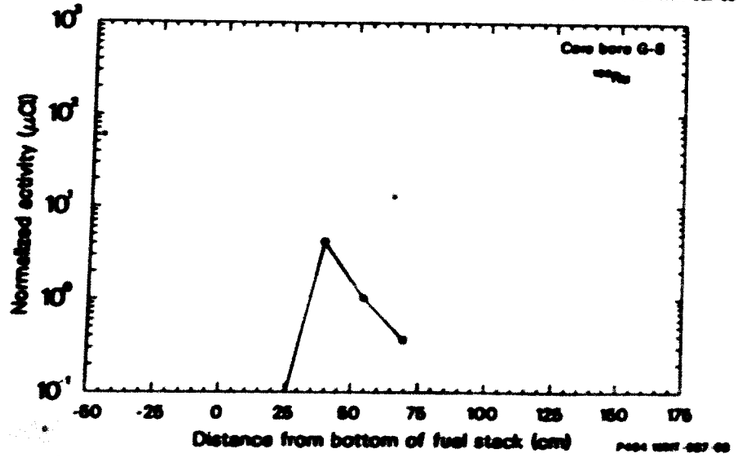

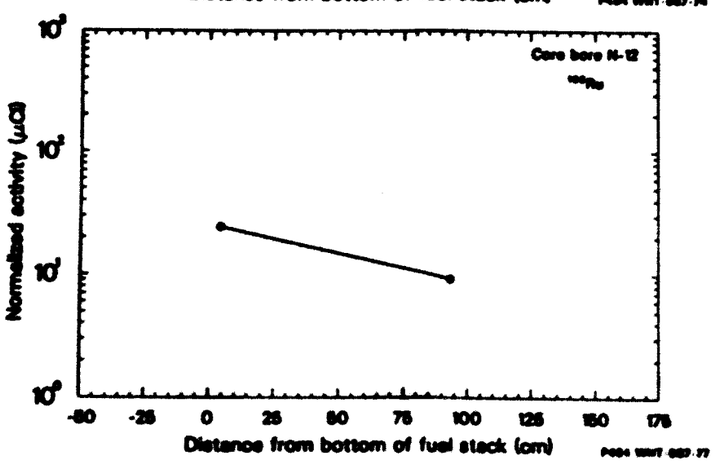

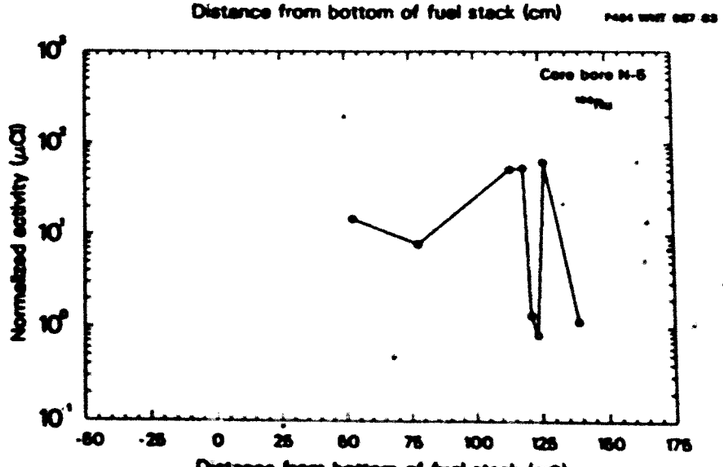

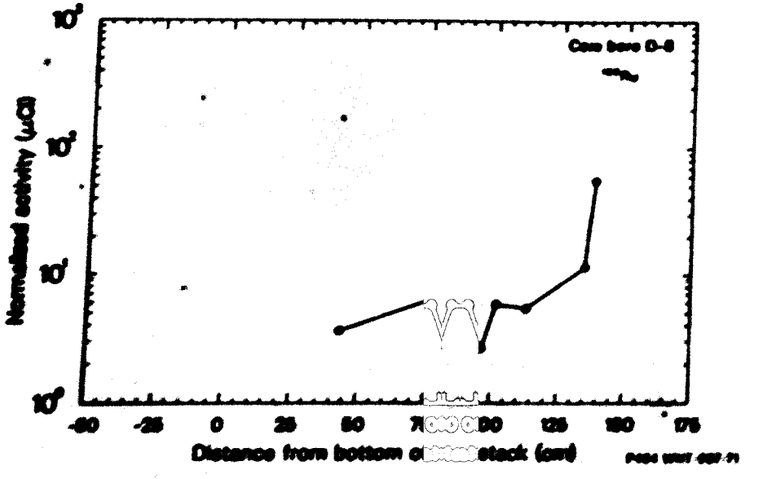

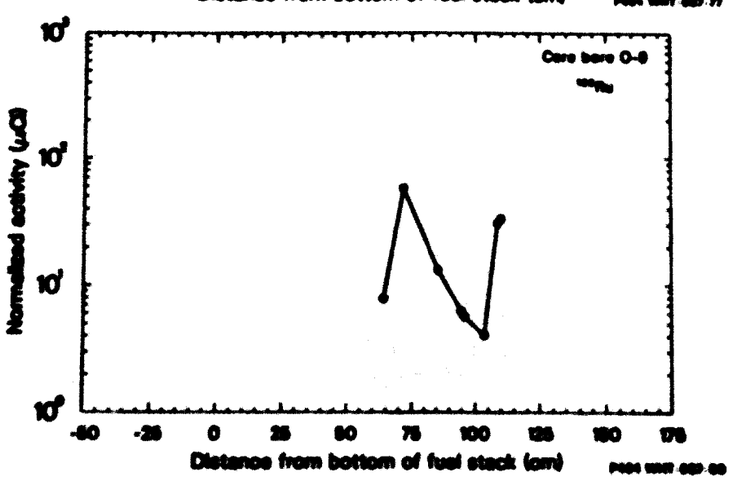

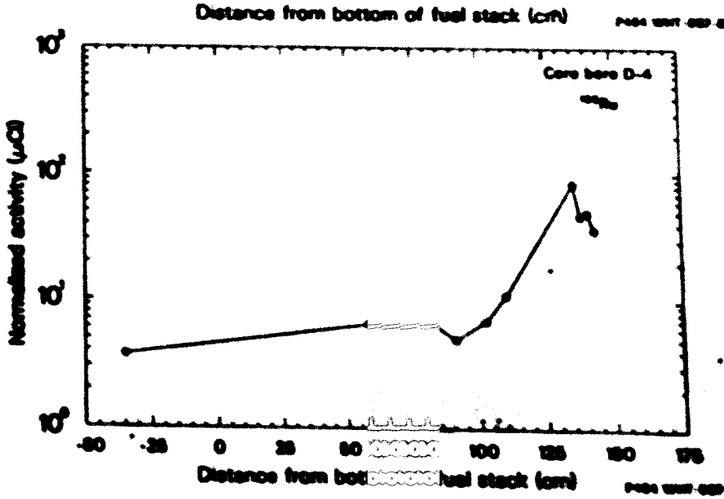

Figure 15. Normalized activity distribution for ^{106}Ru for nine TMI-2 core bore samples.

$^{106}Ru/^{154}Eu$ activity ratios over the regions of the fuel stacks are reasonably constant. The average values of the ratio over the upper regions of the fuel stacks (i.e., the same regions used to compute the average $^{137}Cs/^{154}Eu$ ratios) range from a low of 2.1 for core bore G-8 to a high of 15.7 for core bore N-5. Similar average values for the remaining seven core bore samples are: N-5, 11.3; N-12, 9.2; O-7, 8.9; D-4, 7.3; G-12, 6.6; K-9, 5.3; and D-8, 4.8. The mean value and standard deviation of the mean value of the ratio for all nine fuel stacks is 8 ± 17%. Because the signature gamma rays of ^{106}Ru have about the same energies as the primary gamma rays of ^{154}Eu, one would expect the average values of the $^{106}Ru/^{154}Eu$ activity ratios to be close to the ORIGEN2 value (i.e., 5.1).

The maximum values of the $^{106}Ru/^{154}Eu$ ratio measured at the locations of the large ceramic core segments in core bore samples K-9 and G-12 are 92 and 26, respectively, while the average values of the ratio for the upper regions of the corresponding fuel stacks are 5.3 and 6.6, respectively. Similar results for the large agglomerate core segments that were present in core bores K-9, O-7, and D-8 are 35, 184, and 56, respectively. The relatively high value of the $^{106}Ru/^{154}Eu$ ratio for the agglomerate segment in core bore O-7 is due to the fact that the ^{154}Eu activity measured at this position is low compared to the ^{154}Eu activities of the other two agglomerate segments, having a value of only 0.0009 Ci. Values of the activity ratio for the agglomerate fragments in core bore samples N-5 and D-4 are 62 and 84, respectively. The fact that the average $^{106}Ru/^{154}Eu$ ratios for the upper regions of the fuel stacks are comparable to or larger than the theoretical value of the ratio indicates that the fuel stacks have retained their initial inventories of ^{106}Ru. On the other hand, the fact that the ceramic and agglomerate materials have $^{106}Ru/^{154}Eu$ ratios significantly larger than the average values for the fuel stacks, in spite of the fact that the ^{154}Eu activities of the ceramic and agglomerate materials are typically higher than the ^{154}Eu activities of the fuel stacks, indicates that ^{106}Ru has been concentrated in these materials. These data indicate that the ^{106}Ru

in the ceramic and agglomerate materials cannot be accounted for in terms of the initial inventory of ^{106}Ru in the fuel that is bound up in these materials.

4.2.2.5 Cerium-144 Among the radionuclides detected in the core bore samples, ^{144}Ce is one of the most refractory and it is expected that this radionuclide was retained in the fuel. The ^{144}Ce activity distribution plots shown in Figure 16 indicate that, for each core bore sample except O-9, the level of ^{144}Ce activity remains reasonably constant throughout the region of the fuel stack. Figure 16 also shows that, excluding core bores K-9 and O-9, the average values of the measured ^{144}Ce activities over the regions of the fuel stacks are about equal; they range from a low of about 0.018 Ci for core bores D-8, G-12, and N-5 to a high of 0.022 Ci for core bore N-12. Similar results for core bores K-9 and O-9 are 0.011 and 0.009 Ci, respectively. The fact that the average ^{144}Ce activity for the K-9 fuel stack is only about one-half the average values for the majority of the fuel stacks might be explained by the fact that the K-9 fuel rods are much shorter that the fuel rods of the other eight core bore samples. As was the case with ^{137}Cs, for a number of the fuel stacks the ^{144}Ce activities near the bottoms of the fuel stacks are less than the activities measured at positions farther removed from the bottoms of the fuel stacks. Between 10.2 and 20.3 cm from the bottom of the K-9 fuel stack, ^{144}Ce was not detected at several of the scan locations.

As was previously mentioned, the fuel rods in core bore sample O-9 appeared to be severely damaged in the region between about 62 and 103 cm above the bottom of the fuel stack. The ^{144}Ce activities of the O-9 fuel stack decrease linearly with height, from 0.03 Ci at 36 cm to 0.002 Ci at 96 cm. Because ^{144}Ce is a very refractory material and is expected to have been retained by the fuel, these data indicate that the quantity of fuel within the field of view of the detector decreased with increasing distance from the bottom of the O-9 fuel stack. Over the regions of their fuel stacks, the contours of the ^{144}Ce activity profiles of core bore samples D-8 and D-4 each exhibit an abrupt dip in activity. As was previously discussed, a number of the fuel rods of core bores D-8 and D-4

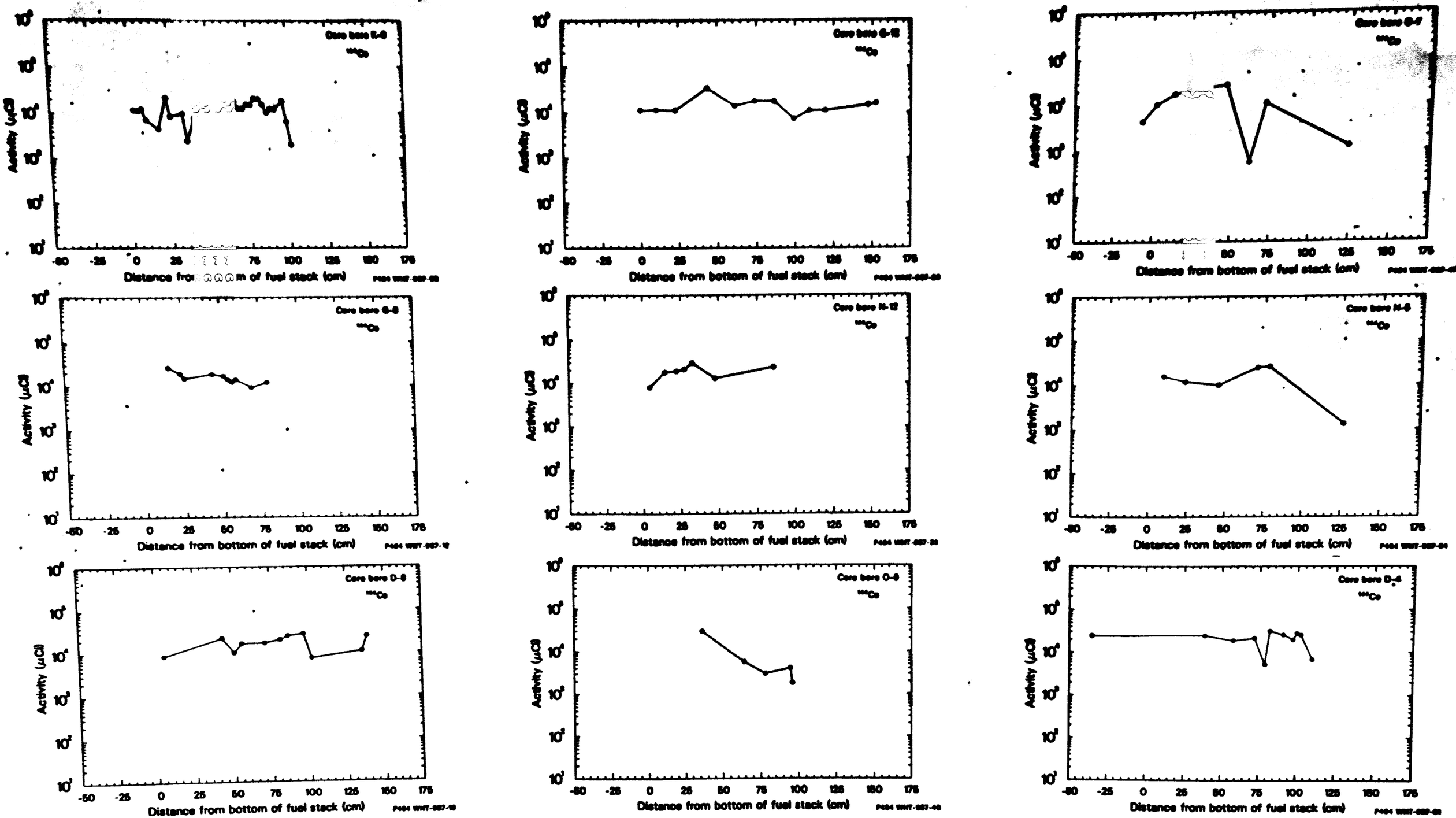

Figure 16. Activity distribution for ^{144}Ce for nine TMI-2 core bore samples.

were breached between the locations of the second and third spacer grids. The locations of the dips very likely correspond to the locations of voids in some of the fuel stacks.

The activity profiles shown in Figure 16 indicate that the ^{144}Ce activities of large ceramic core segments are comparable to the average ^{144}Ce activities of the fuel stacks. The maximum ^{144}Ce activities that were measured for the ceramic core segments in core bore samples K-9 and G-12 are 0.018 and 0.016 Ci, respectively, while the average activities measured for the corresponding fuel stacks are 0.011 and 0.018 Ci, respectively. Three core bore samples (K-9, O-7, and D-8) contained large agglomerate core segments whose maximum ^{144}Ce activities were measured at distances of about 0.48, 0.72, and 1.38 m, respectively, from the bottoms of their fuel stacks. The maximum ^{144}Ce activities measured for these three agglomerate core segments are 0.012, 0.011, and 0.024 Ci, respectively. As was previously stated, several of the core bore samples contained ceramic and/or agglomerate fragments. The maximum ^{144}Ce activities of these fragments range from a low of 0.0013 Ci for agglomerate fragments in core bore N-5 to a high of 0.021 Ci for ceramic fragments in core bore K-9. In general, the ^{144}Ce activities measured for ceramic samples are about the same as those measured for agglomerate samples.

For each position that was scanned, the ratio of the activity of ^{144}Ce to that of ^{154}Eu was calculated. The results for the nine core bore samples are tabulated in Tables D-1 through D-9 and are plotted in Figure 17. Based on the results of ORIGEN2 calculations[1], as of April 1, 1986, the theoretical value of the core inventory of ^{144}Ce to that of ^{154}Eu was about 8.0. The graphs in Figure 17 show that, as was the case with $^{137}Cs/^{154}Eu$ ratios, the $^{144}Ce/^{154}Eu$ ratios generally decrease with increasing height above the bottoms of the fuel stacks. For example, the value of the ratio for the O-7 fuel stack is about 46 at a height of 2.5 cm, but drops to about 15 at 62 cm above the bottom of the fuel stack. The average values of the ratio over the upper regions of the fuel stacks (i.e., the same regions used to compute the average $^{137}Cs/^{154}Eu$ and $^{106}Ru/^{154}Eu$ ratios) range from a low of 11.1 for core bore O-9 to a

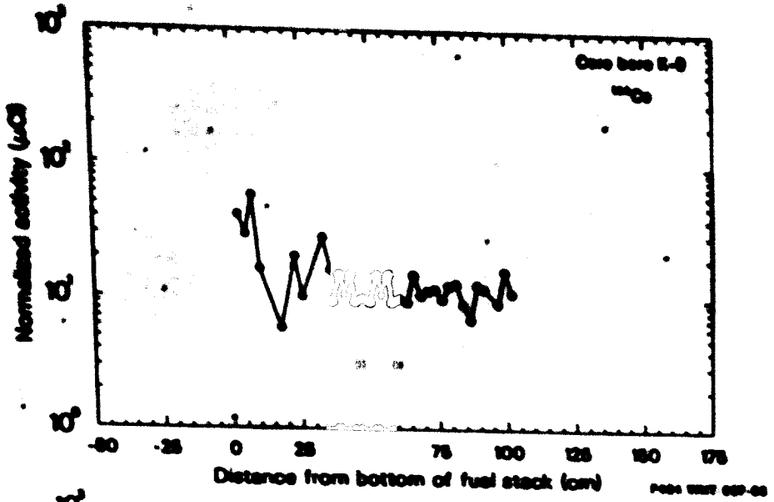

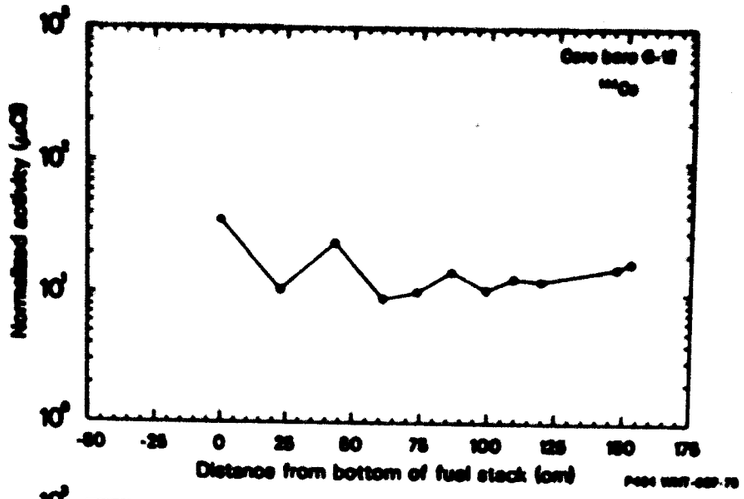

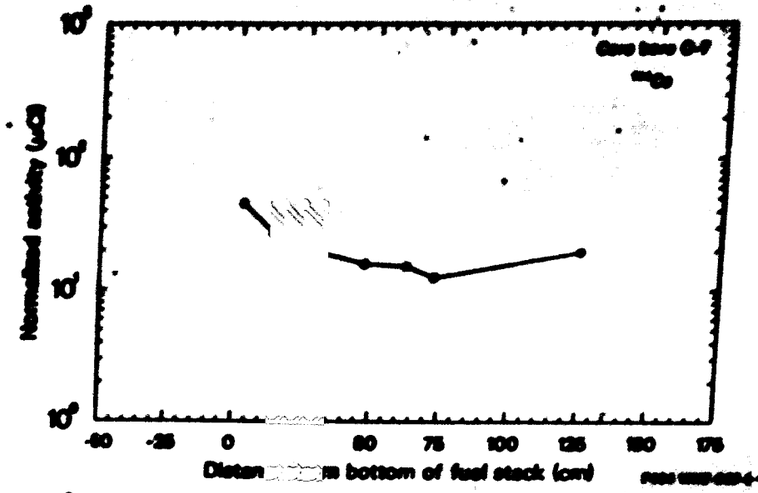

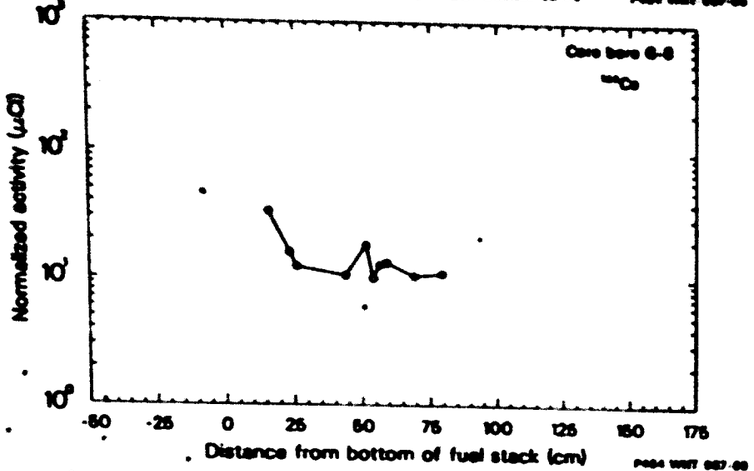

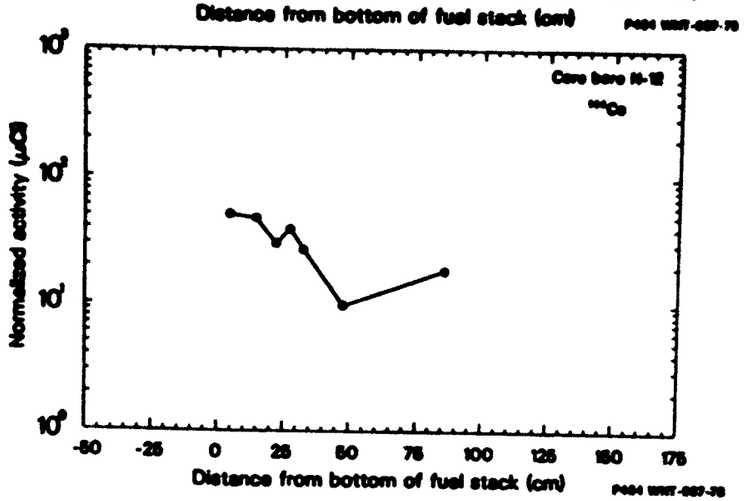

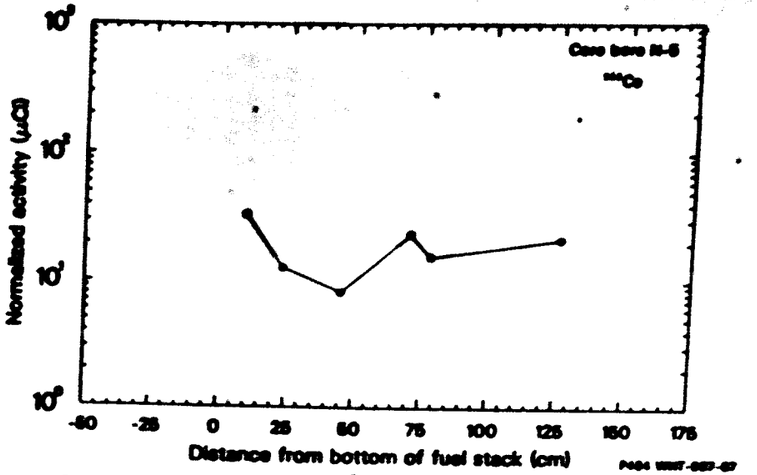

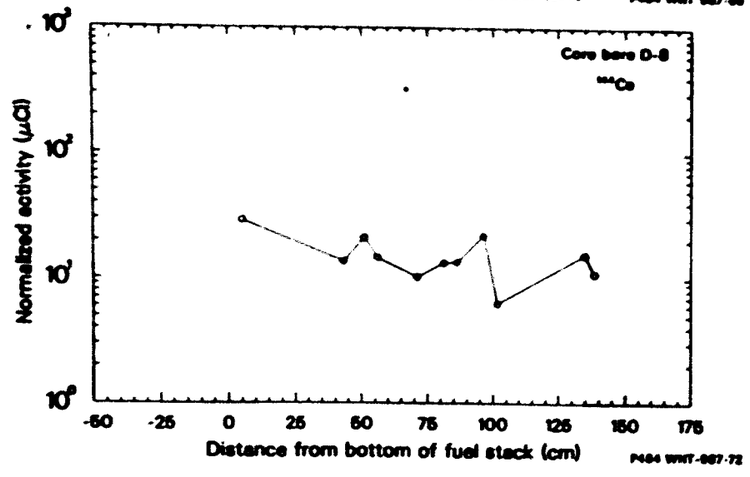

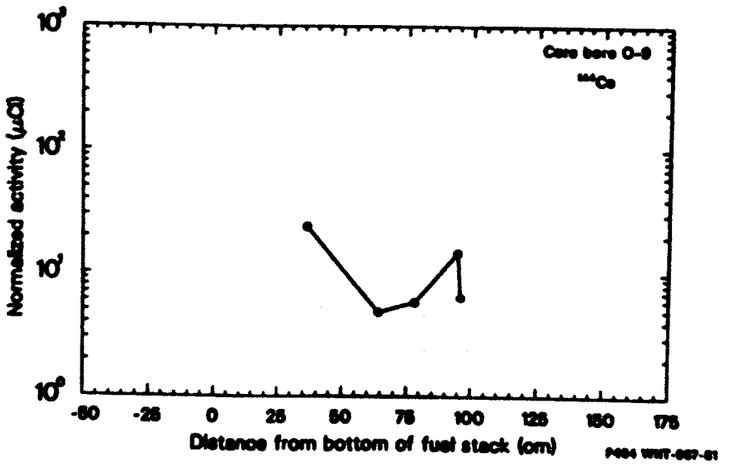

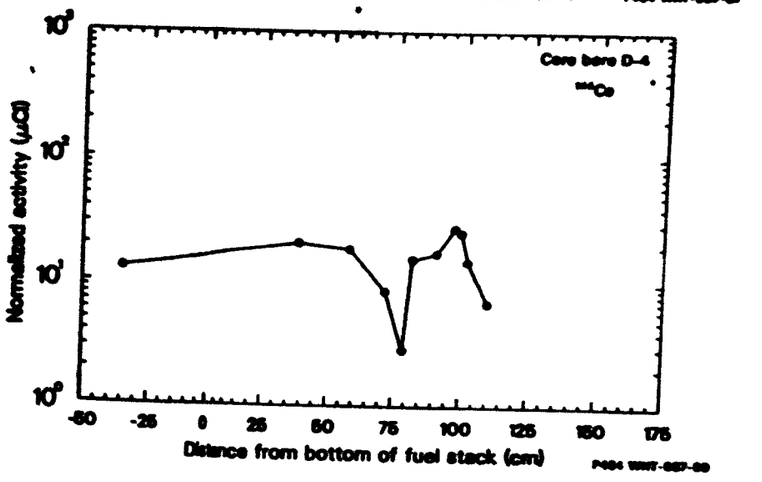

Figure 17. Normalized activity distribution for ^{144}Ce for nine TMI-2 core bore samples.

high of 18.7 for core bore O-7. Similar average values for the remaining seven core bore samples are: N-12, 18.3; D-4, 15.9; N-5, 15.1; D-8, 14.3; G-12, 13.2; G-8, 12.9; and K-9, 12.2. The mean value and standard deviation of the mean value of the ratio for all nine fuel stacks is 15 ± 6%.

The maximum values of the $^{144}Ce/^{154}Eu$ activity ratios that were measured at the locations of the large ceramic core segments in core bore samples K-9 and G-12 are 16.0 and 17.2, respectively. These values agree quite well with the average $^{144}Ce/^{154}Eu$ ratio for the fuel stacks (i.e., 15 ± 18%), which indicates that these two radionuclides were retained by the fuel in the ceramic material to the same degree.

4.2.2.6 Europium-154. Like cerium, europium is a refractory rare earth. The ^{154}Eu activities that were measured at positions along the centerlines of the nine core bore samples are plotted in Figure 10 (p. ??). The plots in Figure 10 show that, in general, ^{154}Eu activities increase with height up to a distance of between 20 to 30 cm from the bottoms of the fuel stacks. This behavior is particularly evident in the activity profiles of core bores K-9, G-12, N-12, and O-7. The data presented in Table 7 and Figure 10 show that, excluding core bore K-9, the average ^{154}Eu activities over the fuel stacks are in good agreement, their mean value and standard deviation of the mean being 0.0012 Ci ± 5%. The corresponding average value for core bore K-9 is about one-half this amount, being 0.0006 Ci. The reason the average ^{154}Eu activity of the K-9 core bore sample is lower than the average values for the other core bores is because the fuel rods in this core bore are shorter than the others.

The maximum ^{154}Eu activities that were measured at the locations of the large ceramic core segments in core bores K-9 and G-12 are about 0.0020 and 0.0009 Ci, respectively, while the maximum activities measured for the corresponding fuel stacks are about 0.001 and 0.002 Ci, respectively. The maximum ^{154}Eu activities measured for the three large agglomerate core segments in core bores K-9, O-7, and D-8 are 0.0012, 0.0009, and 0.002 Ci,

respectively. As was previously mentioned, several of the core bore samples contained ceramic and/or agglomerate fragments. The maximum ^{154}Eu activities of these fragments range from a low of 0.0011 Ci for the agglomerate fragments in core bore G-8 to a high of 0.013 Ci for the agglomerate fragments in core bore N-5. The latter activity is an order of magnitude higher than the average ^{154}Eu activity of the N-5 fuel stack and is the highest ^{154}Eu activity measured. The average ^{154}Eu activity of the ceramic fragments in core bore K-9 is 0.0014 Ci. The unusually high ^{154}Eu concentrations measured for the agglomerate materials in core bore samples O-7, N-5, and O-4 likely indicate that these materials contain a high proportion of fuel pellet remnants.

4.2.2.7 Total Activity. The sums of the activities of ^{134}Cs, ^{137}Cs, ^{60}Co, ^{110m}Ag, ^{125}Sb, ^{106}Ru, ^{144}Ce, and ^{154}Eu at scan positions along the axial centerlines of the core bore samples are plotted as a function of position in Figure 18. The average total activities at positions in selected regions of the fuel stacks of the core bore samples are tabulated in Table 7. The activities presented in Table 7 are not corrected for sample self-attenuation. The data presented in Table 7 show that, excluding core bore K-9, the average total activities in incremental cross sections of the fuel stacks are about the same and range from a low of 0.20 Ci to a high of 0.24 Ci.

Because the upper regions of the O-9 fuel rods were severely damaged, the average total activity in a cross section of the O-9 fuel stack was computed using the activities measured in the region 36.2 to 71.8 cm, a region that appeared to be relatively undamaged. Ignoring the result for the K-9 fuel stack, the average total activity in incremental cross sections of the fuel stacks of the remaining eight core bore samples is 0.221 ± 0.007 Ci, where the standard deviation is the standard deviation of the average value. The average total activity in an incremental cross section of the K-9 fuel stack is about one-half this value, being 0.13 Ci. As has been previously mentioned, the K-9 fuel stack is much shorter than the fuel stacks of the majority of the core bore samples; therefore, its fuel experienced less burnup than the fuel in the upper regions of the other fuel stacks.

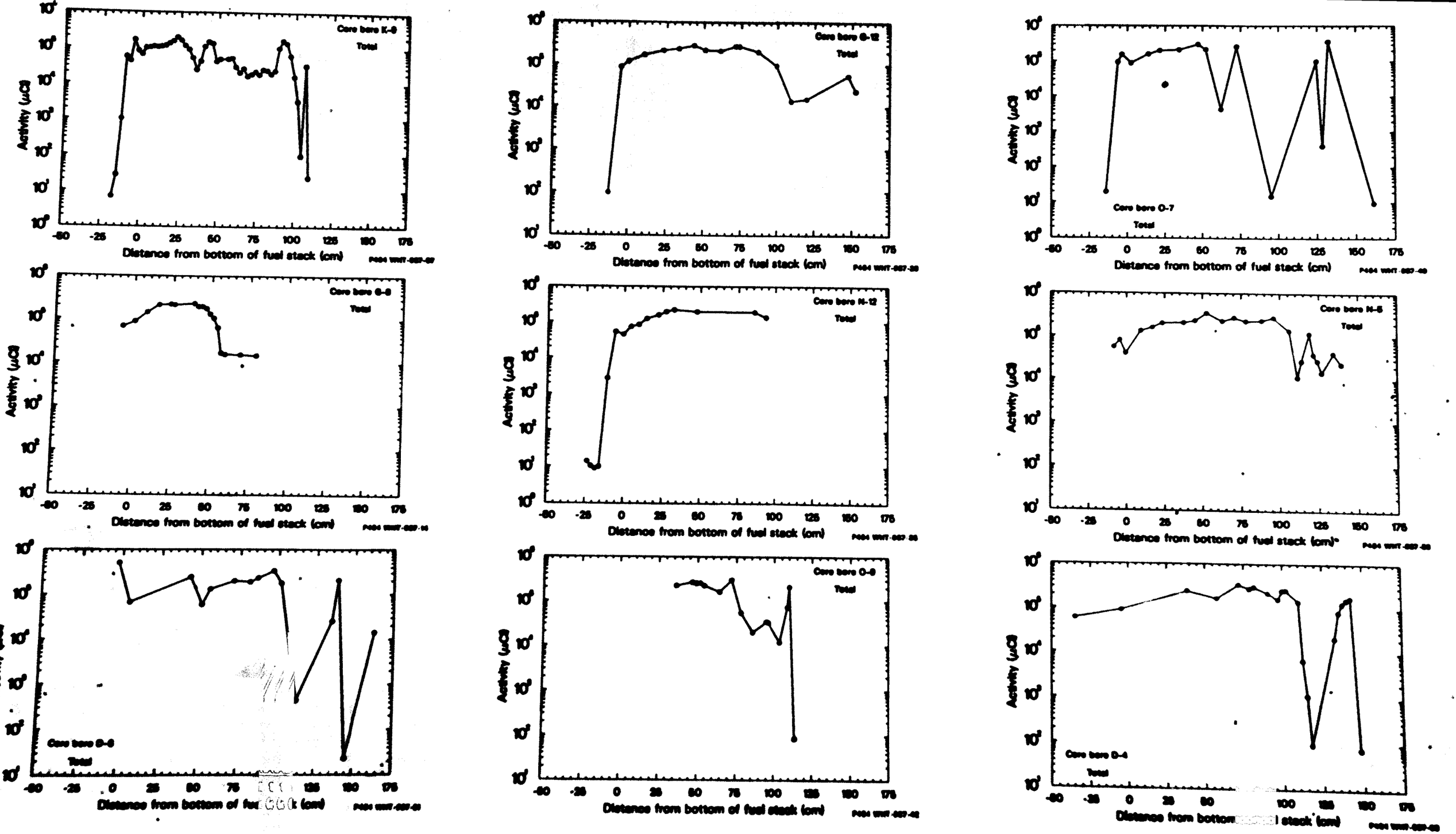

Figure 18. Total activity distribution for nine TMI-2 core bore samples.

Uncorrected for sample self-attenuation, the maximum total activities measured for the large ceramic core segments in core bore samples K-9 and G-12 are 0.17 and 0.05 Ci, respectively, while the maximum total activities of the large agglomerate core segments in core bore samples K-9, O-7, and D-8 are 0.15, 0.26, and 0.21 Ci, respectively. Similar values for the agglomerate fragments in core bore samples N-5 and D-4 are, respectively, 0.12 and 0.17 Ci. These results show that, in general, the total activities in incremental cross sections of the ceramic and agglomerate materials are comparable to the average total activities in incremental cross sections of the fuel rod bundles.

4.2.3 Comparisons with ORIGEN2 Analyses

Comparisons were performed with ORIGEN2 analyses to evaluate the relative abundances of fission products in the intact fuel rods. To provide a basis for comparing theoretical and measured relative activities in the core bore fuel stacks, the average uncorrected radionuclide activities presented in Table 7 were corrected for sample self-attenuation using the correction factors from Table 4. The results are presented in Table 8. In each case, the activity in Table 7 was multiplied by the self-attenuation correction factor for a fuel bundle corresponding to the energy of the intensity-code-1 gamma ray of the radionuclide. For example, for ^{125}Sb, its intensity-code-1 gamma ray has an energy of 427.89 keV (see Table 5 for energies of the radionuclides of interest). The self-attenuation correction factor obtained by interpolating between the values presented in Table 4 for 400 and 600 keV is 10.2. So, the corrected ^{125}Sb activities that are presented in Table 8 are about a factor of ten higher than the uncorrected ^{125}Sb activities listed in Table 7.

For the purpose of comparing measured relative abundances with those calculated using ORIGEN2, the average radionuclide activities presented in Table 8 were converted to percentages of total activity. These results are presented in Table 9, which shows that ^{137}Cs is the dominant activity of the gamma-emitting radionuclides that were detected in the fuel stacks; it constitutes 89.6 ± 0.3% of the total measured activity. The average

TABLE 8. AVERAGE RADIONUCLIDE ACTIVITIES IN INCREMENTAL CROSS SECTIONS OF FUEL STACKS AFTER CORRECTION FOR SAMPLE SELF-ATTENUATION[a]

Core Bore	Region of Fuel Stack[b]	Average Activity (μCi)							
		^{134}Cs	^{137}Cs	^{60}Co	^{125}Sb	^{106}Ru	^{144}Ce	^{154}Eu	Total
K-9	2.5 to 30.5	1.03 E04	6.15 E05	3.62 E03	1.77 E04	1.19 E04	2.54 E04	1.84 E03	6.86 E05
G-8	8.3 to 48.9	1.93 E04	9.61 E05	5.29 E03	1.63 E04	8.39 E03	4.56 E04	3.55 E03	1.06 E06
D-8	43.2 to 101.6	2.30 E04	9.00 E05	2.90 E03	9.57 E03	2.40 E04	4.30 E04	4.06 E03	1.01 E06
G-12	10.2 to 86.4	2.34 E04	1.14 E06	6.80 E02	2.26 E04	2.26 E04	4.16 E04	4.12 E03	1.26 E06
N-12	32.4 to 93.3	1.79 E04	9.00 E05	ND[c]	ND	2.47 E04	5.15 E04	3.91 E03	9.98 E05
O-9	36.2 to 71.8	2.58 E04	1.08 E06	2.55 E04	--[d]	3.06 E04[d]	4.23 E04	3.97 E03	1.21 E06
O-7	2.5 to 52.1	1.79 E04	9.17 E05	9.84 E03	1.31 E03	2.56 E04	4.44 E04	2.73 E03	1.03 E06
N-5	9.5 to 106.0	2.02 E04	1.08 E06	1.59 E04	1.67 E04	4.70 E04	4.16 E04	3.67 E03	1.23 E06
D-4	38.7 to 109.9	2.49 E04	1.11 E06	1.26 E03	1.16 E04	3.29 E04	4.89 E04	4.39 E03	1.23 E06
	Average[e]:	2.16 E04	1.01 E06	8.77 E03	1.50 E04	2.70 E04	4.49 E04	4.03 E03	1.13 E06
	Std. Dev.:	0.11 E04	0.04 E06	3.45 E03	0.19 E04	0.38 E04	0.13 E04	0.26 E03	0.04 E06

a. Activities are corrected for sample self-attenuation using correction factors from Table 6. Activities are decay-corrected to April 1, 1986.

b. Distance in centimeters from the bottom of the fuel stack.

c. ND = not detected. For the purpose of calculating overall average activities ND results were ignored.

d. Activity measured at 71.8 cm was ignored.

e. The results for core bore sample K-9 were omitted when the overall average activities were computed. The standard deviation is the one-sigma standard deviation of the average value.

TABLE 9. AVERAGE RADIONUCLIDE ACTIVITIES IN INCREMENTAL CROSS SECTIONS OF FUEL STACKS AFTER CORRECTION FOR SAMPLE SELF-ATTENUATION, EXPRESSED AS PERCENT OF TOTAL ACTIVITY[a]

Core Bore	Percent of Total Activity							Total (Ci)
	^{134}Cs	^{137}Cs	^{60}Co	^{125}Sb	^{106}Ru	^{144}Ce	^{154}Eu	
K-9	1.50	89.65	0.53	2.58	1.73	3.70	0.27	0.69
G-8	1.82	90.66	0.50	1.54	0.79	4.30	0.34	1.06
D-8	2.28	89.11	0.29	0.95	2.38	4.26	0.40	1.01
G-12	1.86	90.48	0.05	1.79	1.79	3.30	0.33	1.26
N-12	1.79	90.18	ND[b]	ND	2.47	5.16	0.39	1.00
O-9	2.13	89.26	2.11	---[c]	2.53[c]	3.50	0.33	1.21
O-7	1.74	89.03	0.96	1.27	2.49	4.31	0.27	1.03
N-5	1.64	87.80	1.29	1.36	3.82	3.38	0.30	1.23
D 4	2.02	90.24	0.10	0.94	2.67	3.98	0.36	1.23
Average[d]	1.91	89.6	0.8	1.3	2.4	4.0	0.34	1.13
Std. Dev.:	0.08	0.3	0.3	0.1	0.3	0.2	0.02	0.04

a. Activities are corrected for self-attenuation using correction factors for fuel bundles from Table 4. Activities are decay-corrected to April 1, 1986.

b. ND = not detected. For the purpose of computing average percentages, ND values were ignored.

c. Activity measured at 71.8 cm was ignored.

d. The results for core bore K-9 were omitted when the overall average activities were computed. The standard deviation is the one-sigma standard deviation of the average value.

activities of the remaining seven radionuclides, expressed as percentages of total measured activity, are: ^{144}Ce, 4.0 ± 0.2%; ^{106}Ru, 2.4 ± 0.3%; ^{134}Cs, 1.91 ± 0.08%; ^{125}Sb, 1.3 ± 0.1%; ^{60}Co, 0.8 ± 0.3%; and ^{154}Eu 54, 0.34 ± 0.02%. Omitting ^{60}Co, an activation product, the average ratios of these fission products as calculated using ORIGEN2[1] are: ^{137}Cs, 86.2%, ^{144}Ce, 5.1%; ^{106}Ru, 3.3%; ^{134}Cs, 2.2%; ^{125}Sb, 2.6%; and ^{154}Eu, 0.64%, where the results are expressed as percentages of the calculated combined core inventory of the radionuclides as of April 1, 1986. These data indicate that, at positions removed from the bottoms of the fuel stacks, the relative quantities of ^{137}Cs, ^{144}Ce, ^{106}Ru, and ^{134}Cs in the fuel stacks agree quite well with their calculated core average relative abundances. The relative quantities of ^{125}Sb and ^{154}Eu at the same positions in the fuel stacks are, on the other hand, lower than their ORIGEN2 calculated values. The measured relative abundances of these two radionuclides are both about a factor of two lower than their abundances determined using ORIGEN2. Other data suggest that ORIGEN2 may overpredict the production of these radionuclides, because they are produced, respectively, by neutron capture on stable ^{124}Sn and the fission product ^{153}Eu, which would make them more sensitive to variations in neutron flux.

The activities of the previously mentioned radionuclides in incremental cross sections of the large ceramic core segments and agglomerate fragments were corrected for sample self-attenuation by multiplying each measured activity by the self-attenuation correction factor for a (U-Zr-O) core segment corresponding to the energy of the intensity-code-1 gamma ray of the radionuclide. The self-attenuation correction factors were obtained by interpolating between the values presented in Table 4. The results are presented in Tables 10 and 11. After being corrected for self-attenuation, the activities for a given ceramic sample were summed to determine the total activity in a cross section of the sample.

The data presented in Tables 10 and 11 were converted to percentages of the total activities in cross sections of the corresponding ceramic and

TABLE 10. RADIONUCLIDE ACTIVITIES IN INCREMENTAL CROSS SECTIONS OF CERAMIC SEGMENTS AND FRAGMENTS AFTER CORRECTION FOR SAMPLE SELF-ATTENUATION

Core Bore	Scan Location (cm)	Average Activity (μCi)							
		^{134}Cs	^{137}Cs	^{60}Co	^{125}Sb	^{106}Ru	^{144}Ce	^{154}Eu	Total
K-9[a]	91.4	ND[b]	1.20 E04	6.94 E04	1.87 E05	2.68 E05	2.53 E04	2.69 E03	5.64 E05
G-12[a]	147.3	3.98 E02	1.74 E04	1.48 E04	3.92 E04	6.77 E04	3.02 E04	2.44 E03	1.72 E05
K-9[c]	50.8 to 61.0	2.74 E02	7.65 E03	7.74 E03	1.10 E04	1.89 E04	1.23 E04	1.38 E03	5.92 E04

a. Activities were corrected for self-attenuation using the correction factors for a (U-Zr-O) ceramic segment from Table 4. Activities are decay-corrected to April 1, 1986.

b. ND = not detected.

c. Ceramic fragments are present in this region. Activities were corrected for self-attenuation using the correction factors for a (U-Zr-O) pellet from Table 3.

TABLE 11. RADIONUCLIDE ACTIVITIES IN INCREMENTAL CROSS SECTIONS OF AGGLOMERATE SEGMENTS AND FRAGMENTS AFTER CORRECTION FOR SAMPLE SELF-ATTENUATION

Core Bore	Scan Location (cm)	Average Activity (μCi)							
		^{134}Cs	^{137}Cs	^{60}Co	^{125}Sb	^{106}Ru	^{144}Ce	^{154}Eu	Total
K-9[a]	43.2	1.20 E04	3.63 E05	5.53 E04	5.54 E04	7.08 E04	2.04 E04	2.82 E03	5.80 E05
O-7[a]	72.4	1.16 E03	8.74 E04	1.03 E05	2.14 E05	4.51 E05	2.26 E04	2.26 E03	8.81 E05
D-8[a]	138.4	8.25 E02	1.76 E04	3.95 E04	1.45 E05	3.44 E05	4.95 E04	5.69 E03	6.02 E05
D-4[c]	142.9	ND[b]	2.35 E02	1.61 E04	4.56 E04	1.60 E05	ND	6.90 E03	2.29 E05
N-5[c]	118.7	9.83 E02	4.52 E04	1.24 E04	1.75 E04	7.89 E04	ND	1.45 E03	1.56 E05

a. Activities were corrected for self-attenuation using the correction factors for a (U-Zr-O) ceramic segment from Table 4. Activities are decay-corrected to April 1, 1986.

b. ND = not detected.

c. Agglomerate fragments are present at this scan location. Activities were corrected for self-attenuation using the correction factors for a (U-Zr-O) pellet from Table 3.

agglomerate samples. The results are presented in Tables 12 and 13. These data indicate that the relative abundances of the gamma-emitting radionuclides are significantly different in the ceramic and agglomerate materials as compared to their relative abundances in the core bore fuel stacks. While ^{137}Cs comprises about 90% of the total activity in the fuel stacks, it makes up only from 2.1% to 12.9% of the total activity in the ceramic materials and from 0.1% to 62.6% of the total activity in the agglomerate materials. The data presented in Tables 9 and 10 show that ^{137}Cs activities in ceramic and agglomerate materials are generally substantially less than the average ^{137}Cs activity in the core bore fuel stacks.

The data in Tables 12 and 13 show that ^{106}Ru and ^{125}Sb are the dominant activities for the majority of the ceramic and agglomerate samples. Ruthenium-106 comprises from 31.9% to 47.5% of the total activity in the ceramic samples and, excluding the results for the agglomerate segment in core bore K-9, from 50.6% to 69.9% of the total activity in the agglomerate samples. In the case of the agglomerate segment in core bore K-9, ^{106}Ru makes up only 12.2% of the total activity in a cross section of the sample. Ruthenium-106 activities in the agglomerate segments in core bores K-9, O-7, and D-8 are, respectively, factors of 2.6, 16.7,and 12.7 higher than the average ^{106}Ru activity in the core bore fuel stacks.

The data presented in Tables 12 and 13 show that ^{125}Sb constitutes from 18.6% to 33.2% of the total activity in the ceramic samples and, excluding the results for the agglomerate segment in core bore K-9, from 11.2% to 24.3% of the total activity in the agglomerate samples. Antimony-125 activities in the ceramic segments in core bores K-9 and G-12 are respectively, factors of 12.5 and 2.6 higher than the average ^{125}Sb activity in the core bore fuel stacks. As was the case with ^{106}Ru activity, the ^{125}Sb activity measured in a cross section of the K-9 agglomerate sample is substantially lower than the corresponding activities measured in cross sections of the O-7 and D-8 agglomerate samples. The

TABLE 12. RADIONUCLIDE ACTIVITIES IN INCREMENTAL CROSS SECTIONS OF CERAMIC SEGMENTS AND FRAGMENTS AFTER CORRECTION FOR SAMPLE SELF-ATTENUATION, EXPRESSED AS PERCENT OF TOTAL ACTIVITY

Core Bore	Scan Location (cm)	Percent of Total Activity							
		^{134}Cs	^{137}Cs	^{60}Co	^{125}Sb	^{106}Ru	^{144}Ce	^{154}Eu	Total
K-9[a]	91.4	ND[b]	2.13	12.30	33.16	47.52	4.49	0.48	0.564
G-12[a]	147.3	0.23	10.12	8.60	22.79	39.36	17.56	1.42	0.172
K-9[c]	50.8 to 61.0	0.46	12.91	13.06	18.57	31.90	20.78	2.33	0.059

a. Activities were corrected for self-attenuation using the correction factors for (U-Zr-O) ceramic segment from Table 4. Activities are decay-corrected to April 1, 1986.

b. ND = not detected.

c. Ceramic fragments are present in this region. Activities were corrected for self-attenuation using correction factors for a (U-Zr-O) pellet from Table 3.

TABLE 13. RADIONUCLIDE ACTIVITIES IN INCREMENTAL CROSS SECTIONS OF AGGLOMERATE SEGMENTS AND FRAGMENTS AFTER CORRECTION FOR SAMPLE SELF ATTENUATION, EXPRESSED AS PERCENT OF TOTAL ACTIVITY

Core Bore	Scan Location (cm)	Percent of Total Activity							
		^{134}Cs	^{137}Cs	^{60}Co	^{125}Sb	^{106}Ru	^{144}Ce	^{154}Eu	Total
K-9[a]	3.2	2.07	62.59	9.53	9.55	12.21	3.52	0.49	0.580
O-7[a]	72.4	0.13	9.92	11.69	24.29	51.19	2.57	0.26	0.881
D-8[a]	138.4	0.14	2.92	6.56	24.09	57.14	8.22	0.95	0.602
D-4[c]	142.9	ND[b]	0.10	7.03	19.91	69.87	ND	3.01	0.229
N-5[c]	118.7	0.63	28.97	7.95	11.22	50.58	ND	0.93	0.156

a. Activities were corrected for self-attenuation using the correction factors for (U-Zr-O) ceramic segment from Table 4. Activities are decay-corrected to April 1, 1986.

b. ND = not detected.

c. Agglomerate fragments are present in this scan location. Activities were corrected for self-attenuation using correction factors for a (U-Zr-O) pellet from Table 3.

^{125}Sb activities in the above samples are, respectively, factors of 3.7, 14.3, and 9.7 higher than the average ^{125}Sb activity in the core bore fuel stacks.

The data presented in Tables 10 and 11 also indicate that ^{60}Co activities in ceramic and agglomerate samples are generally significantly higher than the average activity of ^{60}Co in the core bore fuel stacks. Cobalt-60 activities in cross sections of the ceramic segments in core bores K-9 and G-12 are, respectively, factors of 7.9 and 1.7 higher than the average ^{60}Co activity in the core bore fuel stacks. Cobalt-60 activities in the three agglomerate segments in core bores K-9, O-7, and D-8 are, respectively, factors of 6.3, 11.7, and 4.5 higher than the average ^{60}Co activity in incremental cross sections of the core bore fuel stacks. Unlike its ^{106}Ru and ^{125}Sb activities, the ^{60}Co activity of the K-9 agglomerate segment is comparable to the ^{60}Co activities measured for the other two agglomerate segments. The average ^{60}Co activity in cross sections of the ceramic fragments in core bore K-9 is 0.0077 Ci, while corresponding activities in the agglomerate fragments in core bores D-4 and N-5 are 0.016 and 0.012 Ci, respectively.

The activities listed in Tables 10 and 11 indicate that ^{154}Eu activities in the ceramic and agglomerate segments are generally comparable to the average ^{154}Eu activity measured for the core bore fuel stacks. The ^{154}Eu activities in incremental cross sections of the ceramic segments in core bores K-9 and G-12 are, respectively, 67% and 61% of the average ^{154}Eu activity in cross sections of the core bore fuel stacks. Europium-154 activities in the three agglomerate segments show more variation. The ^{154}Eu activities in cross sections of the agglomerate segments in core bores K-9, O-7, and D-8 are, respectively, 0.0028, 0.0023, and 0.0057 Ci. These latter activities correspond to about 70%, 56% and 141% of the average ^{154}Eu activity of the core bore fuel stacks. As was mentioned in Section 4.1.3, fuel pellet remnants were visible on the surface of the agglomerate segment in core bore D-8. The anomalously high ^{154}Eu activity of the D-8 agglomerate sample is probably due to the fact that the sample has a higher concentration of fuel pellet remnants than the

other agglomerate samples. Based on the premise that ^{154}Eu activity is proportional to fuel content, the data indicate that the inventories of uranium in cross sections of the ceramic segments and of two of the three agglomerate segments are about equal but are only about 65% of the average inventory of uranium in incremental cross sections of the core bore fuel rod bundles.

The data presented in Tables 10 and 11 show that the total activities in cross sections of the ceramic and agglomerate segments range from a low of 0.172 Ci for the ceramic sample in core bore G-12 to a high of 0.881 Ci for the agglomerate sample in core bore D-7. These total activities correspond to 15% and 78%, respectively, of the average total activity in incremental cross sections of the core bore fuel stacks. The total activity in a cross section of the G-12 ceramic segment is about a factor of three lower than the total activity measured in a cross section of the K-9 ceramic segment. The fact that the total activities of these two ceramic segments are substantially different might indicate that the ceramic sample located 147 cm above the bottom end of the G-12 fuel stack is actually a fragment rather than a core segment having a diameter equal to the diameter of the core bore canister. As was discussed in Section 4.1.4, dark-colored fragments consisting of pieces ranging in size from 1.3 to 2.5 cm filled 53 cm of the G-12 core bore casing directly above the upper ends of the fuel rods. If the self-attenuation correction factors for a (U-Zr-O) pellet are used rather than those for a (U-Zr-O) ceramic segment, the total activity of the G-12 ceramic sample is only 0.068 Ci. This value is similar to the average total activity in cross sections of the ceramic fragments in core bore K-9, which is 0.059 Ci. The total activity in a cross section of the K-9 ceramic segment is 0.564 Ci, which is about 50% of the average total activity in cross sections of the core bore fuel stacks. The total activities in cross sections of the agglomerate segments in core bores K-9 and D-8 are 0.580 and 0.602 Ci, respectively, while the total activities in cross sections of the agglomerate fragments in core bores D-4 and N-5 are 0.229 and 0.156 Ci, respectively.

4.2.4 Summary of Gamma Ray Spectroscopy Results

This section presents a summary of the important differences in the distribution of fission products and ^{60}Co in the core bore samples. Differences in measured activities between the fuel stacks and the large ceramic pieces can generally be attributed to the accumulation of fission products in the different types of materials. Because the large-diameter agglomerate segments in core bore samples K-9, O-7, and D-8 are probably non-homogeneous mixtures of (U-Zr-O) ceramic and remnants of fuel pellets and cladding that are likely randomly oriented within the ceramic, sample geometry is not well defined and, therefore, the results for the agglomerate segments must be viewed as being more qualitative than the results for the fuel stacks and ceramic segments. Because the actual sizes of the individual ceramic and agglomerate fragments that are present in core bores K-9, D-4, and N-5 are not known, the corrections for sample self-attenuation that were made for these small-diameter samples must be viewed as being less exact than the corrections made for the fuel rod stacks and the large-diameter ceramic segments.

The results presented in Table 8 show that, excluding core bore K-9, the average activities of ^{134}Cs, ^{137}Cs, ^{144}Ce, and ^{154}Eu in the fuel rod bundles of the core bore samples remain reasonably constant from one core bore sample to the next. The average activities of these radionuclides in cross sections of the K-9 fuel stack are all approximately one-half their corresponding average activities in the remaining eight fuel stacks.

The results presented in Table 9 show that the relative abundances of ^{134}Cs, ^{137}Cs, ^{106}Ru, and ^{144}Ce in regions of the fuel stacks removed from the bottoms of the fuel stacks agree quite well with their theoretical core average relative abundances. The relative abundances of ^{125}Sb and ^{154}Eu in the same regions of the core bore fuel stacks are both about a factor of two lower than their corresponding abundances calculated using ORIGEN2.

In contrast to the results for the core bore fuel stacks, the data presented in Tables 10 through 13 show that ^{106}Ru and ^{125}Sb are the dominant activities in the majority of the ceramic and agglomerate materials in the core bore samples and are as much as a factor of 15 higher than their corresponding average activities in cross sections of the core bore fuel stacks. Cobalt-60 activities in the ceramic and agglomerate materials are also generally significantly higher than the average ^{60}Co concentration in cross sections of the core bore fuel stacks. The ^{60}Co activities measured in the former samples are as much as an order of magnitude higher than the average ^{60}Co activity measured in cross sections of the fuel stacks.

The results for the fuel stacks and selected results for the large-diameter ceramic and agglomerate segments presented in Tables 8, 10, and 11 are summarized in Table 14. As was previously mentioned, the average activities in cross sections of the core bore fuel stacks were computed omitting the results for core bore K-9; however, because of the uncertainty regarding the actual size of the ceramic sample in core bore G-12, only the results for the ceramic segment in core bore K-9 are presented in Table 14.

The data presented in Table 13 show that the relative abundances of ^{137}Cs, ^{106}Ru, and ^{125}Sb in the K-9 agglomerate segment are much different than their respective relative abundances in the O-7 and D-8 agglomerate segments. Cesium-137 comprises 62.6% of the total activity in the K-9 agglomerate segment, whereas it makes up only 9.9% and 2.9%, respectively, of the total activities in the O-7 and D-8 agglomerate segments. These results suggest that relatively intact fuel pellets containing most of their original inventories of ^{137}Cs are embedded in the K-9 agglomerate segment. The relative abundances of ^{106}Ru and ^{125}Sb in the K-9 agglomerate sample are substantially lower than their corresponding relative abundances in the other two agglomerate segments. Because of these differences, only the results for the agglomerate segments in core bores O-7 and D-8 were used to compute average agglomerate material radionuclide activities. The data presented in Table 14 for ^{137}Cs,

TABLE 14. AVERAGE RADIONUCLIDE ACTIVITIES IN INCREMENTAL CROSS SECTIONS OF FUEL STACKS, CERAMIC SEGMENTS, AND AGGLOMERATE SEGMENTS AFTER CORRECTION FOR SAMPLE SELF-ATTENUATION[a]

Type of Material	Activity (μCi)							Total (Ci)
	^{134}Cs	^{137}Cs	^{60}Co	^{125}Sb	^{106}Ru	^{144}Ce	^{154}Eu	
Fuel stack	2.2 E04	1.01 E06	8.8 E03	1.5 E04	2.7 E04	4.5 E04	4.0 E03	1.13 E06
	0.1 E04[b]	0.04 E06	3.4 E03	0.2 E04	0.4 E04	0.1 E04	0.3 E03	0.04 E06
Ceramic[c]	ND[d]	1.20 E04	6.94 E04	1.87 E05	2.68 E05	2.53 E04	2.69 E03	5.64 E05
Agglomerate[e]	9.9 E02	5.3 E04	7.1 E04	1.8 E05	4.0 E05	3.6 E04	4.0 E03	7.4 E05
	1.7 E02[b]	3.5 E04	3.2 E04	0.4 E05	0.5 E05	1.4 E04	1.7 E03	1.4 E05

a. Activities are corrected for self-attenuation using the correction factors for a (U-Zr-O) ceramic segment from Table 4. Activities are decay-corrected to April 1, 1986.

b. One-sigma standard deviation of mean value.

c. Results for K-9 ceramic segment only.

d. ND = not detected.

e. Average of results for O-7 and O-8 agglomerate segments.

^{125}Sb, ^{106}Ru, and ^{60}Co are plotted in Figure 19, where radionuclide activities are expressed in units of Curies.

While ^{137}Cs is significantly depleted from the ceramic and agglomerate materials, Figure 19 shows that ^{106}Ru, ^{125}Sb and ^{60}Co are highly concentrated in these materials. The data in Table 14 show that the average ^{154}Eu activity in cross sections of the agglomerate segments is equal to the average ^{154}Eu activity in similarly sized cross sections of the core bore fuel stacks. Based on the premise that ^{154}Eu activity is proportional to fuel inventory, the data indicate that the quantity of fuel in a cross section of the ceramic segment is about 30% less than average inventories of fuel in similarly sized cross sections of the agglomerate segments and core bore fuel stacks. This indicates that the quantities of ^{106}Ru and ^{125}Sb in the ceramic and agglomerate materials cannot be accounted for in terms of their initial inventories in the fuel that were assimilated into these materials.

The results presented in Table 14 also show that average ^{137}Cs activities in cross sections of the agglomerate and ceramic sections are only 1.2% and 5.2% of the average ^{137}Cs activity in the core bore fuel stacks. These results indicate that about 98% of the ^{137}Cs that was originally present in the fuel was lost from the ceramic material. The relatively higher $^{137}Cs/^{154}Eu$ ratio of the agglomerate segments indicates that the agglomerate segments contain intact fuel pellet fragments that retained about 5% of their original ^{137}Cs inventories.

4.2.5 Core Materials Distribution

Based on the normal distribution of instrument tubes, guide tubes, and fuel rods in a TMI-2 fuel assembly,[5] each core bore fuel rod bundle should contain one instrument tube, two guide tubes, and about 18 fuel rods. Collectively, these 21 rods have a linear density of about 164.6 g/cm, which includes the mass of the Ag-In-Cd control rods that are inside the two guide tubes. For the case where a core bore fuel bundle contains 18 fuel rods, the fuel rods collectively have a linear UO_2

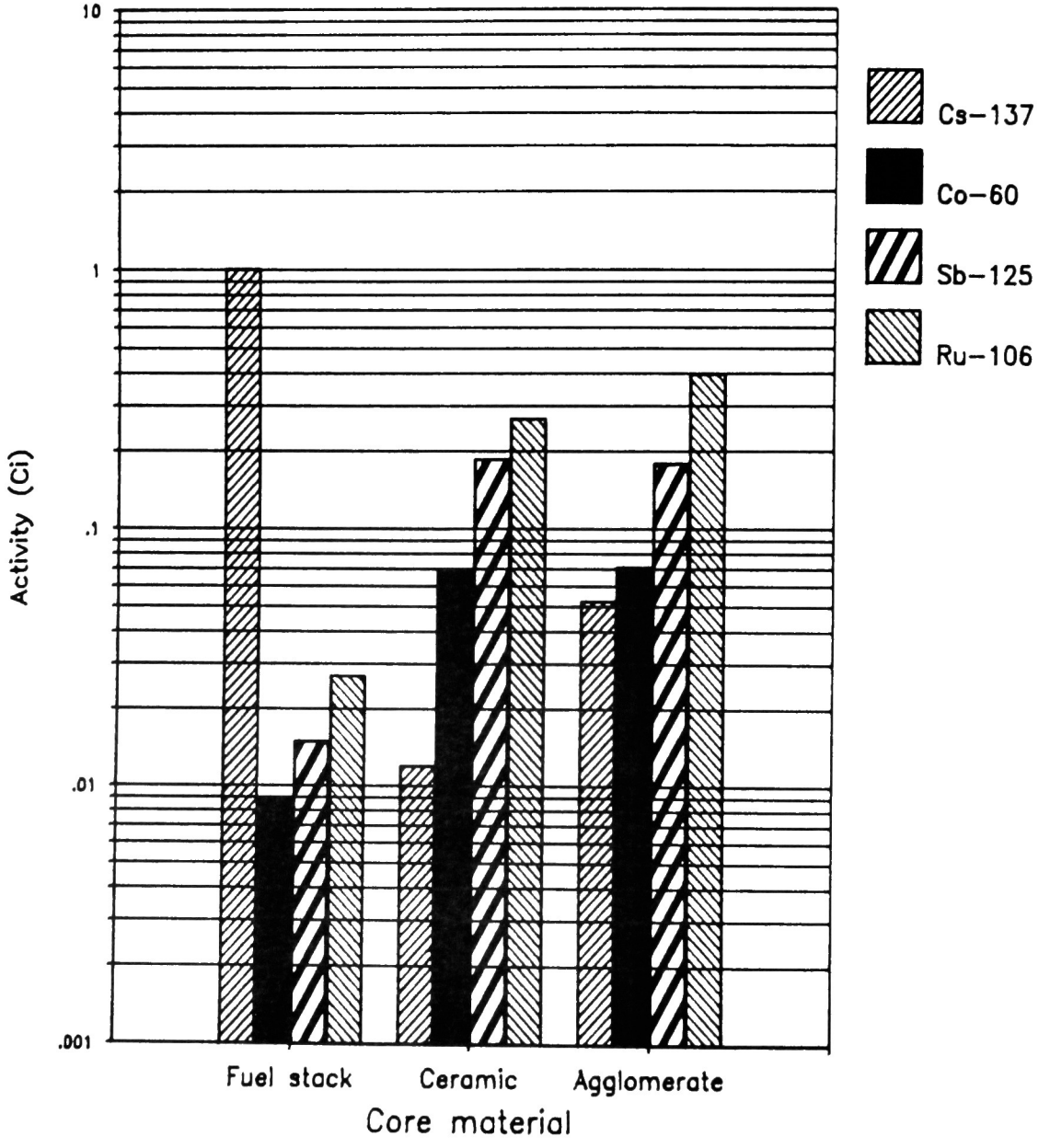

Figure 19. Average activities in incremental cross sections of fuel bundles, ceramic segments, and agglomerate materials.

density of about 126.4 g/cm. Using the pre-accident concentration of uranium in the fuel pellets (i.e., 88.15 wt%), this converts to about 111.4 g of uranium per centimeter. In the case of the ceramic and agglomerate core segments, a solid 6.35-cm-dia right-circular cylinder having a density of 7.5 g/cm^3 has a linear density of about 237.5 g/cm. Using these linear densities, the masses of material within the umbra of the detector's field of view, which is 0.991-cm wide, are: (a) bulk material of 21-rod fuel rod bundle, 163.1 g; (b) uranium in 18 fuel rods, 110.4 g; (c) ceramic and agglomerate segments, 235.4 g. The densities and dimensions of the ceramic and agglomerate materials are assumed to be the same.

The average radionuclide activities presented in Table 14 were converted to concentrations by dividing by the corresponding sample masses listed in the preceding paragraph. The results are presented in Table 15 and are plotted in Figure 20. The concentrations presented in Table 15 for the fuel bundle are the average concentrations in the bulk material of the fuel bundle, which is assumed to have a linear density of 164.6 g/cm. For the purpose of comparison, the core average radionuclide concentrations calculated using ORIGEN2[1] are also presented in Table 15. The ORIGEN2 results were calculated by dividing the calculated core radionuclide inventories by 1.295 E08 g, the total mass of materials in the active core region including the 4.81 E06 g of oxygen that is estimated to have been taken up during the oxidation of the fuel rod cladding.[4] Average radionuclide concentrations in the fuel in the core bore fuel bundles are presented in Table 16, where the concentrations were calculated using a uranium mass of 110.4 g, the calculated mass of uranium in the umbra of the detector's field of view. The theoretical concentrations of radionuclides in the fuel are also presented in Table 16. These latter results were calculated by dividing the ORIGEN2 core radionuclide inventories by 8.357 E07 g,[4] the mass of uranium in the core at the time of the accident. These results are plotted in Figure 21. The ratio of the measured and theoretical concentrations are also given in Table 16 for each radionuclide.

TABLE 15. AVERAGE RADIONUCLIDE CONCENTRATIONS IN CORE MATERIALS COMPARED WITH THEORETICAL CORE AVERAGE CONCENTRATIONS[a]

Core Material	Concentrations (μCi/g)							Total (Ci)
	^{134}Cs	^{137}Cs	^{60}Co	^{125}Sb	^{106}Ru	^{144}Ce	^{154}Eu	
ORIGEN2[b]	1.41 E02	5.59 E03	NA	1.68 E02	2.11 E02	3.33 E02	4.16 E01	6.48 E03
Fuel bundle[c]	1.35 E02	6.19 E03	5.39 E01	9.20 E01	1.65 E02	2.76 E02	2.45 E01	6.94 E03
Ceramic	ND	5.10 E01	2.95 E02	7.95 E02	1.14 E03	1.07 E02	1.14 E01	2.40 E03
Agglomerate	4.21 E00	2.25 E02	3.02 E02	7.65 E02	1.70 E03	1.53 E02	1.70 E01	3.14 E03

a. All concentrations are decay-corrected to April 1, 1986.

b. Calculated using a core mass of 1.295 E08 g that includes 4.81 E06 g of oxygen that is estimated to have been taken up during the oxidation of the zircaloy cladding.

c. Calculated assuming the core bore fuel bundles consist of 1 instrument tube, 2 control rods, and 18 fuel rods. Based on this composition, the mass of the fuel bundle within the umbra of the detector's field of view is 163.1 g.

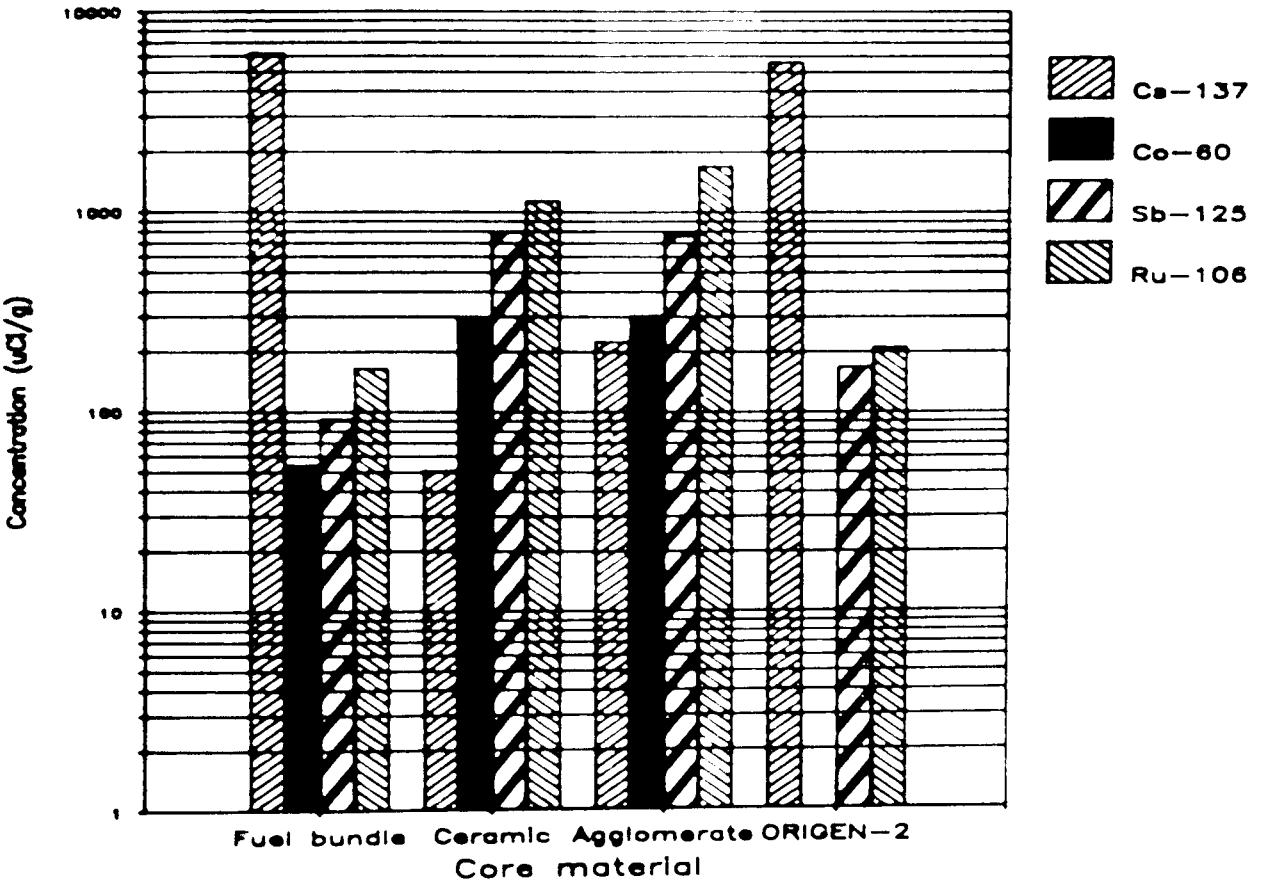

Figure 20. Average radionuclide concentrations in core materials compared with theoretical core average concentrations.

TABLE 16. COMPARISON OF MEASURED AND THEORETICAL FUEL STACK RADIONUCLIDE CONCENTRATIONS

Radionuclide	Concentration (μCi/g of uranium)		
	Fuel Stack	ORIGEN2[a]	Ratio
^{134}Cs	1.99 E02	2.19 E02	0.91
^{137}Cs	9.14 E03	8.66 E03	1.06
^{125}Sb	1.35 E02	2.60 E02	0.52
^{106}Ru	2.45 E02	3.27 E02	0.75
^{144}Ce	4.07 E02	5.16 E02	0.79
^{154}Eu	3.63 E01	6.44 E01	0.56

a. Calculated using core uranium inventory of 8.357 E07 g.

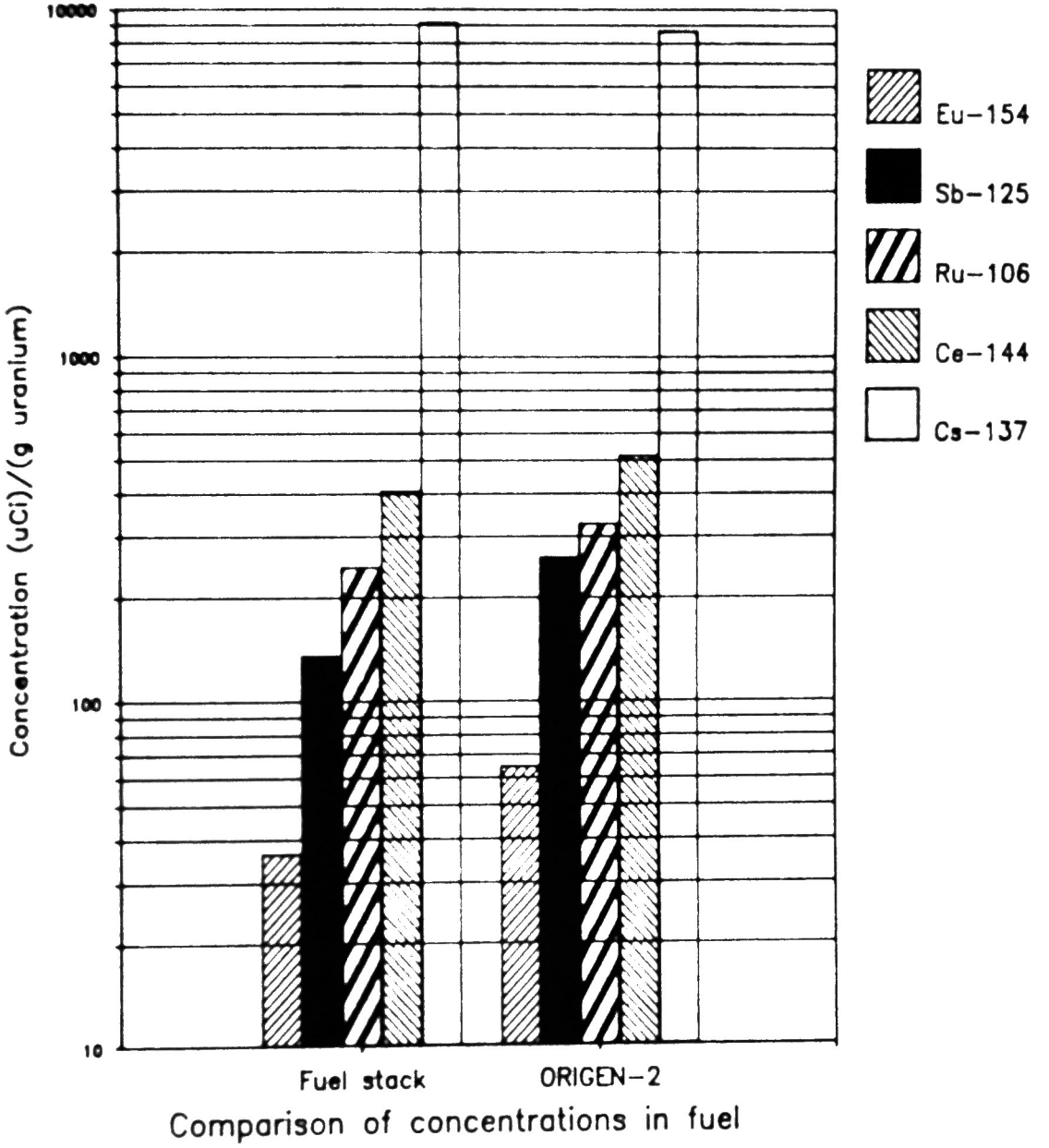

Figure 21. Comparison of measured and theoretical fuel stack radionuclide concentrations.

The results presented in Table 15 show that, using the calculated mass of material in the umbra of the detector's field of view, the measured concentrations of radionuclides in the bulk material of the fuel bundles generally agree quite well with the ORIGEN2 results. The average measured concentrations of ^{134}Cs, ^{137}Cs, ^{106}Ru, and ^{144}Ce in the fuel bundles are, respectively, 135, 6190, 165, and 276 μCi/g, which all agree to within about 20% of their corresponding ORIGEN2 concentrations. The concentrations of ^{125}Sb and ^{154}Eu in the bulk material of the fuel bundles are, on the other hand, significantly lower than their ORIGEN2 values. Their measured concentrations are 92.0 and 24.5 μCi/g, respectively, while their concentrations determined using ORIGEN2 are 168 and 41.6 μCi/g, respectively. Because ^{125}Sb is both a fission product and an activation product and ^{154}Eu is purely an activation product, it is probable that the ORIGEN2 inventories of these two radionuclides are not correct. The data indicate that the ORIGEN2 inventories for these two radionuclides are both too high by about a factor of two. The cumulative concentration of the detected radionuclides in the fuel bundles is 6940 μCi/g, which is about 7% higher than the corresponding ORIGEN2 value.

The results presented in Table 15 show that the concentrations of ^{137}Cs in the ceramic and agglomerate segments are, respectively, only about 1% and 4% of the average ^{137}Cs concentration in the bulk material of the fuel bundles. The concentrations of ^{60}Co, ^{125}Sb, and ^{106}Ru are, on the other hand, between factors of 5 and 10 higher in the previously molten material than in the bulk material of the fuel bundles. The concentrations of ^{144}Ce and ^{154}Eu in the ceramic segment are between 40% and 50% of their respective average concentrations in the bulk material of the core bore fuel bundles. The average concentrations of these same radionuclides in the agglomerate segments are somewhat higher, being between 55% and 70% of their respective average concentrations in the fuel bundles.

The data presented in Table 16 show that, using the calculated mass of uranium in the umbra of the detector's field of view, the measured average radionuclide concentrations in the fuel in the fuel bundles generally agree

quite well with similar ORIGEN2 results. The only exceptions are ^{125}Sb and ^{154}Eu; as was the case in the bulk material of the fuel bundles, the measured concentrations of ^{125}Sb and ^{154}Eu in the fuel are only about one-half of their corresponding ORIGEN2 concentrations.

5. OBSERVATIONS AND CONCLUSIONS

Principal observations made and conclusions determined from the photographic examinations and high-resolution gamma ray spectroscopy measurements performed on the nine core bore samples include the following:

- The lengths of the fuel rods in the core bore samples as determined from examinations of the photographs are: K-9, 0.5 m; G-8, 0.65 m; O-7, 0.76 m; D-8, 1.14 m; G-12, 1.19 m; N-12, 1.23 m; N-5, 1.25 m; D-4, 1.26 m; and O-9, 1.66 m.

- The lengths of the fuel rods as determined from examinations of the photographs of the core bore samples differ from the lengths determined via the CCTV inspections of the core bore holes. Five of the core bore samples contained fuel rods that are shorter than the lengths determined via the CCTV inspections of their core bore holes. The differences in length range from 5 cm for core bore D-4 to 42 cm for core bore O-7. The fuel rods in core bore samples O-9 and N-5 are, respectively, 48 and 6 cm longer than their lengths determined via the CCTV inspections of their core bore holes.

- A number of core bore samples contained large-diameter ceramic and/or agglomerate core segments. Ceramic core segments, each about 7-cm long, were present in core bore samples K-9, D-8, and G-12. Agglomerate core segments, from 8- to 13-cm long, were present in core bore samples K-9, G-8, D-8, and O-7.

- Ceramic and/or agglomerate fragments, ranging in diameter from 0.6 to 5.1 cm, were present in most of the core bore samples.

- The average activities of ^{134}Cs, ^{137}Cs, ^{144}Ce, and ^{154}Eu in undamaged regions of the fuel rod stacks removed from the bottoms of the rods are reasonably constant throughout the core. Excluding the data for core bore sample K-9, the average

activities of these radionuclides in cross sections of the fuel bundles are: ^{134}Cs, 0.022 ± 0.001 Ci; ^{137}Cs, 1.01 ± 0.04 Ci; ^{144}Ce, 0.045 ± 0.001 Ci; and ^{154}Eu, 0.0040 ± 0.0003 Ci. The activities are corrected for sample self-attenuation and are decay-corrected to April 1, 1986.

- The average activities of ^{60}Co, ^{106}Ru, and ^{125}Sb in cross sections of the fuel stacks (except K-9) are: ^{60}Co, 0.009 ± 0.003 Ci, ^{106}Ru, 0.027 ± 0.004 Ci; and ^{125}Sb, 0.015 ± 0.002 Ci.

- The average activities of the previously mentioned radionuclides in cross sections of the K-9 fuel bundle are typically one-half their corresponding average activities in the other eight fuel bundles.

- The relative abundances of ^{134}Cs, ^{137}Cs, ^{106}Ru, and ^{144}Ce in the fuel bundles agree quite well with their core average relative abundances calculated using ORIGEN2. This indicates that the inventories of these radionuclides in undamaged regions of the fuel bundles have not been appreciably depleted.

- The relative abundances of ^{125}Sb and ^{154}Eu in the same regions of the fuel bundles are both about one-half their core average relative abundances calculated using ORIGEN2. Because ^{125}Sb is both a fission product and an activation product and ^{154}Eu is purely an activation product, it is plausible that the ORIGEN2 results for these two radionuclides are not correct. The results indicate that the ORIGEN2 core average inventories for these two radionuclides are both about a factor of two too high.

- In contrast to the results for the fuel bundles, the data indicate that ^{106}Ru, ^{125}Sb, and ^{60}Co are the dominant activities in the majority of the ceramic and agglomerate materials in the core bore samples.

- The measured activities and per cent of total measured activity in a cross section of the ceramic segment in core bore K-9 for ^{106}Ru, ^{125}Sb, and ^{60}Co are: ^{106}Ru, 0.27 Ci and 47.5%; ^{125}Sb, 0.19 Ci and 33.2%; and ^{60}Co, 0.069 Ci and 12.3%.

- The average activities of ^{106}Ru, ^{125}Sb, and ^{60}Co in cross sections of the large-diameter agglomerate segments in core bore samples O-7 and D-8 are, respectively, 0.40, 0.18, and 0.071 Ci. These activities correspond to 54.1%, 24.3%, and 9.5% of the average total activity in cross sections of the samples.

- While the average ^{137}Cs activity in cross sections of the fuel bundles is 1.01 ± 0.04 Ci, its average activities in cross sections of the ceramic and agglomerate core segments are only 0.012 and 0.052 Ci, respectively. These activities correspond to only 1.2% and 5.2% of the average ^{137}Cs activity in cross sections of the fuel bundles.

- The data indicate that about 98% of the ^{137}Cs originally retained in the fuel that was assimilated into the ceramic material was lost from the ceramic material and that about 95% of the original inventory of ^{137}Cs associated with the fuel in the agglomerate material was lost from the agglomerate material.

- Using the mass of material in the umbra of the detector's field of view, the average concentrations of ^{134}Cs, ^{137}Cs, ^{106}Ru, and ^{144}Ce in the bulk material of the fuel bundles are, respectively, 135, 6190, 165, and 276 μCi/g. These concentrations agree to within about 20% of their corresponding core average concentrations calculated using ORIGEN2.

- The measured concentrations of ^{125}Sb and ^{154}Eu in the bulk material of the fuel bundles are 92 and 24.5 μCi/g, respectively. These values are both about a factor of two lower than their corresponding core average concentrations calculated using ORIGEN2.

- Using the mass of uranium in the umbra of the detector's field of view, the average concentrations of ^{134}Cs, ^{137}Cs, ^{106}Ru, and ^{144}Ce in the fuel in the fuel bundles are, respectively, 199, 9100, 245, and 407 μCi/g uranium. These concentrations agree to within 25% of similar values calculated using ORIGEN2.

- The measured concentrations of ^{125}Sb and ^{154}Eu in the fuel in the fuel bundles are, respectively, 135 and 36.3 μCi/g uranium. These values are about one-half the corresponding values calculated using ORIGEN2.

- The results indicate that the concentrations of ^{137}Cs in the large-diameter ceramic and agglomerate core segments are only about 1% and 4% of the average ^{137}Cs concentration in the bulk material of the fuel bundles.

- The concentrations of ^{60}Co, ^{125}Sb, and ^{106}Ru are, on the other hand, factors of between 5 and 10 higher in the previously molten material than in the bulk material of the fuel bundles. Apparently these radionuclides have been concentrated in the ceramic and agglomerate materials.

- The concentrations of ^{144}Ce and ^{154}Eu in the ceramic core segment in core bore sample K-9 are between 40% and 50% of their respective concentrations in the bulk material of the fuel bundles. The average concentrations of these same radionuclides in the large-diameter agglomerate core segments are between 55% and 70% of their respective average concentrations in the bulk material of the fuel bundles.

6. REFERENCES

1. D. W. Akers, et. al, TMI-2 Core Debris Grab Samples--Examination and Analysis, Part 1, GEND-INF-075, September 1986.

2. L. Beller and H. Brown, Design and Operation of the Core Topography Data Acquisition System for TMI-2, GEND-INF-012, May 1984.

3. E. Tolman et al, TMI-2 Core Bore Acquisition Summary Report, EGG-TMI-7385, Rev. 1, February 1987.

4. E. Tolman et al, TMI-2 Accident Scenario Update, EGG-TMI-7489, December 1986.

5. NSAC/25, TMI-2 Accident Core Heat-Up Analysis - A Supplement, Nuclear Safety Analysis Center (NSAC), Electric Power Research Institute (EPRI), Palo Alto, CA.

6. J. O. Carlson, TMI-2 Core Examination Plan, EGG-TMI-6169, July 1984.

7. A. E. Proctor and D. W. Akers, "TMI Spectrometer Design Package,"

8. H. H. Bolotin et al., "Simple Technique for Precise Determinations of Counting Losses in Nuclear Pulse Processing Systems," Nucl. Instr. and Meth., 83, 1970, pp. 1-12.

9. A. E. Proctor, RICKI: A Compact Gamma Analysis Code for the IBM Personal Computer, EGG-PHY-7545, February 1987.

10. T. Mukoyama, "Fitting of Gaussian to Peaks by Non-Iterative Method," Nucl. Instr. and Meth., 125, 1975, pp. 289-291.

11. Gulf General Atomic, Inc., Self-Shielding Correction for Photon Irradiation of Slab and Cylindrical Samples, Progress Report GA-9614 (July 1, 1968- June 30, 1969).

12. J. L. Parker, The Use of Calibration Standards and the Correction for Sample Self-Attenuation in Gamma-Ray Nondestructive Assay, LA-10045, August 1984.

13. R. L. Bunting, "ISOLIB Gamma-Ray Library Listing for Gamma-Ray Library from INEL(DDMF) DATAMASTER", August 23, 1979.

APPENDIX A

GAMMA RAY SPECTROMETER/SCANNER SYSTEM

APPENDIX A

GAMMA RAY SPECTROMETER/SCANNER SYSTEM

Detailed schematics of the gamma ray spectrometer/scanner system are given as Figures A-1 through A-3.

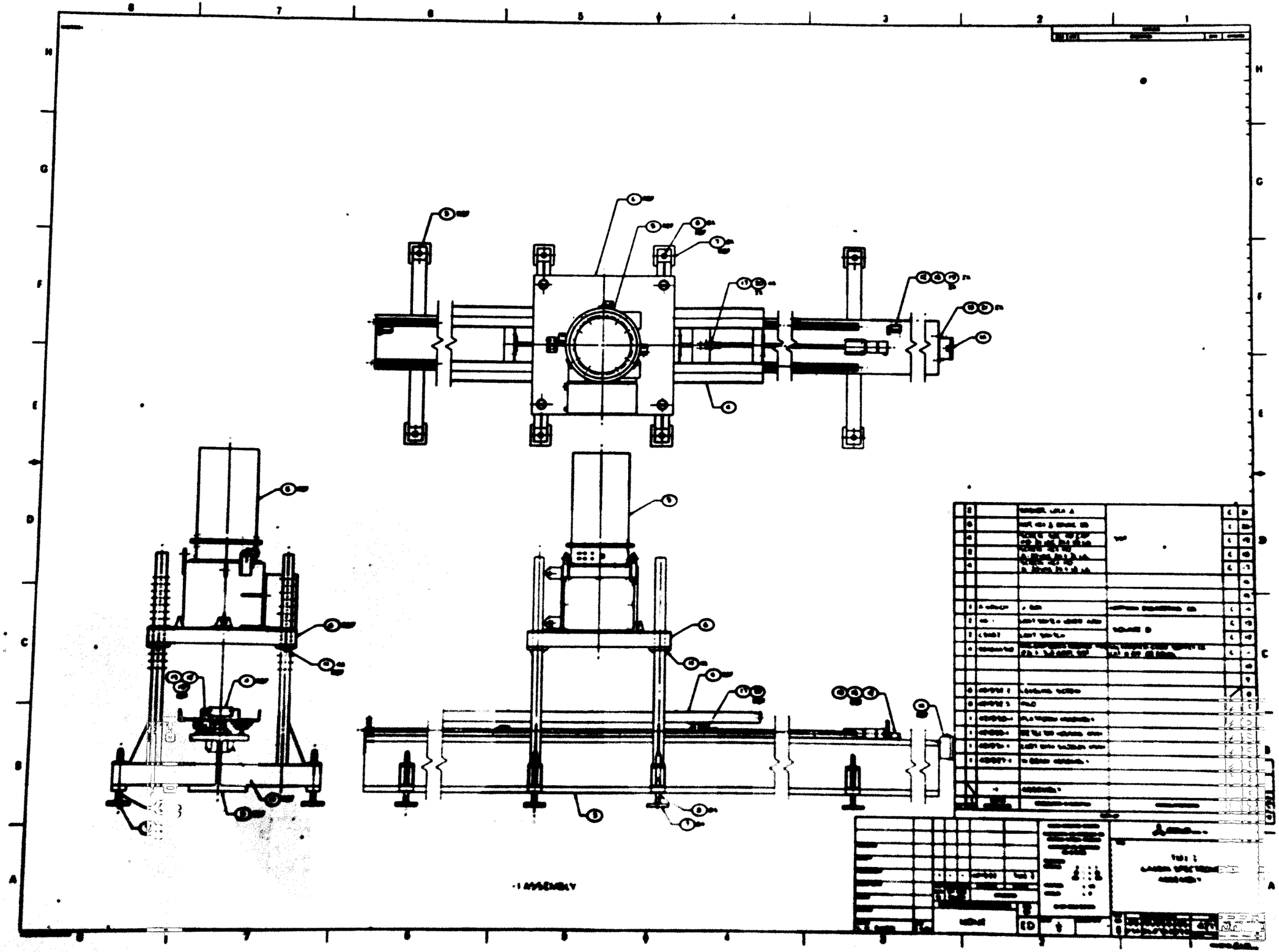

Figure A-1. Gamma spectrometer assembly.

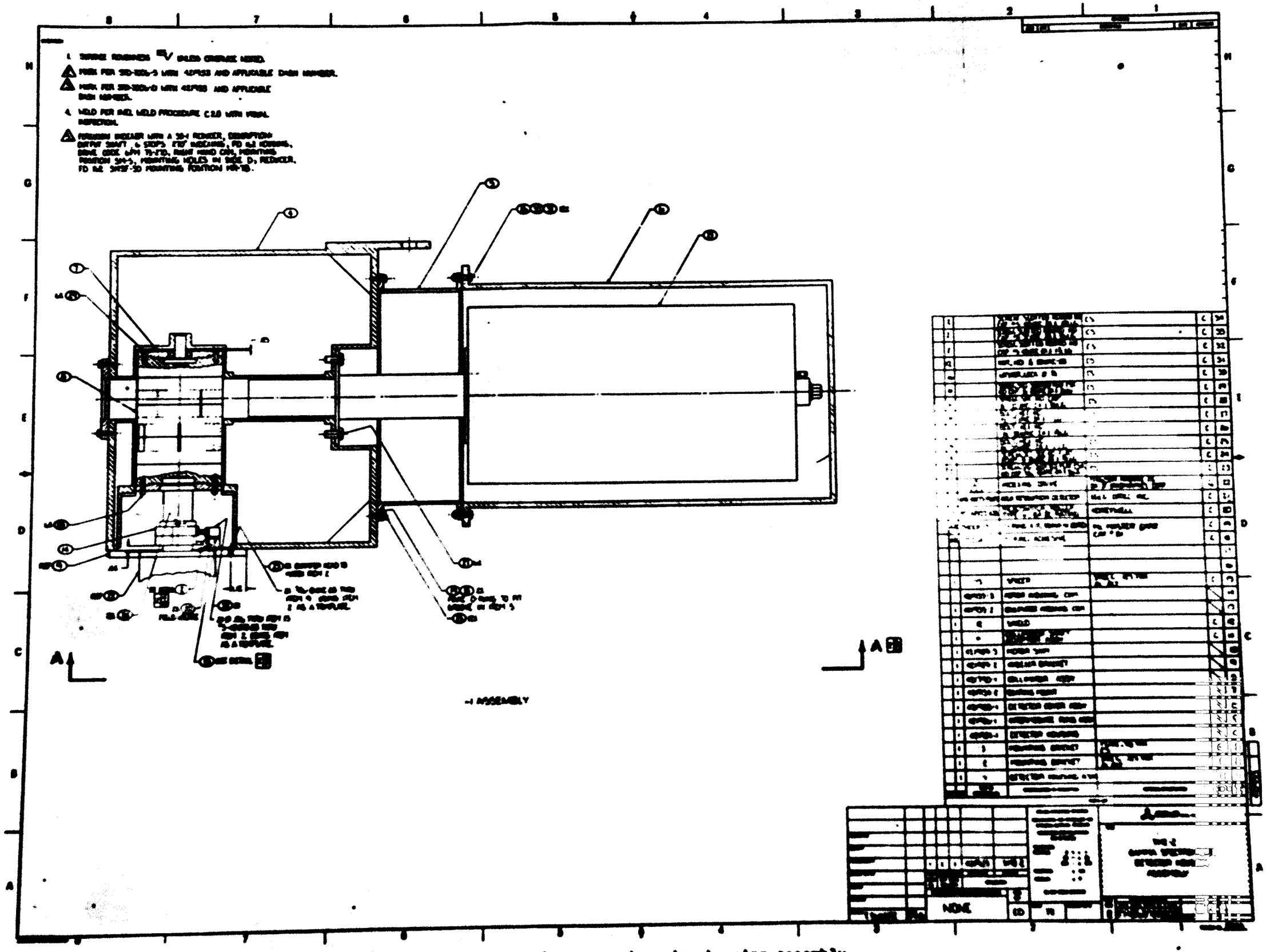

Figure A-2. Gamma spectrometer housing assembly.

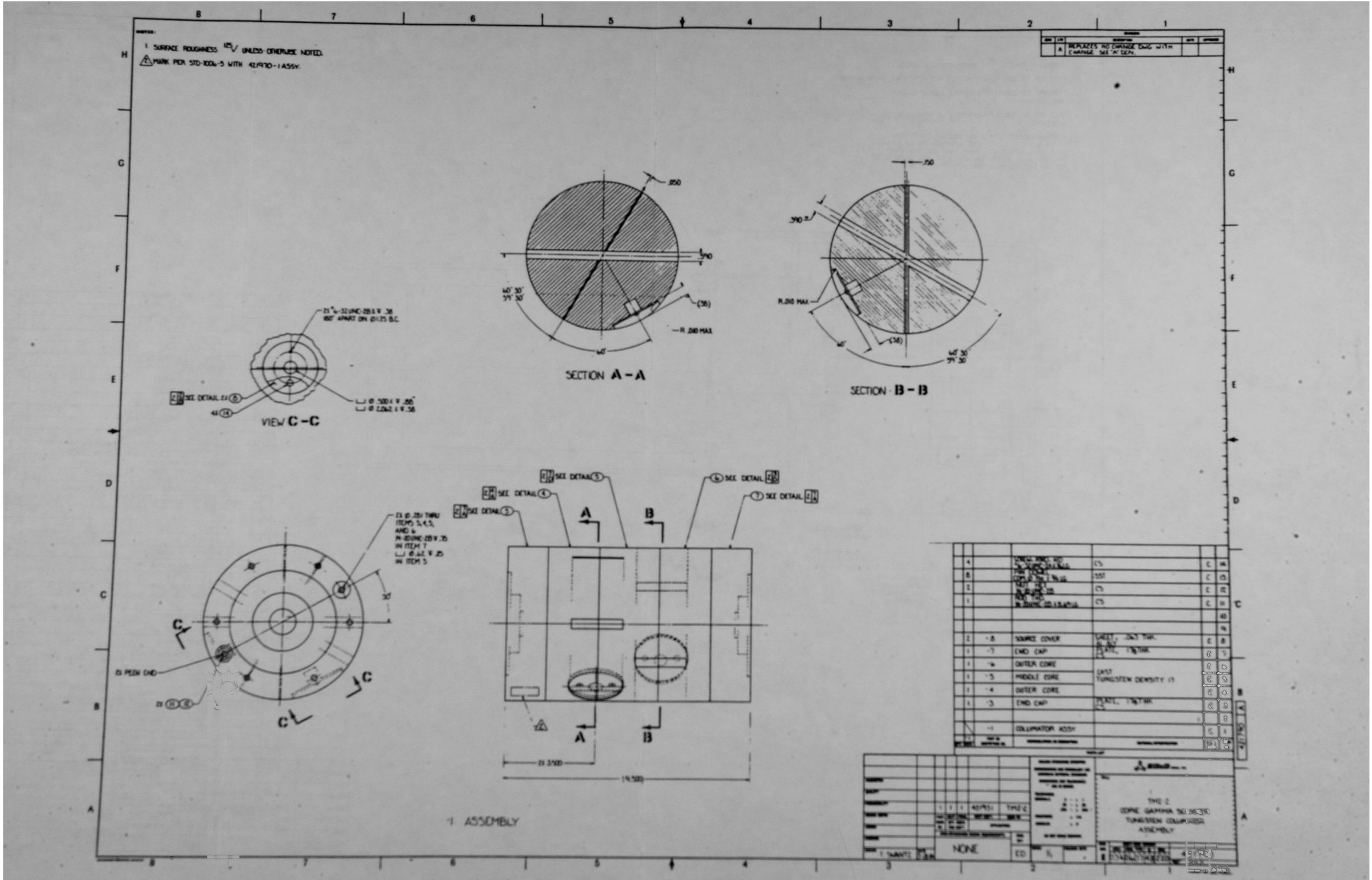

Figure A-3. Core gamma scanner tungsten collimator assembly.

APPENDIX B

PHOTOGRAPHS OF CORE BORE SAMPLES

APPENDIX B

PHOTOGRAPHS OF CORE BORE SAMPLES

The following photographs were taken of the nine TMI-2 core bore samples after their arrival at the INEL (Figures B-1 through B-9).

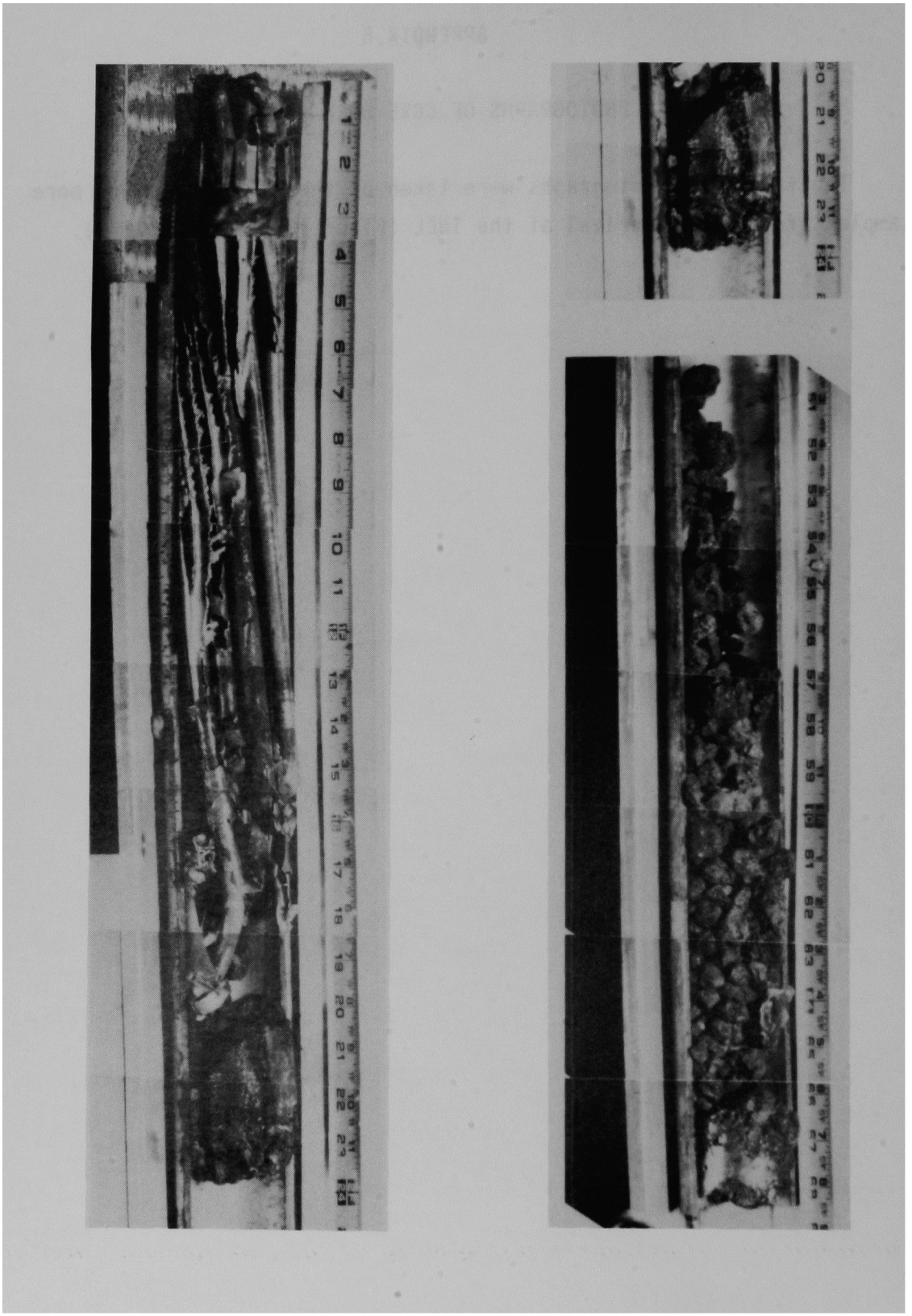

Figure B-1. Photograph of core bore K-9.

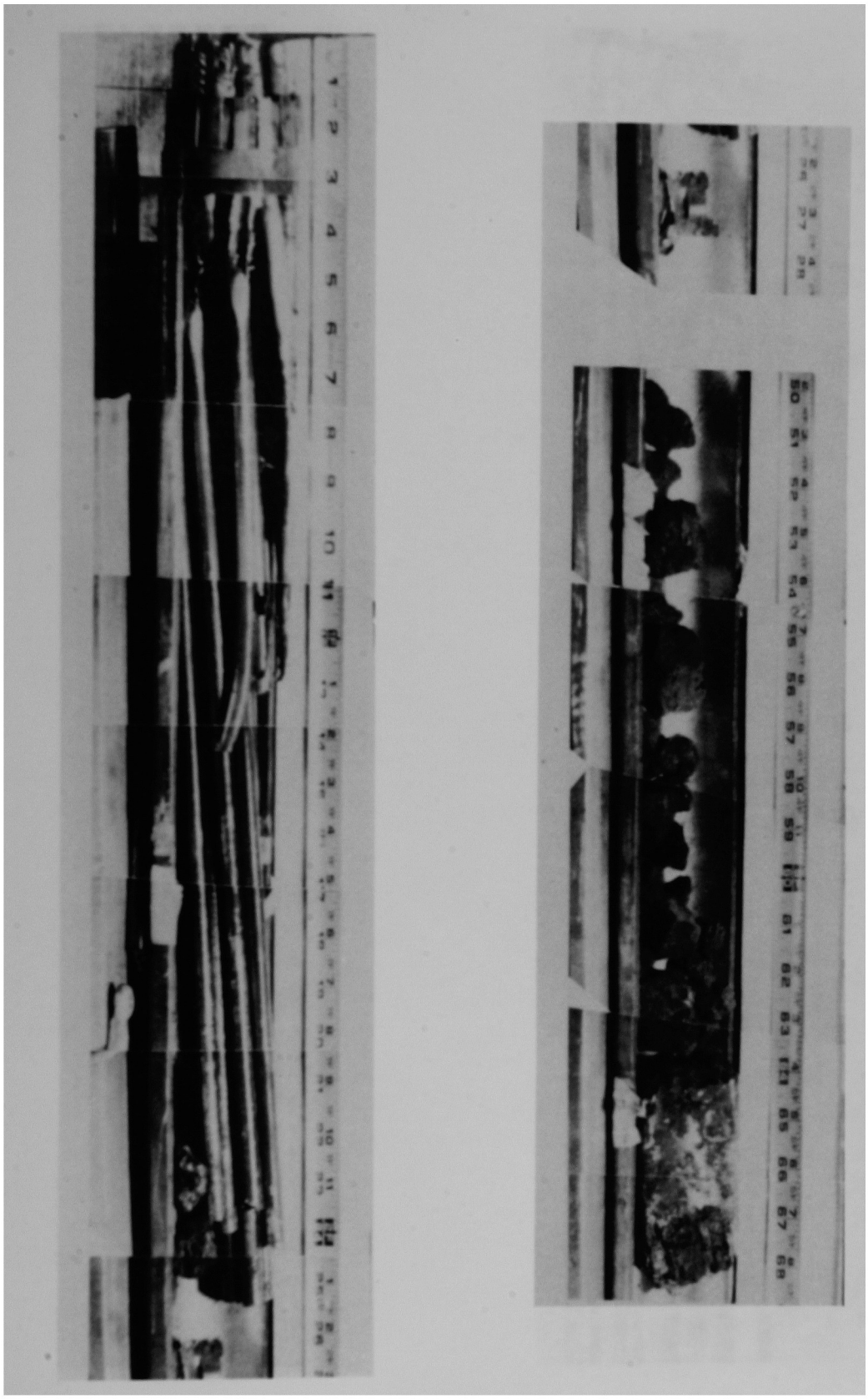

Figure B-2. Photograph of core bore G-8.

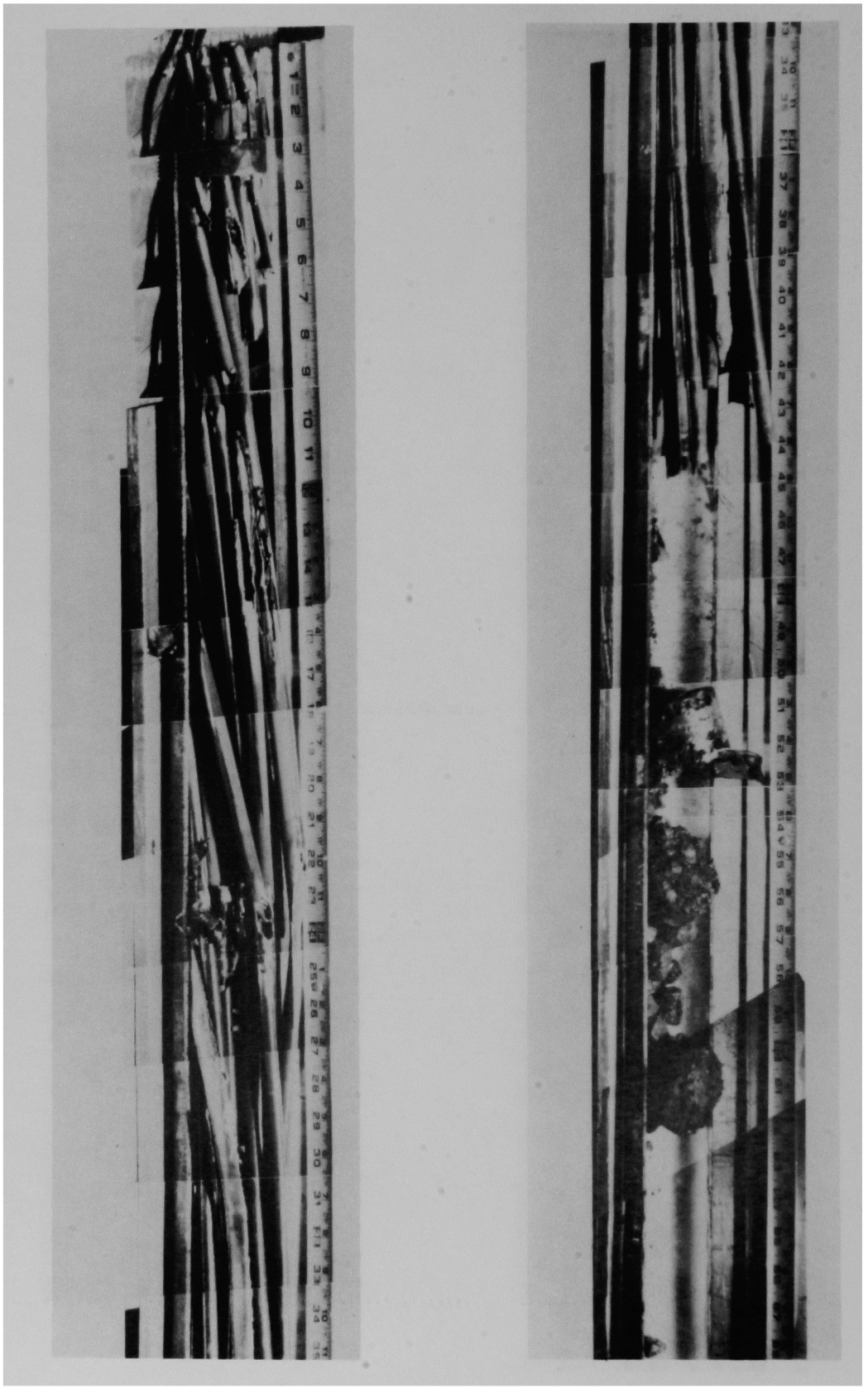

Figure B-3. Photograph of core bore D-8.

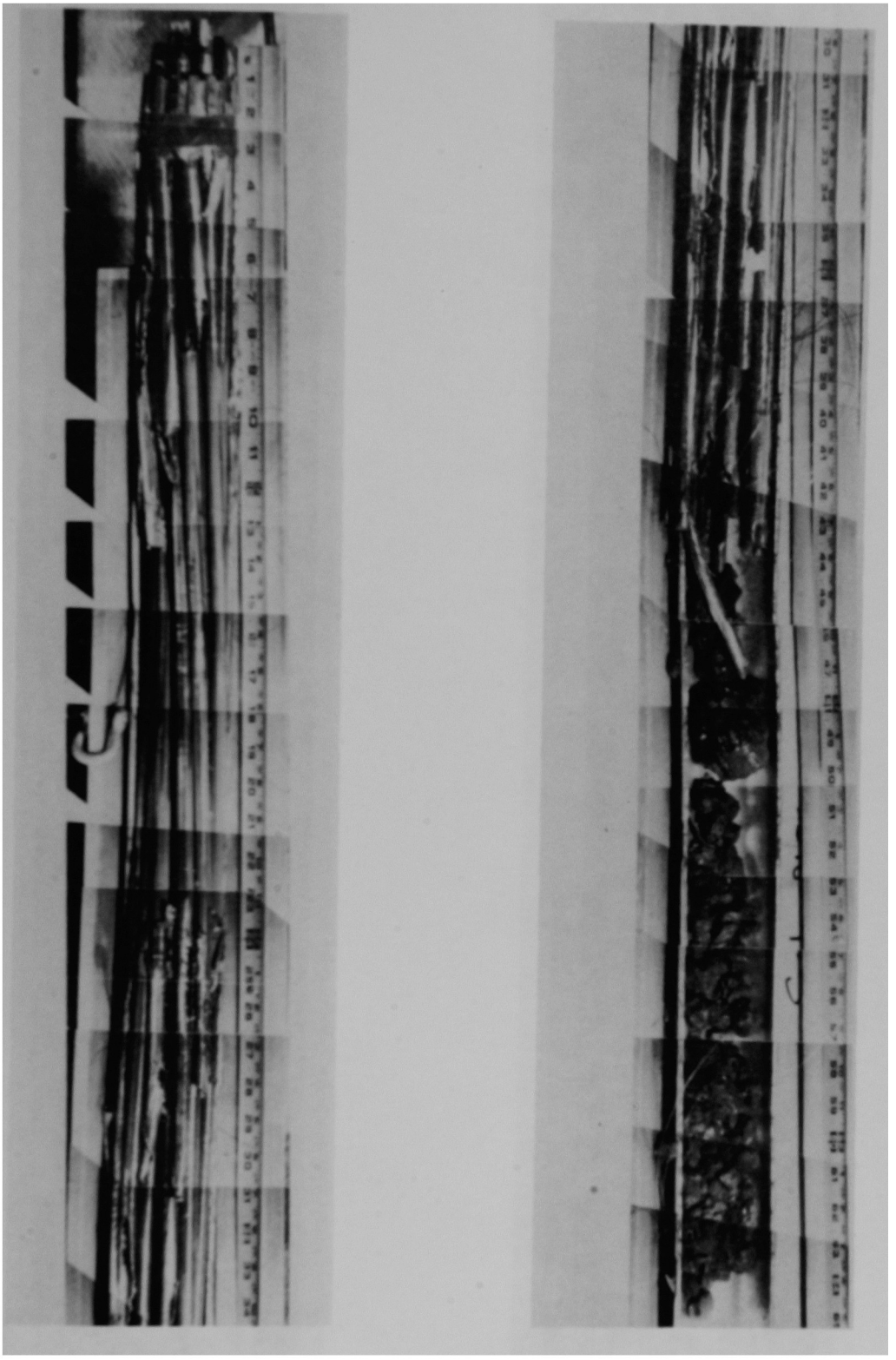

Figure B-4. Photograph of core bore G-12.

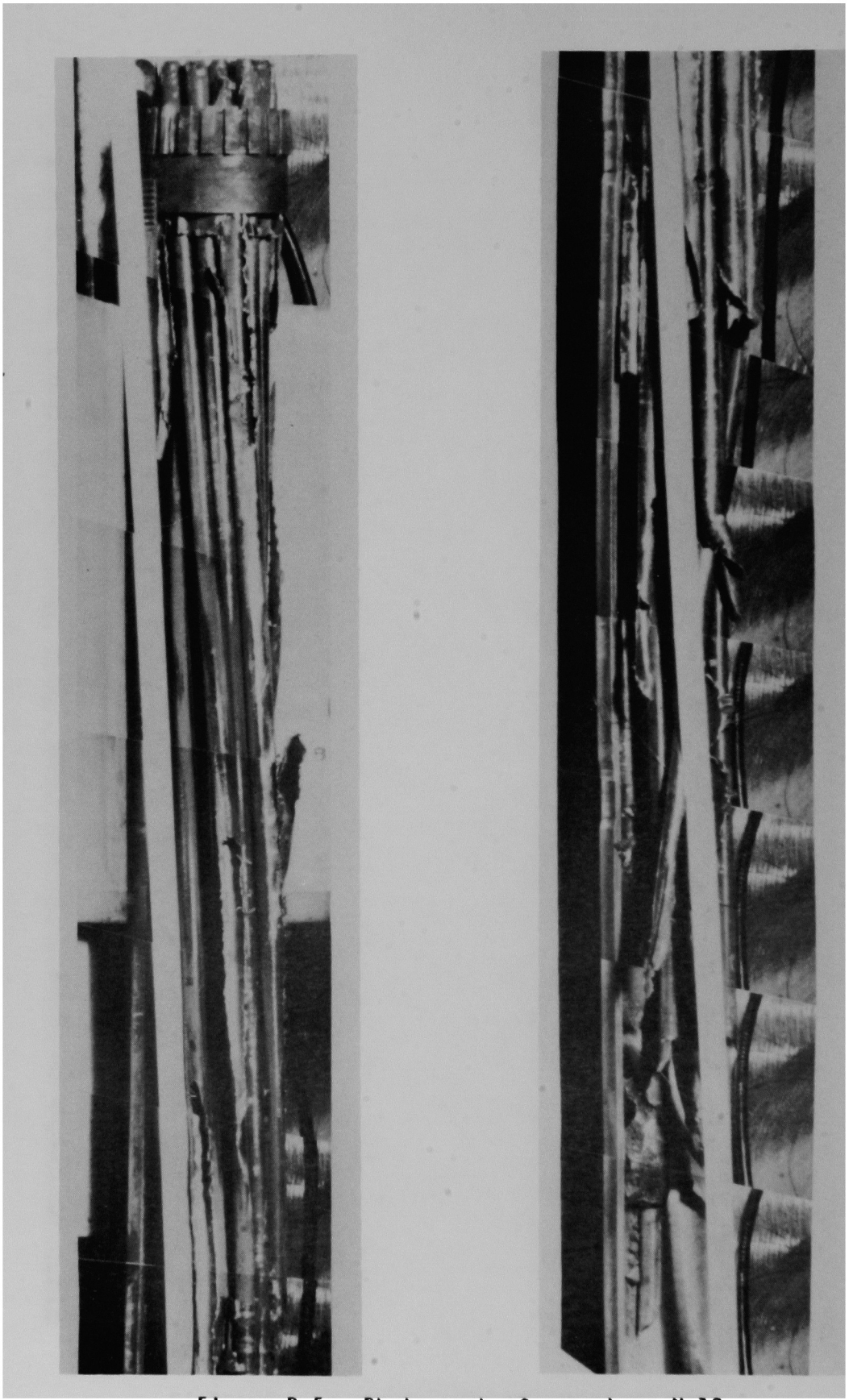

Figure B-5. Photograph of core bore N-12.

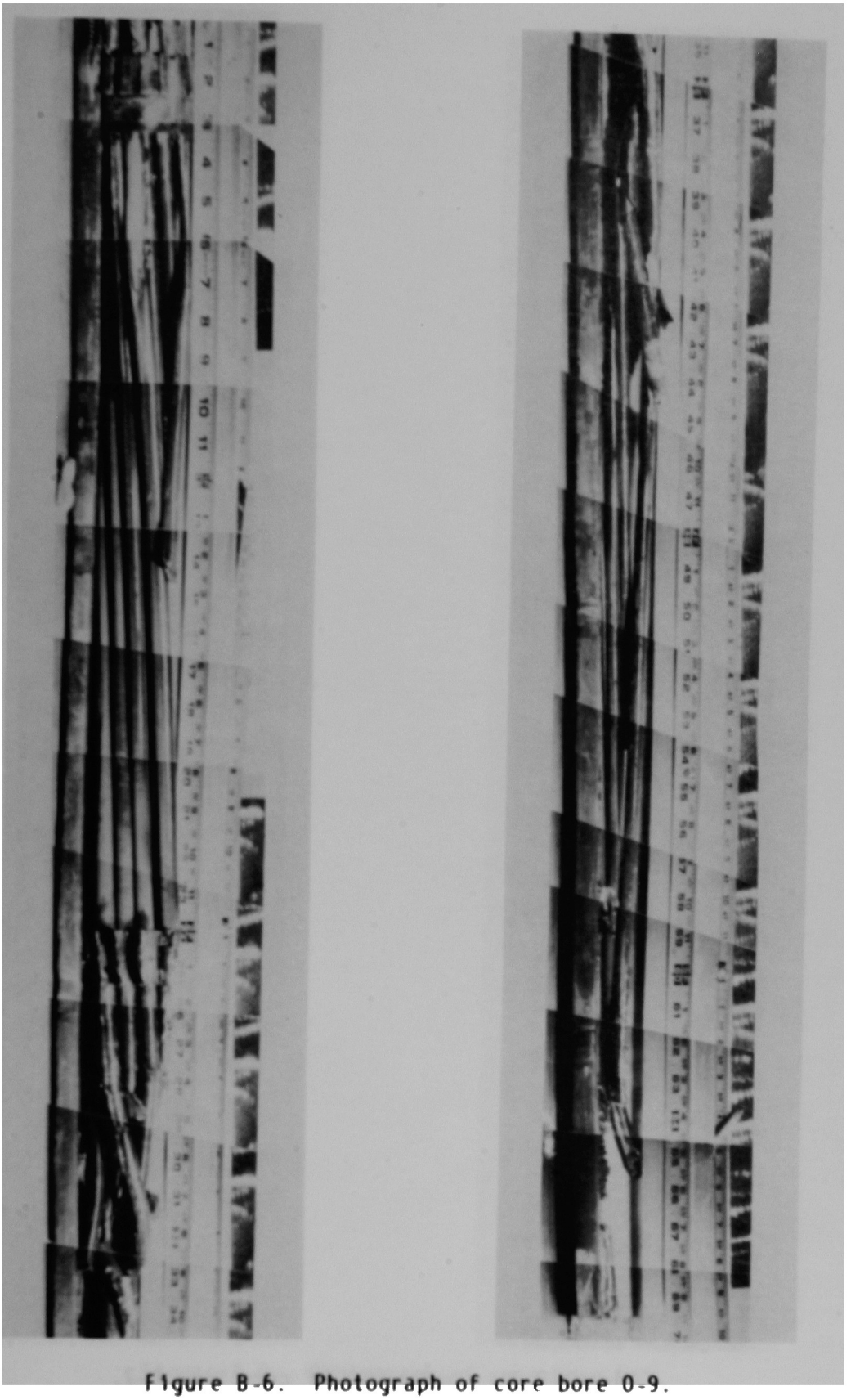

Figure B-6. Photograph of core bore O-9.

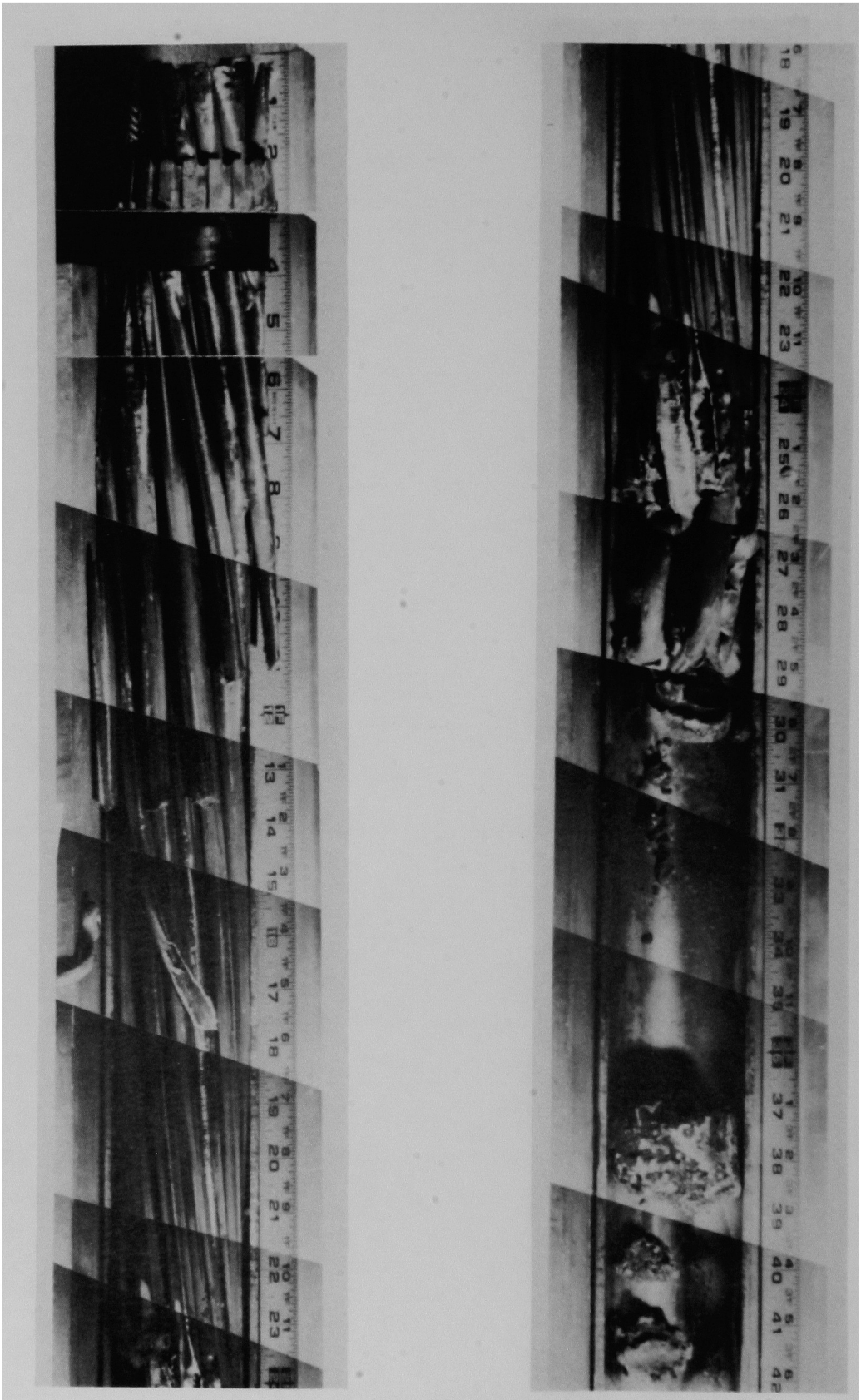

Figure B-7. Photograph of core bore 0-7.

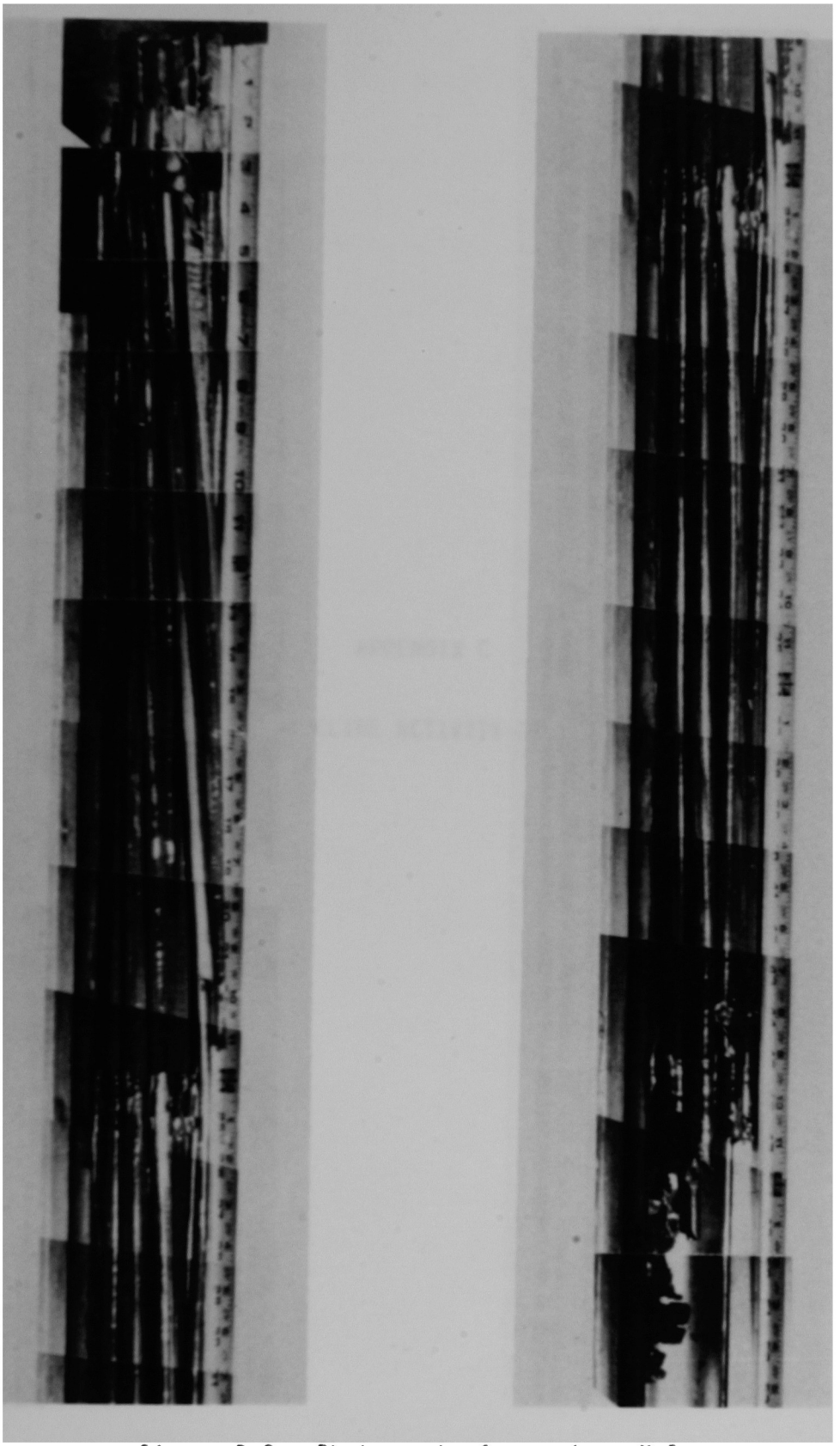

Figure B-8. Photograph of core bore N-5.

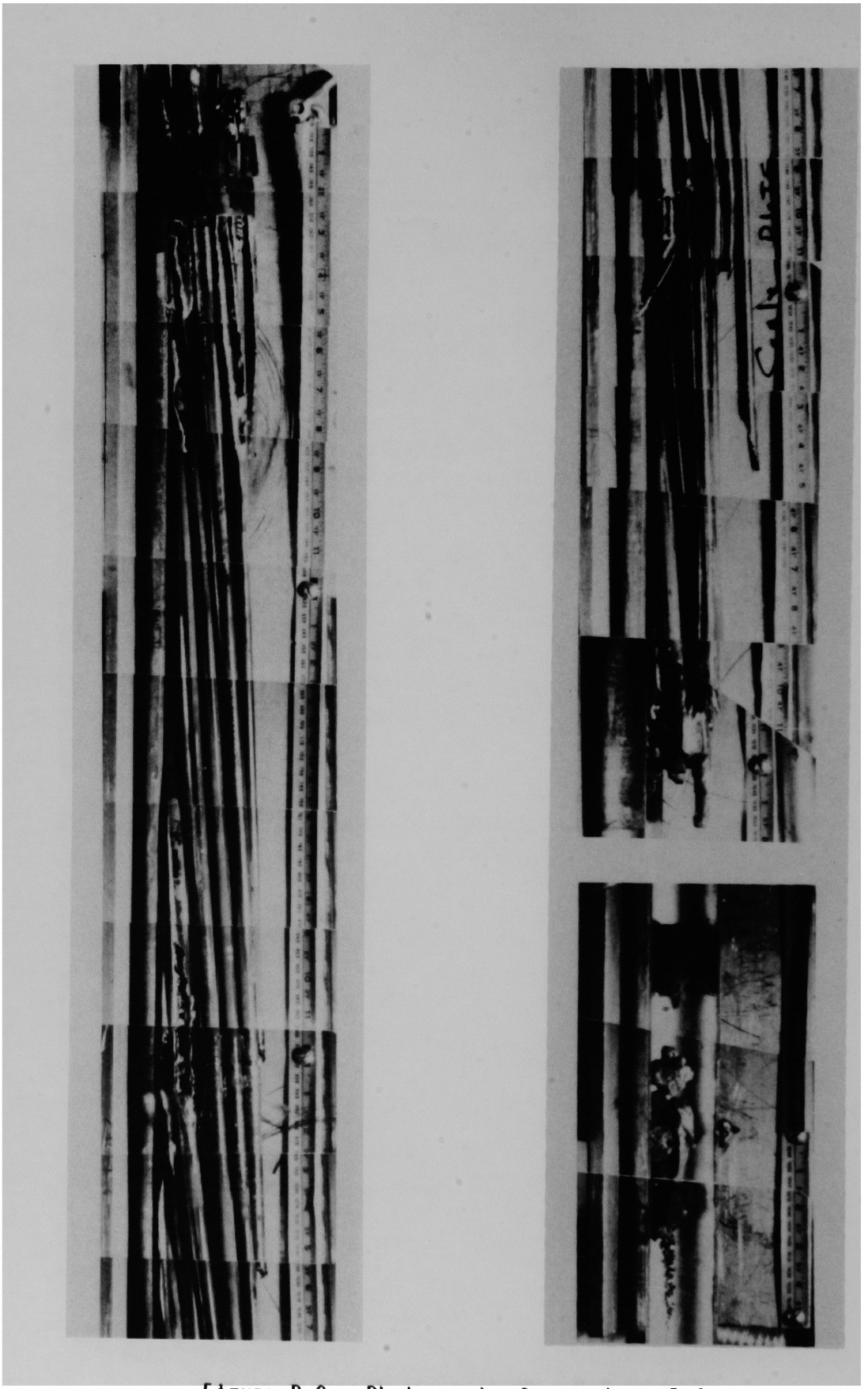

Figure B-9. Photograph of core bore D-4.

APPENDIX C

RADIONUCLIDE ACTIVITY PROFILES

APPENDIX C

RADIONUCLIDE ACTIVITY PROFILES

Radionuclide activity profiles for the nine TMI-2 core bore samples are presented in Tables C-1 through C-9.

TABLE C-1. CORE BORE K-9 RADIONUCLIDE ACTIVITIES IN MICROCURIES (DECAY-CORRECTED TO 4/1/86)

Position[a]	^{134}Cs	^{137}Cs	^{60}Co	^{110m}Ag	^{125}Sb	^{106}Ru	^{144}Ce	^{154}Eu	Total
124.5	ND[b]	ND	ND	ND	ND	ND	ND	ND	ND
121.9	ND	ND	ND	ND	ND	ND	ND	ND	ND
119.4	ND	ND	ND	ND	ND	ND	ND	ND	ND
116.8	ND	ND	ND	ND	ND	ND	ND	ND	ND
114.3	ND	ND	ND	ND	ND	ND	ND	ND	ND
111.8	ND	ND	ND	ND	ND	ND	ND	ND	ND
109.2	ND	ND	2.40 E+01	ND	ND	ND	ND	ND	2.40 E+01
106.7	3.66 E+01	6.75 E+02	4.57 E+03	ND	5.60 E+03	1.56 E+04	ND	5.35 E+02	3.34 E+04
104.1	ND	ND	9.80 E+01	ND	ND	ND	ND	ND	9.80 E+01
101.6	ND	1.06 E+02	1.72 E+02	ND	1.24 E+02	5.71 E+02	2.06 E+03	1.88 E+02	3.30 E+03
99.1	ND	3.71 E+02	1.49 E+03	ND	1.34 E+03	6.09 E+03	6.61 E+03	4.12 E+02	1.63 E+04
96.5	ND	3.17 E+03	1.28 E+04	ND	4.58 E+03	3.32 E+04	1.82 E+04	1.98 E+03	6.34 E+04
94.0	ND	5.76 E+03	3.13 E+04	ND	2.13 E+04	1.02 E+05	ND	1.98 E+03	6:34 E+04
91.4	ND	2.68 E+03	2.72 E+04	ND	2.37 E+04	9.51 E+04	1.22 E+04	1.03 E+03	1.68 E+05
88.9	ND	2.33 E+03	1.36 E+04	ND	3.00 E+04	4.93 E+04	1.26 E+04	1.00 E+03	1.04 E+05
86.4	5.64 E+01	2.30 E+03	1.88 E+03	ND	2.10 E+03	5.82 E+03	1.04 E+04	1.50 E+03	2.42 E+05
83.8	5.05 E+01	1.68 E+03	5.03 E+02	ND	ND	ND	1.56 E+04	1.73 E+03	1.96 E+05
81.3	6.46 E+01	1.76 D+03	5.52 E+02	ND	ND	ND	2.05 E+04	1.59 E+03	2.45 E+04
78.7	ND	1.47 E+03	8.30 E+02	ND	1.50 E+02	9.89 E+02	2.08 E+04	1.69 E+03	2.59 E+04
76.2	ND	1.22 E+03	6.56 E+02	ND	ND	ND	1.53 E+04	1.56 E+03	1.87 E+04
73.7	ND	1.43 E+03	1.69 E+03	ND	4.76 E+02	2.20 E+03	1.56 E+04	1.33 E+03	2.27 E+04
71.1	4.13 E+01	1.42 E+03	1.27 E+03	ND	5.57 E+02	1.89 E+03	1.27 E+04	1.11 E+03	1.90 E+04
68.6	4.96 E+01	1.09 E+03	7.88 E+02	ND	ND	1.02 E+03	1.27 E+04	1.21 E+03	1.69 E+04
66.0	5.37 E+01	1.19 E+03	2.44 E+03	ND	1.03 E+03	3.90 E+03	1.78 E+04	1.20 E+03	2.76 E+04
63.5	6.47 E+01	1.86 E+03	2.14 E+03	ND	7.15 E+02	2.67 E+03	1.22 E+04	1.31 E+03	2.10 E+04
61.0	1.49 E+02	1.86 E+03	2.90 E+03	ND	1.47 E+02	5.23 E+03	1.51 E+04	1.53 E+03	3.01 E+04
58.4	1.77 E+02	6.15 E+03	6.75 E+03	ND	9.50 E+03	1.78 E+04	1.22 E+04	1.21 E+03	5.38 E+04
55.9	1.72 E+02	3.92 E+03	7.81 E+03	ND	8.35 E+03	2.00 E+04	9.37 E+03	8.74 E+02	5.05 E+04
50.8	3.38 E+02	8.19 E+03	8.51 E+03	ND	5.79 E+03	1.93 E+04	6.80 E+03	1.03 E+03	5.00 E+04
48.3	3.18 E+02	8.31 E+03	5.76 E+03	ND	3.45 E+03	1.18 E+04	1.22 E+04	1.15 E+03	4.30 E+04
45.7	1.92 E+03	5.93 E+04	2.34 E+04	ND	7.21 E+03	4.33 E+04	ND	1.22 E+03	1.36 E+05
43.2	3.30 E+03	8.15 E+04	2.17 E+04	ND	7.01 E+03	2.52 E+04	9.84 E+03	1.08 E+03	1.50 E+05
40.6	2.46 E+03	7.96 E+04	1.63 E+04	ND	4.33 E+03	ND	7.71 E+03	8.29 E+02	1.11 E+05
38.1	6.89 E+02	2.33 E+04	9.71 E+03	ND	2.76 E+03	6.63 E+03	ND	3.71 E+02	4.35 E+05

TABLE C-1. (CONTINUED)

Position[a]	^{134}Cs	^{137}Cs	^{60}Co	^{110m}Ag	^{125}Sb	^{106}Ru	^{144}Ce	^{154}Eu	Total
35.6	5.72 E+02	1.80 E+04	1.81 E+03	ND	8.14 E+02	1.37 E+03	2.45 E+03	1.32 E+02	2.52 E+04
33.0	8.66 E+02	3.34 E+04	4.74 E+03	ND	1.96 E+03	2.83 E+03	9.70 E+03	3.42 E+02	5.38 E+04
30.5	2.07 E+03	8.11 E+04	5.61 E+03	ND	2.30 E+03	ND	ND	5.82 E+02	9.17 E+04
27.9	2.83 E+03	1.03 E+05	2.89 E+03	ND	1.11 E+03	6.91 E+03	ND	6.91 E+02	1.17 E+05
25.4	4.03 E+03	1.46 E+05	2.36 E+03	ND	1.00 E+03	1.96 E+03	8.44 E+03	8.25 E+02	1.65 E+04
22.9	4.35 E+03	1.64 E+05	5.40 E+02	ND	5.11 E+03	4.86 E+03	2.12 E+04	1.04 E+03	2.01 E+05
20.3	3.28 E+03	1.48 E+05	1.72 E+02	ND	ND	6.12 E+03	ND	9.14 E+02	1.58 E+05
17.8	2.53 E+03	1.25 E+05	4.67 E+02	ND	8.93 E+02	3.84 E+03	4.51 E+03	7.71 E+02	1.38 E+05
15.2	2.14 E+03	1.12 E+05	2.35 E+02	ND	ND	2.38 E+03	ND	7.56 E+02	1.18 E+05
12.7	1.91 E+03	1.07 E+05	4.95 E+02	ND	ND	2.31 E+03	ND	4.85 E+02	1.12 E+05
10.2	1.43 E+03	9.50 E+04	3.28 E+02	ND	1.73 E+03	1.33 E+03	6.98 E+03	4.25 E+02	1.07 E+05
7.6	1.42 E+03	9.35 E+04	6.70 E+02	ND	ND	3.37 E+03	1.19 E+04	2.04 E+02	1.11 E+05
5.1	1.10 E+03	8.63 E+04	5.74 E+02	ND	9.60 E+02	3.77 E+03	1.10 E+04	3.70 E+02	1.04 E+05
2.5	8.83 E+02	8.50 E+04	5.60 E+02	1.42 E+02	7.08 E+02	2.84 E+03	1.14 E+04	2.75 E+02	1.02 E+05
0.0	6.60 E+02	6.16 E+04	2.89 E+03	2.06 E+02	ND	1.24 E+03	ND	6.73 E+01	6.67 E+04
-2.5	ND	7.66 E+03	7.45 E+04	ND	ND	ND	ND	ND	8.22 E+04
-5.1	ND	ND	1.68 E+05	ND	ND	ND	ND	ND	1.68 E+05
-7.6	ND	ND	4.29 E+04	ND	ND	ND	ND	ND	4.29 E+04
-10.2	ND	1.81 E+03	5.49 E+04	ND	ND	ND	ND	ND	5.67 E+04
-12.7	ND	8.76 E+01	4.13 E+02	1.11 E+02	ND	4.20 E+02	ND	ND	1.03 E+03
-15.2	ND	ND	2.75 E+01	ND	ND	ND	ND	ND	2.75 E+01
-17.8	ND	ND	6.87 E+00	ND	ND	ND	ND	ND	6.87 E+00

a. Distance in centimeters from bottom of fuel stack.

b. ND--not detected.

TABLE C-2. CORE BORE G-8 RADIONUCLIDE ACTIVITIES IN MICROCURIES (DECAY-CORRECTED TO 4/1/86)

Position[a]	^{134}Cs	^{137}Cs	^{60}Co	^{110m}Ag	^{125}Sb	^{106}Ru	^{144}Ce	^{154}Eu	Total
79.4	4.26 E+01	1.36 E+03	5.02 E+02	ND[b]	ND	ND	1.19 E+04	1.09 E+03	1.49 E+04
69.2	1.17 E+02	4.12 E-03	3.56 E+02	ND	5.15 E+02	3.23 E+02	9.17 E+03	8.83 E+02	1.55 E+04
59.1	ND	5.96 E+02	4.95 E+02	ND	ND	ND	1.37 E+04	1.04 E+03	1.58 E+04
56.5	8.92 E+01	3.11 E+03	5.13 E+02	ND	ND	ND	1.22 E+04	9.55 E+02	1.69 E+04
54.0	1.37 E+03	4.51 E+04	8.89 E+02	ND	6.30 E+02	1.41 E+03	1.37 E+04	1.38 E+03	6.45 E+04
51.4	2.45 E+03	7.65 E+04	5.72 E+03	ND	3.47 E+03	ND	1.66 E+04	9.13 E+02	1.06 E+05
48.9	3.19 E+03	1.22 E+05	4.24 E+03	ND	1.92 E+03	ND	ND	9.65 E+02	1.32 E+05
46.4	4.60 E+03	1.70 E+05	1.80 E+03	ND	ND	ND	ND	1.40 E+03	1.78 E+05
43.8	5.08 E+03	1.70 E+05	1.51 E+03	ND	ND	ND	1.83 E+04	1.74 E+03	1.97 E+05
41.3	5.29 E+03	1.88 E+05	1.04 E+03	ND	ND	ND	ND	1.56 E+03	1.96 E+05
38.7	5.98 E+03	2.13 E+05	4.66 E+03	ND	ND	5.04 E+03	ND	1.21 E+03	2.30 E+05
26.0	4.75 E+03	1.92 E+05	9.91 E+02	ND	ND	ND	1.46 E+04	1.19 E+03	2.15 E+05
23.5	4.68 E+03	1.94 E+05	6.11 E+02	ND	1.28 E+03	6.50 E+01	1.86 E+04	1.17 E+03	2.20 E+05
15.9	3.98 E+03	1.83 E+05	7.31 E+02	ND	ND	ND	2.59 E+04	7.72 E+02	2.14 E+05
8.3	1.87 E+03	1.40 E+05	7.39 E+02	ND	ND	ND	ND	5.99 E+03	1.43 E+05
0.6	ND	2.88 E+04	5.95 E+04	ND	ND	ND	ND	ND	8.83 E+04
-7.0	ND	1.20 E+04	5.63 E+04	ND	ND	ND	ND	ND	6.83 E+04
-12.1	ND	ND	ND	ND	ND	ND	ND	ND	ND

a. Distance in centimeters from bottom of fuel stack.

b. ND--not detected.

TABLE C-3. CORE BORE D-8 RADIONUCLIDE ACTIVITIES IN MICROCURIES (DECAY-CORRECTED TO 4/1/86)

Position[a]	^{134}Cs	^{137}Cs	^{60}Co	^{110m}Ag	^{125}Sb	^{106}Ru	^{144}Ce	^{154}Eu	Total
165.1	ND[b]	ND	ND	ND	ND	ND	ND	ND	ND
162.6	4.54 E+02	4.26 E+02	1.06 E+03	ND	7.91 E+03	4.59 E+03	ND	ND	1.41 E+04
154.9	ND	ND	ND	ND	ND	ND	ND	ND	ND
144.8	ND	ND	2.30 E+01	ND	ND	ND	ND	ND	2.30 E+01
138.4	2.26 E+02	3.94 E+03	1.55 E+04	2.05 E+04	1.83 E+04	1.22 E+05	2.39 E+04	2.18 E+03	2.07 E+05
134.9	ND	1.48 E+03	1.66 E+03	ND	2.31 E+03	8.05 E+03	1.08 E+04	7.00 E+02	2.50 E+04
113.0	ND	9.26 E+01	3.34 E+01	ND	7.52 E+01	1.90 E+02	ND	3.50 E+01	4.26 E+02
101.6	4.86 E+03	1.55 E+05	6.25 E+02	ND	1.73 E+03	6.96 E+03	7.48 E+03	1.20 E+03	1.78 E+05
96.5	9.62 E+03	2.93 E+05	8.58 E+02	ND	ND	3.31 E+03	2.75 E+04	1.25 E+03	3.36 E+05
86.4	6.52 E+03	1.87 E+05	1.81 E+02	ND	1.74 E+03	9.79 E+03	2.48 E+04	1.86 E+03	2.32 E+05
81.3	4.81 E+03	1.50 E+05	1.00 E+02	ND	4.42 E+02	1.04 E+04	2.03 E+04	1.54 E+03	1.88 E+05
71.1	5.91 E+03	1.73 E+05	2.89 E+02	ND	9.18 E+02	ND	1.70 E+04	1.68 E+03	1.99 E+05
55.0	3.18 E+03	1.09 E+05	3.05 E+02	ND	5.22 E+02	ND	1.66 E+04	1.14 E+03	1.31 E+05
50.8	1.30 E+03	4.11 E+04	5.48 E+03	ND	2.67 E+02	ND	1.02 E+04	4.87 E+02	5.88 E+04
43.2	5.60 E+03	2.06 E+05	1.14 E+02	ND	ND	5.93 E+03	2.23 E+04	1.64 E+03	2.42 E+05
5.1	5.81 E+02	5.66 E+04	2.09 E+02	ND	1.21 E+03	ND	8.50 E+03	2.92 E+02	6.74 E+04
-2.5	ND	ND	5.10 E+05	ND	ND	ND	ND	ND	5.10 E+05

a. Distance in centimeters from bottom of fuel stack.

b. ND--not detected.

TABLE C-4. CORE BORE G-12 RADIONUCLIDE ACTIVITIES IN MICROCURIES (DECAY-CORRECTED TO 4/1/86)

Position[a]	^{134}Cs	^{137}Cs	^{60}Co	^{110m}Ag	^{125}Sb	^{106}Ru	^{144}Ce	^{154}Eu	Total
152.4	2.03 E+02	1.94 E+03	2.09 E+03	ND[b]	ND	2.52 E+03	1.59 E+04	9.22 E+02	2.36 E+04
147.3	1.09 E+02	3.91 E+03	5.80 E+03	ND	4.95 E+03	2.40 E+04	1.46 E+04	9.36 E+02	5.43 E+04
119.4	3.33 E+01	1.22 E+03	1.21 E+03	ND	1.04 E+02	8.35 E+02	1.10 E+04	8.91 E+02	1.53 E+04
109.2	3.93 E+01	1.54 E+03	1.42 E+02	ND	ND	ND	1.10 E+04	8.44 E+02	1.36 E+04
99.1	2.39 E+03	7.94 E+04	9.58 E+01	ND	1.81 E+03	3.32 E+03	7.25 E+03	6.82 E+02	9.49 E+04
86.4	5.34 E+03	1.69 E+05	2.22 E+02	ND	ND	9.62 E+03	1.76 E+04	1.21 E+03	2.03 E+05
73.7	7.60 E+03	2.41 E+05	2.71 E+02	ND	3.02 E+03	ND	1.77 E+04	1.74 E+03	2.71 E+05
71.1	6.42 E+03	2.65 E+05	4.52 E+02	ND	ND	ND	ND	ND	2.72 E+05
61.0	5.67 E+03	1.79 E+05	2.47 E+02	ND	1.60 E+03	8.62 E+03	1.40 E+04	1.55 E+03	2.11 E+05
50.8	4.23 E+03	2.14 E+05	ND	ND	ND	ND	ND	ND	2.18 E+05
43.2	6.52 E+03	2.33 E+05	ND	ND	1.98 E+03	ND	3.40 E+04	1.41 E+03	2.77 E+05
33.0	5.39 E+03	2.27 E+05	ND	ND	ND	ND	ND	1.26 E+03	2.34 E+05
22.9	4.21 E+03	1.87 E+00	1.29 E+02	ND	2.23 E+03	8.70 E+03	1.13 E+04	1.07 E+03	2.15 E+05
10.2	2.36 E+03	1.53 E+05	7.68 E+01	ND	ND	5.20 E+02	1.14 E+04	ND	1.67 E+05
0.0	8.64 E+02	1.03 E+05	4.62 E+02	ND	7.04 E+02	ND	1.13 E+04	3.13 E+02	1.17 E+05
-5.1	ND	7.45 E+03	7.81 E+04	ND	ND	ND	ND	ND	8.56 E+04
-12.7	ND	ND	ND	ND	ND	ND	ND	9.70 E+01	9.70 E+01

a. Distance in centimeters from bottom of fuel stack.

b. ND--not detected.

TABLE C-5. CORE BORE N-12 RADIONUCLIDE ACTIVITIES IN MICROCURIES (DECAY-CORRECTED TO 4/1/86)

Position[a]	^{134}Cs	^{137}Cs	^{60}Co	^{110m}Ag	^{125}Sb	^{106}Ru	^{144}Ce	^{154}Eu	Total
113.7	ND[b]	ND	ND	ND	ND	ND	ND	ND	ND
93.3	3.47 E+03	1.25 E+05	ND	ND	ND	7.51 E+03	ND	8.17 E+02	1.37 E+05
85.7	4.55 E+03	1.63 E+05	ND	ND	ND	ND	2.32 E+04	1.26 E+03	1.92 E+05
47.6	3.88 E+03	1.80 E+05	ND	ND	ND	ND	1.30 E+04	1.33 E+03	1.98 E+05
32.4	4.28 E+03	1.88 E+05	ND	ND	ND	ND	2.94 E+04	1.10 E+03	2.23 E+05
27.3	3.44 E+03	1.72 E+05	ND	ND	ND	ND	2.09 E+04	5.35 E+02	1.97 E+05
22.2	2.33 E+03	1.37 E+05	7.95 E+01	ND	ND	ND	1.91 E+04	6.39 E+02	1.59 E+05
14.6	1.34 E+03	1.04 E+05	ND	ND	ND	ND	1.80 E+04	3.78 E+02	1.24 E+05
9.5	8.43 E+02	8.27 E+04	1.56 E+02	ND	ND	ND	ND	2.66 E+02	8.40 E+04
4.4	5.14 E+02	6.01 E+04	1.91 E+02	ND	5.78 E+02	3.82 E+03	8.07 E+03	1.58 E+02	7.34 E+04
-0.6	ND	1.11 E+04	3.41 E+04	ND	ND	ND	ND	ND	4.52 E+04
-5.7	ND	2.49 E+03	5.08 E+04	ND	ND	ND	ND	ND	5.33 E+04
-10.8	3.20 E+01	1.83 E+03	8.99 E+02	ND	ND	ND	ND	ND	2.76 E+03
-15.9	ND	ND	9.91 E+00	ND	ND	ND	ND	ND	9.91 E+00
-18.4	ND	ND	8.96 E+00	ND	ND	ND	ND	ND	8.96 E+00
-21.0	ND	ND	1.04 E+01	ND	ND	ND	ND	ND	1.04 E+01
-23.5	ND	ND	1.40 E+01	ND	ND	ND	ND	ND	1.40 E+01

a. Distance in centimeters from bottom of fuel stack.

b. ND--not detected.

TABLE C-6. CORE BORE 0-9 RADIONUCLIDE ACTIVITIES IN MICROCURIES (DECAY-CORRECTED TO 4/1/86)

Position[a]	^{134}Cs	^{137}Cs	^{60}Co	^{110m}Ag	^{125}Sb	^{106}Ru	^{144}Ce	^{154}Eu	Total
113.7	ND[b]	8.47 E+01	ND	ND	ND	ND	ND	ND	8.47 E+01
109.9	ND	5.61 E+02	1.57 E+04	ND	3.28 E+04	1.53 E+05	ND	4.60 E+03	2.07 E+05
108.6	5.50 E+01	1.30 E+02	5.92 E+03	ND	1.11 E+04	5.27 E+04	ND	1.72 E+03	7.28 E+04
103.5	3.76 E+02	1.05 E+04	3.16 E+01	ND	3.28 E+02	4.30 E+02	ND	1.06 E+02	1.18 E+04
95.9	9.05 E+02	2.72 E+04	2.91 E+01	ND	8.08 E+02	1.59 E+03	1.80 E+03	2.83 E+02	3.26 E+04
94.6	9.33 E+02	2.63 E+04	2.52 E+01	ND	5.50 E+02	1.72 E+03	4.04 E+03	2.77 E+02	3.38 E+04
85.7	5.46 E+02	1.62 E+04	2.84 E+01	ND	5.47 E+02	2.18 E+03	ND	1.68 E+02	1.97 E+04
78.1	1.59 E+03	4.73 E+04	7.14 E+01	ND	1.14 E+03	ND	2.99 E+03	5.16 E+02	5.36 E+04
71.8	3.92 E+03	1.22 E+05	2.18 E+04	ND	2.06 E+04	1.23 E+05	ND	2.14 E+03	2.93 E+05
64.1	4.64 E+03	1.38 E+05	1.03 E+02	ND	ND	9.29 E+03	5.72 E+03	1.19 E+03	1.59 E+05
54.0	6.17 E+03	2.10 E+05	1.84 E+03	ND	ND	ND	ND	8.90 E+02	2.19 E+05
51.4	6.88 E+03	2.35 E+05	1.12 E+04	ND	ND	ND	ND	1.21 E+03	2.54 E+05
48.9	7.17 E+03	2.38 E+05	ND	ND	ND	ND	ND	1.77 E+03	2.47 E+05
46.4	7.26 E+03	2.53 E+05	ND	ND	ND	ND	ND	7.48 E+02	2.61 E+05
36.2	4.86 E+03	1.84 E+05	ND	ND	ND	ND	3.02 E+04	1.27 E+03	2.20 E+05

a. Distance in centimeters from bottom of fuel stack.

b. ND--not detected.

TABLE C-7. CORE BORE 0-7 RADIONUCLIDE ACTIVITIES IN MICROCURIES (DECAY-CORRECTED TO 4/1/86)

Position[a]	^{134}Cs	^{137}Cs	^{60}Co	^{110m}Ag	^{125}Sb	^{106}Ru	^{144}Ce	^{154}Eu	Total
161.3	ND[b]	6.55 E+00	3.09 E+00	ND	ND	ND	ND	ND	9.65 E+00
132.1	ND	4.72 E+02	2.86 E+04	ND	4.00 E+04	2.84 E+05	ND	7.50 E+03	3.61 E+05
128.3	ND	1.54 E+01	2.80 E+01	ND	1.09 E+02	2.39 E+02	ND	ND	3.91 E+02
124.5	1.07 E+02	4.27 E+03	8.86 E+03	1.59 E+01	1.63 E+04	6.90 E+04	1.24 E+03	6.38 E+01	9.99 E+04
95.3	ND	1.49 E+01	ND	ND	ND	ND	ND	ND	1.49 E+01
72.4	3.19 E+02	1.96 E+04	4.03 E+04	ND	2.71 E+04	1.60 E+05	1.09 E+04	8.66 E+02	2.59 E+05
62.2	6.19 E+01	1.98 E+03	8.05 E+02	ND	4.05 E+02	4.47 E+02	5.64 E+02	3.69 E+01	4.30 E+03
52.1	5.51 E+03	1.90 E+05	1.88 E+04	ND	ND	ND	ND	5.25 E+02	2.15 E+05
47.0	7.30 E+03	2.46 E+05	1.78 E+02	ND	1.91 E+03	1.17 E+04	2.72 E+04	1.71 E+03	2.98 E+05
34.3	5.18 E+03	1.95 E+05	1.38 E+02	ND	ND	8.54 E+03	ND	1.39 E+03	2.10 E+05
21.6	3.61 E+03	1.60 E+05	1.77 E+02	ND	1.46 E+03	1.31 E+04	2.05 E+04	9.53 E+02	2.01 E+05
14.0	2.07 E+03	1.37 E+05	1.32 E+02	ND	ND	3.30 E+03	1.74 E+04	6.39 E+02	1.61 E+05
2.5	7.30 E+02	7.32 E+04	8.21 E+02	2.27 E+02	4.57 E+02	2.26 E+03	1.04 E+04	2.28 E+02	8.83 E+04
-3.8	ND	1.02 E+04	1.43 E+05	ND	ND	ND	ND	ND	1.53 E+05
-6.4	ND	5.75 E+03	7.63 E+04	ND	ND	ND	4.43 E+03	ND	9.41 E+04
-14.0	ND	ND	1.96 E+01	ND	ND	ND	ND	ND	1.96 E+01
ND									

a. Distance in centimeters from bottom of fuel stack.

b. ND--not detected.

TABLE C-8. CORE BORE N-5 RADIONUCLIDE ACTIVITIES IN MICROCURIES (DECAY-CORRECTED TO 4/1/86)

Position[a]	^{134}Cs	^{137}Cs	^{60}Co	^{110m}Ag	^{125}Sb	^{106}Ru	^{144}Ce	^{154}Eu	Total
139.1	ND[b]	ND	2.36 E+03	ND	1.65 E+03	1.02 E+04	ND	8.88 E+03	2.31 E+04
134.0	ND	7.68 E+01	6.41 E+03	ND	5.10 E+03	2.98 E+04	ND	ND	4.14 E+04
126.4	8.39 E+01	2.74 E+03	7.46 E+02	ND	6.02 E+03	3.76 E+03	1.30 E+03	6.06 E+01	1.47 E+04
123.8	4.01 E+01	1.51 E+03	9.63 E+02	ND	8.59 E+03	7.44 E+03	ND	8.99 E+03	2.75 E+04
121.3	7.41 E+01	2.45 E+03	2.76 E+03	ND	1.89 E+03	1.80 E+04	ND	1.34 E+04	3.86 E+04
118.7	7.49 E+02	3.25 E+04	1.04 E+04	ND	1.00 E+04	6.50 E+04	ND	1.22 E+03	1.19 E+05
113.7	7.77 E+01	3.49 E+03	2.81 E+03	ND	3.10 E+03	1.74 E+04	ND	3.35 E+02	2.72 E+04
111.1	3.51 E+02	6.13 E+03	4.05 E+01	ND	4.66 E+03	ND	ND	1.44 E+02	1.13 E+04
106.0	3.34 E+03	1.29 E+05	5.29 E+03	ND	ND	ND	ND	1.08 E+03	1.39 E+05
95.9	7.49 E+03	2.67 E+05	ND	ND	1.31 E+03	ND	ND	1.83 E+03	2.78 E+05
88.3	4.86 E+03	2.32 E+05	ND	ND	ND	ND	ND	ND	2.37 E+05
78.1	5.30 E+03	1.81 E+05	3.89 E+01	ND	1.42 E+03	1.29 E+04	2.59 E+04	1.65 E+03	2.28 E+05
70.5	5.54 E+03	2.25 E+05	1.60 E+04	ND	2.34 E+03	ND	2.50 E+04	1.06 E+03	2.75 E+07
62.9	6.16 E+03	2.19 E+05	ND	ND	ND	ND	ND	1.64 E+03	2.27 E+05
52.7	5.54 E+03	2.25 E+05	1.60 E+04	ND	8.25 E+04	1.56 E+04	ND	1.06 E+03	3.46 E+05
45.1	5.08 E+03	2.15 E+05	ND	ND	1.49 E+03	ND	1.01 E+04	1.23 E+03	2.33 E+05
37.5	4.38 E+03	2.04 E+05	ND	ND	ND	ND	ND	ND	2.08 E+05
23.5	3.62 E+03	1.85 E+05	2.17 E+02	ND	ND	ND	1.20 E+04	9.40 E+03	2.02 E+05
17.1	2.41 E+03	1.57 E+05	2.64 E+02	ND	ND	ND	ND	ND	1.60 E+05
9.5	1.34 E+03	1.14 E+05	2.13 E+02	ND	ND	ND	1.57 E+04	4.69 E+02	1.32 E+05
-0.6	ND	2.49 E+04	1.41 E+04	ND	1.12 E+03	ND	ND	ND	4.01 E+04
-4.4	ND	4.75 E+03	7.55 E+04	ND	ND	ND	ND	ND	8.03 E+04
-8.3	ND	3.23 E+03	5.29 E+04	ND	ND	ND	ND	ND	5.61 E+04
-15.9	ND	ND	ND	ND	ND	ND	ND	ND	ND

a. Distance in centimeters from bottom of fuel stack.

b. ND--not detected.

TABLE C-9. CORE BORE D 4 RADIONUCLIDE ACTIVITIES IN MICROCURIES (DECAY-CORRECTED TO 4/1/86)

Position[a]	^{134}Cs	^{137}Cs	^{60}Co	^{110m}Ag	^{125}Sb	^{106}Ru	^{144}Ce	^{154}Eu	Total
148.0	ND[b]	7.69 E+01	ND	ND	ND	ND	ND	ND	7.69 E+01
142.9	ND	1.69 E+02	1.35 E+04	ND	2.60 E+04	1.32 E+05	ND	3.63 E+03	1.75 E+05
140.3	ND	5.67 E+02	1.34 E+04	2.16 E+04	2.54 E+04	9.49 E+04	ND	1.92 E+03	1.58 E+05
137.8	ND	5.61 E+02	1.31 E+04	ND	2.50 E+04	8.93 E+04	ND	1.92 E+03	1.30 E+05
135.3	ND	3.34 E+01	1.14 E+04	ND	1.87 E+04	5.24 E+04	ND	6.23 E+02	8.32 E+04
132.7	ND	1.04 E+02	3.13 E+03	ND	8.17 E+03	9.92 E+03	ND	ND	2.13 E+04
117.5	ND	8.80 E+01	9.58 E+00	ND	ND	ND	ND	ND	9.76 E+01
114.9	3.67 E+01	1.09 E+03	1.27 E+01	ND	ND	ND	ND	ND	1.14 E+03
112.4	1.79 E+02	6.18 E+03	2.04 E+02	ND	2.76 E+02	ND	ND	ND	6.84 E+03
109.9	2.99 E+03	1.19 E+05	1.08 E+03	ND	8.25 E+02	1.08 E+04	6.86 E+03	9.95 E+02	1.43 E+05
102.2	6.40 E+03	2.11 E+05	2.26 E+02	ND	9.27 E+02	1.18 E+04	2.56 E+04	1.72 E+03	2.58 E+05
99.7	6.09 E+03	2.16 E+05	ND	ND	6.39 E+02	ND	2.79 E+04	1.09 E+03	2.52 E+05
97.2	3.84 E+03	1.37 E+05	ND	ND	ND	ND	1.97 E+04	7.08 E+02	1.61 E+05
90.8	5.64 E+03	1.80 E+05	1.10 E+02	ND	6.08 E+02	7.29 E+03	2.56 E+04	1.48 E+03	2.21 E+05
81.9	7.37 E+03	2.59 E+05	3.50 E+02	ND	1.50 E+03	ND	3.19 E+04	2.05 E+03	3.02 E+05
78.9	7.17 E+03	2.46 E+05	ND	ND	1.86 E+03	1.36 E+04	5.29 E+03	1.84 E+03	2.76 E+05
71.8	8.41 E+03	3.09 E+05	ND	ND	ND	ND	2.13 E+04	2.48 E+03	3.41 E+05
57.8	3.76 E+03	1.35 E+05	3.88 E+02	ND	8.92 E+02	6.53 E+03	1.89 E+04	1.02 E+03	1.66 E+05
38.7	4.80 E+03	2.10 E+05	ND	ND	1.86 E+03	ND	2.46 E+04	1.19 E+03	2.42 E+05
-4.4	ND	1.34 E+04	7.66 E+04	ND	ND	ND	ND	ND	9.00 E+04
-34.9	8.05 E+02	2.48 E+04	4.68 E+02	ND	ND	6.94 E+03	2.44 E+04	1.89 E+03	5.93 E+04

a. Distance in centimeters from bottom of fuel stack.

b. ND--not detected.

APPENDIX D

NORMALIZED RADIONUCLIDE ACTIVITY PROFILES

APPENDIX D

NORMALIZED RADIONUCLIDE ACTIVITY PROFILES

Normalized radionuclide activity profiles for the nine TMI-2 core bore samples are presented in Tables D-1 through D-9.

TABLE D-1. CORE BORE K-9 NORMALIZED ACTIVITIES

Position[b]	Normalized Activity[a] ^{137}Cs	^{106}Ru	^{144}Cs
124.5	NA[c]	NA	NA
121.9	NA	NA	NA
119.4	NA	NA	NA
116.8	NA	NA	NA
114.3	NA	NA	NA
111.8	NA	NA	NA
109.2	NA	NA	NA
106.7	1.26 E+00	2.92 E+01	NA
104.1	NA	NA	NA
101.6	5.64 E-01	3.04 E+00	1.10 E+01
99.1	9.01 E-01	1.48 E+01	1.60 E+01
96.5	1.60 E+00	1.68 E+01	9.19 E+00
94.0	4.11 E+00	7.27 E+01	ERR
91.4	2.60 E+00	9.23 E+01	1.18 E+01
88.9	2.32 E+00	4.91 E+01	1.26 E+01
86.4	1.53 E+00	3.87 E+00	6.91 E+00
83.8	9.70 E-01	NA	9.00 E+00
81.3	1.10 E+00	NA	1.29 E+01
78.7	8.72 E-01	5.87 E-01	1.24 E+01
76.2	7.86 E-01	NA	9.83 E+00
73.7	1.07 E+00	1.65 E+00	1.17 E+01
71.1	1.28 E+00	1.70 E+00	1.14 E+01
68.6	9.01 E-01	8.43 E-01	1.05 E+01
66.0	9.92 E-01	3.26 E+00	1.49 E+01
63.5	1.43 E+00	2.04 E+00	9.33 E+00
61.0	2.45 E+00	3.42 E+00	9.85 E+00
58.4	5.08 E+00	1.47 E+01	1.01 E+01
55.9	4.49 E+00	2.29 E+01	1.07 E+01
50.8	7.93 E+00	1.87 E+01	6.58 E+00
48.3	7.22 E+00	1.02 E+01	1.06 E+01
45.7	4.86 E+01	3.55 E+01	NA
40.6	9.60 E+01	NA	9.30 E+00
38.1	6.28 E+01	1.79 E+01	NA
35.6	1.18 E+02	9.01 E+00	1.61 E+01
33.0	9.77 E+01	8.28 E+00	2.84 E+01
30.5	1.39 E+02	NA	NA
27.9	1.49 E+02	9.99 E+00	NA
25.4	1.77 E+02	2.37 E+00	1.02 E+01
22.9	1.58 E+02	4.67 E+00	2.04 E+01
20.3	1.61 E+02	6.70 E+00	NA
17.8	1.62 E+02	4.97 E+00	5.85 E+00
15.2	1.49 E+02	3.15 E+00	NA
12.7	2.20 E+02	4.77 E+00	NA
10.2	2.24 E+02	3.13 E+00	1.64 E+01

TABLE D-1. (CONTINUED)

Position[b]	Normalized Activity[a]		
	^{137}Cs	^{106}Ru	^{144}Cs
7.6	4.58 E+02	1.65 E+01	5.80 E+01
5.1	2.33 E+02	1.02 E+01	2.97 E+01
2.5	3.09 E+02	1.03 E+00	4.15 E+01
0.0	9.15 E+02	1.84 E+01	NA
-2.5	NA	NA	NA
-5.1	NA	NA	NA
-7.6	NA	NA	NA
-10.2	NA	NA	NA
-12.7	NA	NA	NA
-15.2	NA	NA	NA
-17.8	NA	NA	NA

a. Ratio of activity of radionuclide to activity of ^{154}Eu.

b. Distance in centimeters from bottom of fuel stack.

c. NA--activity ratio not determined.

TABLE D-2. CORE BORE G-8 NORMALIZED ACTIVITIES

Position[b]	Normalized Activity[a] ^{137}Cs	^{106}Ru	^{144}Cs
79.4	1.25 E+00	NA[c]	1.09 E+01
69.2	4.67 E+00	3.66 E-01	1.04 E+01
59.1	5.73 E-01	NA	1.32 E+01
54.0	3.27 E+01	1.03 E+00	9.96 E+00
51.4	8.38 E+01	NA	1.82 E+01
48.9	1.27 E+02	NA	NA
46.4	1.21 E+02	NA	NA
43.8	9.78 E+01	NA	1.05 E+01
41.3	1.21 E+02	NA	NA
38.7	1.77 E+02	4.16 E+00	NA
26.0	1.62 E+02	NA	1.23 E+01
23.5	1.66 E+02	5.58 E-02	1.59 E+01
15.9	2.37 E+02	NA	3.35 E+01
8.3	2.34 E+02	NA	NA
0.6	NA	NA	NA
-7.0	NA	NA	NA
-12.1	NA	NA	NA

a. Ratio of activity of radionuclide to activity of ^{154}Eu.

b. Distance in centimeters from bottom of fuel stack.

c. NA--activity ratio not determined.

TABLE D-3. CORE BORE D-8 NORMALIZED ACTIVITIES

Position[b]	Normalized Activity[a] ^{137}Cs	^{106}Ru	^{144}Cs
165.1	NA[c]	NA	NA
162.6	NA	NA	NA
154.9	NA	NA	NA
144.8	NA	NA	NA
138.4	1.80 E+00	5.57 E+01	1.09 E+01
134.9	2.12 E+00	1.15 E+01	1.54 E+01
113.0	2.65 E+00	5.42 E+00	NA
101.6	1.29 E+02	5.82 E+00	6.26 E+00
96.5	2.35 E+02	2.65 E+00	2.20 E+01
86.4	1.00 E+00	5.27 E+00	1.34 E+01
71.1	1.03 E+02	NA	1.02 E+01
55.9	9.55 E+01	NA	1.45 E+01
50.8	8.44 E+01	NA	2.09 E+01
43.2	1.26 E+02	3.62 E+00	1.36 E+01
5.1	1.94 E+02	NA	2.91 E+01
-2.5	NA	NA	NA

a. Ratio of activity of radionuclide to activity of ^{154}Eu.

b. Distance in centimeters from bottom of fuel stack.

c. NA--activity ratio not determined.

TABLE D-4. CORE BORE G-12 NORMALIZED ACTIVITIES

Position[b]	Normalized Activity[a]		
	^{137}Cs	^{106}Ru	^{144}Cs
152.4	2.10 E+00	2.74 E+00	1.72 E+01
147.3	4.18 E+00	2.56 E+01	1.56 E+01
119.4	1.37 E+00	9.37 E-01	1.24 E+01
109.2	1.82 E+00	NA[c]	1.30 E+01
99.1	1.16 E+02	4.86 E+00	1.06 E+01
86.4	1.40 E+02	7.96 E+00	1.46 E+01
73.7	1.39 E+02	NA	1.02 E+01
71.1	NA	NA	NA
61.0	1.16 E+02	5.56 E+00	9.06 E+00
50.8	NA	NA	NA
43.2	1.66 E+02	NA	2.42 E+01
33.0	1.80 E+02	NA	NA
22.9	1.75 E+02	8.13 E+00	1.06 E+01
10.2	NA	NA	NA
0.0	3.28 E+02	NA	3.61 E+01
-5.1	NA	NA	NA
-12.7	NA	NA	NA

a. Ratio of activity of radionuclide to activity of ^{154}Eu.

b. Distance in centimeters from bottom of fuel stack.

c. NA--activity ratio not determined.

TABLE D-5. CORE BORE N-12 NORMALIZED ACTIVITIES

Position[b]	Normalized Activity[a] ^{137}Cs	^{106}Ru	^{144}Cs
113.7	NA[c]	NA	NA
93.3	1.53 E+02	9.20 E+00	NA
85.7	1.29 E+02	NA	1.84 E+01
47.6	1.35 E+02	NA	9.78 E+00
32.4	1.71 E+02	NA	2.68 E+01
27.3	3.21 E+02	NA	3.90 E+01
22.2	2.15 E+02	NA	3.00 E+01
14.6	2.74 E+02	NA	4.75 E+01
9.5	3.11 E+02	NA	NA
4.4	3.80 E+02	2.42 E+01	5.10 E+01
-0.6	NA	NA	NA
-5.7	NA	NA	NA
-10.8	NA	NA	NA
-15.9	NA	NA	NA
-18.4	NA	NA	NA
-21.0	NA	NA	NA
-23.5	NA	NA	NA

a. Ratio of activity of radionuclide to activity of ^{154}Eu.

b. Distance in centimeters from bottom of fuel stack.

c. NA--activity ratio not determined.

TABLE D-6. CORE BORE O-9 NORMALIZED ACTIVITIES

Position[b]	Normalized Activity[a] ^{137}Cs	^{106}Ru	^{144}Cs
113.7	NA[c]	NA	NA
109.9	1.22 E-01	3.32 E+01	NA
108.6	7.60 E-01	3.07 E+01	NA
103.5	9.92 E+01	4.06 E+00	NA
95.9	9.60 E+01	5.61 E+00	6.35 E+00
94.6	9.49 E+01	6.20 E+00	1.46 E+01
85.7	9.62 E+01	1.30 E+01	NA
78.1	9.16 E+01	NA	5.78 E+00
71.8	5.69 E+01	5.75 E+01	NA
64.1	1.16 E+02	7.82 E+00	4.82 E+00
54.0	2.35 E+02	NA	NA
51.4	1.94 E+02	NA	NA
48.9	1.35 E+02	NA	NA
46.4	3.39 E+02	NA	NA
36.2	1.45 E+02	NA	2.39 E+01

a. Ratio of activity of radionuclide to activity of ^{154}Eu.

b. Distance in centimeters from bottom of fuel stack.

c. NA--activity ratio not determined.

TABLE D-7. CORE BORE 0-7 NORMALIZED ACTIVITIES

Position[b]	Normalized Activity[a] ^{137}Cs	^{106}Ru	^{144}Cs
161.3	NA[c]	NA	NA
132.1	6.32 E-02	3.78 E+01	NA
128.3	NA	NA	NA
124.5	6.69 E+01	1.08 E+03	1.95 E+01
95.3	NA	NA	NA
72.4	2.26 E+01	1.84 E+02	1.26 E+01
62.2	5.37 E+01	1.21 E+01	1.53 E+01
52.1	3.63 E+02	NA	NA
47.0	1.44 E+02	6.85 E+00	1.59 E+01
34.3	1.40 E+02	6.13 E+00	NA
21.6	1.67 E+02	1.37 E+01	2.15 E+01
14.0	2.14 E+02	5.16 E+00	2.71 E+01
2.5	3.21 E+02	9.89 E+00	4.56 E+01
-3.8	NA	NA	NA
-6.4	NA	NA	NA
-14.0	NA	NA	NA

a. Ratio of activity of radionuclide to activity of ^{154}Eu.

b. Distance in centimeters from bottom of fuel stack.

c. NA--activity ratio not determined.

TABLE D-8. CORE BORE N-5 NORMALIZED ACTIVITIES

Position[b]	Normalized Activity[a] ^{137}Cs	^{106}Ru	^{144}Cs
139.1	NA[c]	1.15 E+00	NA
134.0	NA	NA	NA
126.4	4.52 E+01	6.20 E+01	2.15 E+01
123.8	1.68 E-01	8.27 E-01	NA
121.3	1.83 E-01	1.35 E+00	NA
118.7	2.67 E+01	5.34 E+01	NA
113.7	1.04 E+01	5.18 E+01	NA
111.1	4.25 E+01	NA	NA
106.0	1.19 E+02	NA	NA
95.9	1.46 E+02	NA	NA
88.3	NA	NA	NA
78.1	1.10 E+02	7.85 E+00	1.57 E+01
70.5	2.13 E+02	NA	2.36 E+01
62.9	1.33 E+02	NA	NA
52.7	2.13 E+02	1.47 E+01	NA
45.1	1.75 E+02	NA	8.24 E+00
37.5	NA	NA	NA
23.5	1.96 E+02	NA	1.28 E+01
17.1	NA	NA	NA
9.5	2.43 E+02	NA	3.35 E+01
-0.6	NA	NA	NA
-4.4	NA	NA	NA
-8.3	NA	NA	NA
-15.9	NA	NA	NA

a. Ratio of activity of radionuclide to activity of ^{154}Eu.

b. Distance in centimeters from bottom of fuel stack.

c. NA--activity ratio not determined.

TABLE D-9. CORE BORE D-4 NORMALIZED ACTIVITIES

Position[b]	Normalized Activity[a] ^{137}Cs	^{106}Ru	^{144}Cs
148.0	NA[c]	NA	NA
142.9	4.66 E-02	3.64 E+01	NA
140.3	2.95 E-01	4.94 E+01	NA
137.8	2.92 E-01	4.65 E+01	NA
135.3	5.37 E-02	8.41 E+01	NA
132.7	NA	NA	NA
117.5	NA	NA	NA
114.9	NA	NA	NA
112.4	NA	NA	NA
109.9	1.20 E+02	1.09 E+01	6.90 E+00
102.2	1.22 E+02	6.84 E+00	1.48 E+01
99.7	1.98 E+02	NA	2.55 E+01
97.2	1.93 E+02	NA	2.78 E+01
90.8	1.22 E+02	4.93 E+00	1.73 E+01
81.9	1.26 E+02	NA	1.55 E+01
78.9	1.34 E+02	7.40 E+00	2.88 E+00
71.8	1.25 E+02	NA	8.58 E+00
57.8	1.33 E+02	6.41 E+00	1.86 E+01
38.7	1.77 E+02	NA	2.07 E+01
-4.4	NA	NA	NA
-34.9	1.31 E+01	3.68 E+00	1.29 E+01

a. Ratio of activity of radionuclide to activity of ^{154}Eu.

b. Distance in centimeters from bottom of fuel stack.

c. NA--activity ratio not determined.